ADVANCED RESEARCH PROJECTS AGENCY

Contract SD-88

Technical Report No. ARPA-12

THEORY OF SEMICONDUCTOR-TO-METAL TRANSITIONS

By

David Adler

August 28, 1964

DIVISION OF ENGINEERING AND APPLIED PHYSICS
HARVARD UNIVERSITY - CAMBRIDGE, MASSACHUSETTS

DISCLAIMER NOTICE

THIS DOCUMENT IS THE BEST QUALITY AVAILABLE.

COPY FURNISHED CONTAINED A SIGNIFICANT NUMBER OF PAGES WHICH DO NOT REPRODUCE LEGIBLY.

THEORY OF SEMICONDUCTOR-TO-METAL TRANSITIONS

by

David Adler

Technical Report No. ARPA-12

Contract SD-88

August 26, 1964

Submitted to:

Advanced Research Projects Agency

The Department of Defense

Division of Engineering and Applied Physics

Harvard University

Cambridge, Massachusetts

TABLE OF CONTENTS

LIST OF FIGURES

BLANK PAGE

ABSTRACT

Several materials undergo transitions from a semiconducting to a metallic state at a critical temperature. Previous theoretical attempts to understand such transitions have been generally qualitative and have not been able to account for all the specific experimental results.

In this work, an explanation of semiconductor-to-metal transitions is presented using a band model. It is shown thermodynamically that the energy gap of a semiconductor closes down significantly with the number of excited carriers if the gap has a large pressure coefficient, as is found in several of these materials. This shrinkage of the energy gap is due to explicit variation of the crystalline volume. There may also be a constant volume carrier concentration dependence of the gap, which cannot be evaluated thermodynamically.

Two specific models are discussed. If the energy gap arises from the splitting of the first Brillouin zone by an antiferromagnetic exchange interaction, the gap will decrease linearly with the number of free carriers. The relationship is demonstrated by means of a one-dimensional model, a three-dimensional tight binding model, and a virtual crystal approximation. In all three cases, the same result is obtained. An analogous situation occurs if the energy gap is due to a crystalline structure distortion to lower symmetry. In particular, the pairing of ions in a one-dimensional crystal is analyzed. The relationship between gap and free carrier concentration is derived for the two cases of a contact interaction and a Mathieu inter-

action. The results found are quite similar to those when the gap is caused by antiferromagnetism.

These relationships, together with the application of Fermi-Dirac statistics to the conduction electrons, enable us to calculate the electrical conductivity as a function of temperature in two opposing limits, the effective mass approximation and the limit of narrow bands. It is found in both cases that a singular increase in the carrier concentration, and thus the conductivity, occurs at a given temperature. This leads to the disappearance of the energy gap, and therefore to a semiconductor-to-metal transition.

The transition temperature is evaluated in terms of the zero temperature energy gap. A number of results, relating experimentally measurable quantities such as the pressure coefficients of the transition temperature and energy gap, are derived.

The experimental results dealing with the crystals which exhibit semiconductor-to-metal transitions are presented, and the predictions of the theory are tested. Very good agreement is obtained.

The theory, taken together with the available experimental information, is used to suggest possible band schemes for each of the materials under investigation. It is found that the crystalline symmetry in every case is compatible with an energy gap which arises from either a pairing of cations or antiferromagnetism.

Finally, the effects on the theory of spin-disorder scattering, polaron formation, and non-stoichiometry are discussed quantitatively.

Chapter I

INTRODUCTION

A. Transition Metal Oxides which are Insulators at all Temperatures

The transition metal oxides provide a striking example of the inadequacy of simple band theory when an attempt is made to predict the electrical transport properties of crystals. Most of these oxides are insulators [1], despite the apparent presence of a partially filled 3d band. The materials which remain non-conducting at all temperatures shall be referred to as the NiO class. These include NiO, MnO, and Fe_2O_3. The experimental situation has been reviewed by Morin [2] and by Jonker and van Houten [3]; the only information of direct interest to us here is that, where the magnetic structure has been determined, these oxides are all antiferromagnetic, and they are insulating both below and above the Néel temperature. We are, however, interested in discussing the proposed theoretical models.

Many attempts have been made to explain the non-conducting nature of these materials. DeBoer and Verwey [1] assumed that the movement of electrons between neighboring cations is impeded by a high potential barrier. Thus the 3d electrons are essentially localized, conductivity being possible only via tunneling of electrons through the barriers. Verwey [4] later extended the model, showing that the activation energy was due to the ionization of the cations.

Heikes and Johnston [5] noted that the observed ionization energies

are not large enough to account for the measured activation energies of the NiO class, which are of the order of 0.5 eV. They suggested that the activation energy should be associated with the mobility, rather than with the carrier concentration. The activation energy in this theory arises from Landau trapping [6], which occurs when an electron is localized around a lattice point in a polar crystal long enough to cause a deformation of the crystal. The electron is then able to form a bound state with the potential well due to the polarization. Heikes and Johnston ascribe the conductivity to a hopping or diffusion of electrons from one site to a neighboring site, which will occur when the lattice polarization around both is momentarily the same.

Yamashita and Kurosawa [7] attempted to work out the theory, starting with a Heitler-London approach. They found it necessary to assume that the electrons are localized around the cations, and were then able to show that the electrons could be trapped by the resulting lattice polarization, and that conductivity could occur by means of equal-site hopping. However, no reason was given for the localization in the first place.

Anderson [8], taking up a suggestion of Mott [9], put the theory on a somewhat firmer footing by pointing out that the localization could be due to the large correlation energy we should expect in a low density system. Anderson called U the energy necessary to remove one electron from a given cation and put it on another cation which is far away. U is thus an intra-ionic Coulomb integral, and can be estimated from the free cation ionization energies. Anderson approximates U as of the order of 10 eV, although there are reasons to believe this is too

high. If U is larger than half the bandwidth, it outweighs the kinetic energy loss which could be accomplished by spreading through the crystal, and the electrons would remain localized. Although this argument appears to justify the procedure of Yamashita and Kurosawa, it, too, is only a self-consistent hypothesis, since the presence of many free electrons would reduce U significantly by means of screening. Thus, the large order of magnitude given by Anderson for U is accurate only when the electrons are known to be localized, and it is possible for a metallic state to be self-consistently lower in total energy.

Holstein [10] has applied the theory of polaron formation of Frohlich [11] to the situation in the transition metal oxides. A polaron is a bound state of an electron and its associated lattice deformation which can be treated as a quasiparticle moving through the crystal. Holstein considered in particular the "small" polaron, whose dimensions are of the order of a lattice constant. The polaron will be "small" if the electronic bandwidth is much less than the maximum binding energy of the polaron, a constant which is proportional to the square of the strength of the electron-phonon interaction. Holstein found that at low temperatures there is sufficient overlap to form a polaron band through which the electron, together with its lattice deformation, can move. An unfilled polaron band carries a current which decreases exponentially with increasing temperature. Since the width of the polaron band is also an exponentially decreasing function of temperature, and since the polaron states have a finite lifetime, eventually the point is reached when the bandwidth is smaller than the uncertainty in energy associated with the lifetime, and the bands lose their physical meaning. Above this temperature, estimated by Holstein as half the

Debye temperature, conduction occurs when the interaction of phonons with the deformation potential causes ionic rearrangements at neighboring sites, enabling the polaror to jump from one to the other. This mechanism is just thermally activated hopping of polarons.

An entirely different approach was suggested by Slater [12]. He retained the band picture and suggested that the antiferromagnetic ordering can bring about an extra band splitting. Slater's argument goes as follows: According to the Hartree-Fock approximation, an electron will be repelled much less strongly by electrons with parallel spins than by those with antiparallel spins. Since the crystal is antiferromagnetic, each electron feels a potential which has the periodicity of the superlattice rather than that of the lattice. Such a potential will split the first Brillouin zone in half, each half containing 1/2 N V states for each direction of spin, where N is the concentration of cations per unit volume and V is the volume of the crystal. Thus even when there is one electron per cation, the first zone could in principle be filled, the second empty. Two difficulties with this theory immediately emerge. The 3d band should be highly degenerate, particularly for cubic lattices, such as MnO and CoO, and Slater does not attempt to show how such crystals, containing 5 and 7 3d electrons per cation, respectively, can have anything but a partially filled valence band, even with the antiferromagnetic splitting. Furthermore, Slater gives no explanation of the non-conductivity of the NiO class of materials above the Néel temperature.

Recently, Hubbard [13] considered another band approach which removed the latter objection. Hubbard showed that electronic corre-

lation could result in the splitting of a narrow band into two sub-bands, analogous to the splitting due to exchange energy in Slater's model, but independent of the magnetic ordering of the system. Thus the crystals, if insulating at T = 0, should remain insulating, even above the Néel temperature. This correlation splitting is essentially a manifestation of the Anderson effect [8], in that it represents a partial localization.

B. Transition Metal Oxides which Exhibit Insulator-to-Metal Transitions

The lack of electrical conductivity is not the only enigma provided by the transition metal oxides. Another subclass, referred to here as the V_2O_3 class, consists of several oxides of vanadium and titanium, which are non-conducting at low temperatures, but undergo a transition to a metallic state above a critical temperature. These are the materials with which we are concerned in this work.

The first hint of unusual behavior in this class of oxides came when Perakis [14] discovered that the magnetic susceptibilities of VO_2 and V_2O_3 each went through a sharp transition at a given temperature. Anderson [15] found a specific heat anomaly in V_2O_3 in the vicinity of $150^{\circ}K$, with a latent heat of approximately 700 calories per mole measured over a $20^{\circ}K$ temperature interval. Foëx [16] investigated the electrical properties of V_2O_3, and discovered a sharp increase of a factor of 10^6 in conductivity at the temperature of the specific heat anomaly. He also reported a volume contraction at the same point. Foëx and Loriers [17] found a transition in Ti_2O_3 at about $475^{\circ}K$, the electrical conductivity jumping by a factor of 10. Jaffray and Dumas [18] verified the transition in V_2O_3, and also reported an insulator-to-metal

transition as well as a small contraction in volume in VO_2 at the temperature of the magnetic susceptibility anomaly. Pearson [19] noted an absorption edge of 0.15 eV in a sample of powdered Ti_2O_3 in KBr, but did not obtain a break in the conductivity curve. He did find that the conductivity as well as the lattice constants were rapidly changing in the vicinity of 500°K.

The situation with regard to the electrical properties of the lower oxides of titanium and vanadium was resolved by the work of Morin [20], who performed measurements of conductivity as a function of temperature on single crystals of Ti_2O_3, V_2O_3, TiO, VO, and VO_2. His results are given in Fig. I-1. As can be seen, all these materials with the exception of TiO are semiconducting at low temperatures, but undergo a transition to the metallic state at a given temperature, which we shall call T_o.

The experimental situation since Morin's work has been reviewed in great detail by Feinleib [21], and we shall at this point mention only three important discoveries of recent years. Yahia and Frederikse [22] were able to measure the Hall coefficient in Ti_2O_3, and found that the Hall activation energy was virtually the same as the conductivity activation energy. Abrahams [23] performed neutron diffraction experiments on Ti_2O_3, and determined that it was antiferromagnetic with a small moment of 0.2 Bohr magnetons per cation, the Néel temperature being in the vicinity of the semiconductor-to-metal transition. Most recently, Feinleib [24] performed optical measurements on single crystals of stoichiometric, semiconducting V_2O_3, and

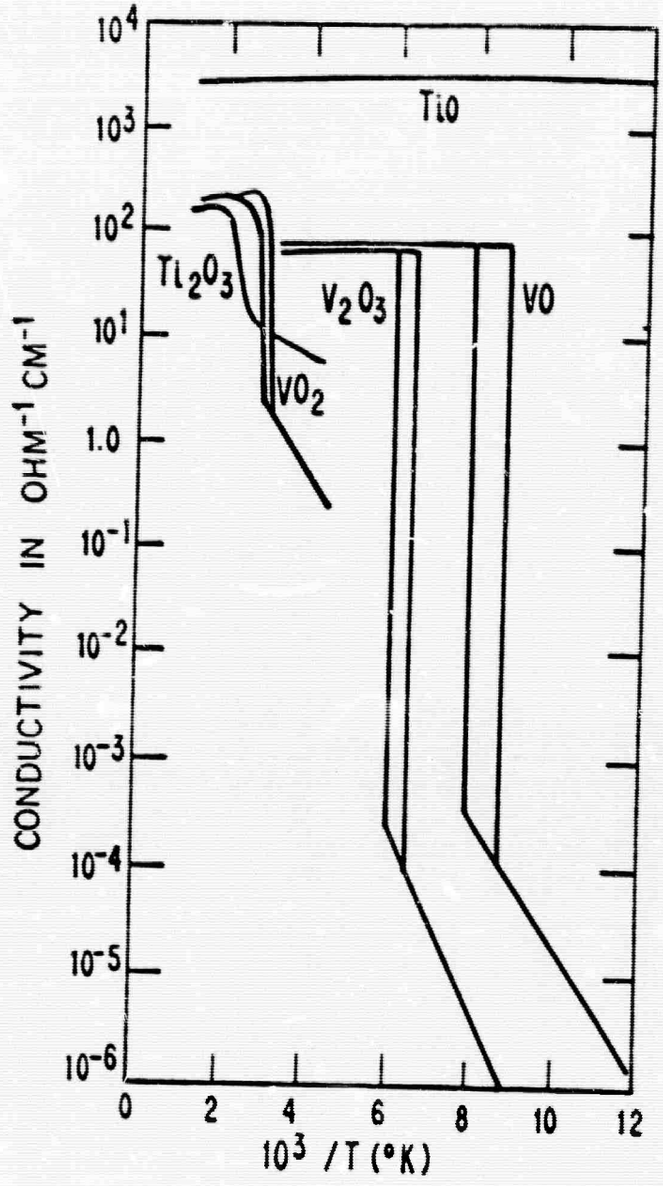

FIG. I-1 CONDUCTIVITY vs. TEMPERATURE FOR SEVERAL V AND Ti OXIDES [after Morin (20)]

observed an absorption edge at approximately 0.1 eV.

The first attempt at an explanation of the sharp discontinuities in conductivity was given by Morin [20], who adapted the theory of Slater [12]. If these materials were semiconducting due to a band splitting arising from antiferromagnetism, then a transition to the metallic state would be expected at the Néel temperature.

Callaway [25] made the Slater-Morin model a little more quantitative by studying the energy band structure of a body-centered cubic antiferromagnet. Considering only the first Fourier component of the exchange potential, a major simplification, he found that an insulating state exists whenever an interaction parameter (proportional to the effective mass, to the strength of the exchange potential, and to the square of the lattice constant) is sufficiently large. Neither Callaway nor Morin discussed the nature of the semiconductor-to-metal transition beyond noting that the band gap should disappear at the Néel temperature.

There are three difficulties with the Slater-Morin theory, outside of the fact that it has never been quantitatively applied to the oxides of titanium and vanadium. Firstly, the existence of antiferromagnetism has been demonstrated only in Ti_2O_3, and even in that material the antiferromagnetic moment is extremely small. Secondly, no model for the structure of the degenerate 3d bands has been presented which explains how Ti_2O_3, V_2O_3, and VO_2 can be semiconducting even with the antiferromagnetic splitting. Finally, it has not been proven that the energy gap must vanish with the disappearance of long-range order; it is conceivable that the large amount of short

range order present until two or three times the Néel temperature is sufficient to maintain the effective double periodicity seen by the slowly moving 3d electrons, and thus maintain an energy gap.

A different approach to the problem was presented by Mott [26], who proposed that there would be a sharp transition from an insulating to a conducting state at a critical value of the lattice parameter, R_c. Mott argued that a free electron and a free hole attract each other with a Coulomb potential, $V(r) = -e^2/\epsilon r$, and form a bound state, similar to an exciton, from which neither can participate in conduction. However, if a large number of free carriers exist, the attraction between an electron and a hole is a screened Coulomb potential, $V(r) = -e^2 e^{-qr}/\epsilon r$. When q becomes sufficiently large, this potential becomes too weak for the formation of bound states, and a discontinuous increase in the number of free carriers brings about a transition to the metallic state. Mott [27] assumed Fermi-Thomas screening, and roughly estimated R_c as :

$$R_c \sim z \frac{\epsilon}{m^*/m} 2.1 \text{ Å}$$

where z is the number of 3d electrons per cation, ϵ is the dielectric constant, and m^* is the effective mass of an electron in the conduction band. Mott did not attempt to apply quantitatively his theory to the vanadium and titanium oxides, but it is possible that a crystalline contraction at a given temperature could indeed lower the lattice parameters in such a way as to bring about a transition to the metallic state. Since there is evidence of phase transformations at or near T_o in all four materials which undergo semiconductor-to-metal transitions,

it is possible that this model applies. However, the temperature variation of the lattice constants often produces changes greater than those which occur during the phase transformation, but in the opposite direction. Furthermore, the expression derived for R_c should favor metallic conductivity in VO, where $z = 3$, over that in TiO, where $z = 2$, the lattice parameters and ionic radii of the two crystals being roughly the same. Actually, the reverse is the case, TiO being the metal at all temperatures. Other objections to this theory will be presented in Chapter VI.

Goodenough [28] accepted Mott's hypothesis of a critical cation separation, and proposed that, due to the anisotropy of 3d orbitals and complex crystalline structures, localized and collective electrons could be present simultaneously in a given crystal. By considering the entire class of transition metal oxides, he was able to estimate $R_c \sim 2.9$ Å. Noting that the lattice parameters in the V_2O_3 class are smaller than R_c, Goodenough [29] suggested that, due to direct cation-cation interaction, all would-be conduction electrons could be trapped in homopolar bonds at low temperatures. Above a critical temperature, the free energy associated with a metallic state may become lower than that of the bonding state, because of the extra entropy associated with the continuum of electronic states in the metallic phase, and a transition would then occur. Goodenough [30] did apply his hypothesis to the oxides of vanadium and titanium, and was able to account for many of the previously unexplained symmetry changes. However, the theory does not lend itself to quantitative investigation, and has other difficulties which will be detailed in

Chapter VI.

Two recent theoretical discussions are quite relevant, although neither has been applied to the V_2O_3 class of materials. Kohn [31] developed a characterization of the insulating state, which essentially makes quantitative part of Mott's original proposal [9]. Kohn considered a ring of hydrogen atoms, and showed that if the separation between nearest neighbors is sufficiently large, one can express each wave function as a sum of localized functions which do not overlap, and such wave functions correspond to an insulating system. Kohn also investigated the Mott transition [27] by considering a ferromagnetic simple cubic array of hydrogen atoms. If the potential between a spin-up hole and a spin-down electron were a Coulomb attraction, an insulating spin-wave state is lowest, independent of the weakness of the interaction. However, for a delta function interaction, a critical strength exists, below which only a continuum of states, characterizing a metal, is present. Thus, an insulator-to-metal transition can occur at a critical value of the lattice parameter.

Hubbard [32] extended his own theory of correlations in narrow bands, and found that at a critical ratio of the bandwidth, E_b, to the intraionic correlation energy, U:

$$\frac{E_b}{U} = \frac{2}{\sqrt{3}}$$

the energy gap due to correlation has shrunk to zero, and a semiconductor-to-metal transition occurs. However, the energy gap shrinks continuously as the ratio of E_b to U increases, so that slightly below the critical value, the material has an infinitesimal band gap, while

just above the transition point, the density of states at the Fermi surface is negligibly small, so that the material is a poor metal. This type of transition is unlikely to be responsible for a change in conductivity of a factor of 10^8 at T_c, as is found in V_2O_3 and VO. It is possible that Hubbard's neglect of interactions of electrons on different ions camouflaged the sharpness of the transition, but until worked out explicitly, this remains a speculation. If the nature of the disappearance of the energy gap is as Hubbard has found, then Mott's hypothesis of a sharp increase in the number of carriers is incorrect.

It is clear that all theories of insulator-to-metal transitions have serious deficiencies when applied to the V_2O_3 class of materials. In this work, we shall attempt to present a model which overcomes the objections discussed above. We shall retain the band picture, and assume the non-conducting state of these materials is that of a normal semiconductor, having a filled valence band separated from an empty conduction band by an energy gap. In Chapter II, we shall show how such a gap can arise in the transition metal oxides from antiferromagnetism and also from a crystalline structure distortion to lower symmetry. It will be demonstrated that in these two cases the energy gap will shrink as carriers are excited across it, and the decrease in the gap will be quantitatively estimated. A thermodynamic argument will be presented to relate this decrease to the observed pressure coefficient of the gap. In Chapter III, the theory of conductivity will be worked out in two limits, the effective mass approximation and the limit of narrow bands. We shall demonstrate that a

sharp semiconductor-to-metal transition occurs, and calculate the transition temperature in terms of observable quantities. In Chapter IV, the theory of Chapters II and III will be applied to the experimental data on the oxides of titanium and vanadium. Certain relationships predicted by the theory will be critically tested quantitatively. Chapter V will consist of suggested energy band models for the materials investigated, based on a combination of the experimental data available and the predictions of the theory. Finally, in Chapter VI, we shall discuss the effects of spin-disorder scattering and broadening, polaron formation, and non-stoichiometry, as well as demonstrate additional inconsistencies with some of the other models which have been presented.

Chapter II

DEPENDENCE OF ENERGY GAP ON CARRIER CONCENTRATION

A. General Hypothesis

Consider an intrinsic semiconductor for which the top of the valence band is separated from the bottom of the conduction band by an energy gap, E_g. In general, E_g depends on the concentration of carriers in the conduction band, n, and on the temperature, T:

$$E_g = E_g(n, T).$$

At low temperatures, the concentration of carriers is also small, and we can write:

$$E_g = E_{go} - \alpha T - \beta n$$

where E_{go} is the gap at T = 0, $\alpha \equiv -\left(\frac{\partial E_g}{\partial T}\right)_n$, and $\beta \equiv -\left(\frac{\partial E_g}{\partial n}\right)_T$. Although the term linear in T is responsible for the major part of the decrease in band gap at very low temperatures, it does not contribute to the semiconductor-to-metal transition and therefore will be dropped. In Appendix A, we shall show that only a small error is introduced into the calculation by ignoring this term. We are left with:

$$E_g = E_{go} - \beta n \qquad (2.1)$$

which is our fundamental relation. The remainder of this chapter will be devoted to demonstrating the applicability of Eq. (2.1) in two particular situations, where the energy gap is due to antiferromagnetism and where the gap arises from a crystalline structure distortion

to lower symmetry. We shall evaluate β for both of these cases, and show that Eq. (2.1) remains valid as n becomes relatively large.

B. Thermodynamic Argument

In this section, we shall present a thermodynamic calculation of the change in energy gap of a semiconductor with the concentration of excited carriers. This will provide us with a general expression for β in Eq. (2.1). The first part of this argument follows closely a recent paper by Figielski [33].

The differential form of the Gibbs' free energy for a system where the number of particles may vary is:

$$dG = -S\,dT + V\,dP + \sum_j \mu_j\,dN_j \tag{2.2}$$

where N_j is the number of particles in the j^{th} phase and μ_j is the chemical potential of the j^{th} phase. Treating electrons in the valence and conduction bands as different phases and ignoring inner orbitals, we can write:

$$\sum_j \mu_j\,dN_j = \mu_c\,dN_c + \mu_v\,dN_v\,. \tag{2.3}$$

For an intrinsic semiconductor, $N_v + N_c$ = constant, and (2.3) becomes:

$$\sum_j \mu_j\,dN_j = (\mu_c - \mu_v)\,dN \tag{2.4}$$

where N is the number of carriers.

Since $\frac{\partial^2 G}{\partial P \partial N} = \frac{\partial^2 G}{\partial N \partial P}$, (2.2) and (2.4) give:

$$\left(\frac{\partial V}{\partial N}\right)_{P,T} = \frac{1}{V}\left(\frac{\partial V}{\partial n}\right)_{P,T} = \left(\frac{\partial \mu_c}{\partial P}\right)_{n,T} - \left(\frac{\partial \mu_v}{\partial P}\right)_{n,T} \tag{2.5}$$

where $n \equiv N/V$ is the concentration of carriers. The chemical

potential, μ_v, must be calculated from the relation:

$$n_v = \int_{-\infty}^{\infty} \rho_v(E)\, f\left(\frac{E - \mu_v}{kT}\right) dE$$

where n_v is the concentration of electrons in the valence band, $\rho_v(E)$ is the density of states in the valence band, and $f(x) = [e^x + 1]^{-1}$. The chemical potential μ_c, is determined from an entirely analogous relation. It is clear that at $T = 0$, $\mu_v = E_v$ and $\mu_c = E_c$, where E_v is the energy of the top of the valence band and E_c is the energy of the bottom of the conduction band. In general, $\mu_c - \mu_v$ is the change in free energy when an electron is removed from the valence band and placed in the conduction band. It can be shown that $\mu_c - \mu_v$ differs from $E_c - E_v$ by small terms proportional to kT, which we can essentially neglect. Substituting this result in (2.5):

$$\frac{1}{V}\left(\frac{\partial V}{\partial n}\right)_{P,T} = \left(\frac{\partial E_c}{\partial P}\right)_{n,T} - \left(\frac{\partial E_v}{\partial P}\right)_{n,T} = \left(\frac{\partial E_g}{\partial P}\right)_{n,T} \qquad (2.6)$$

where $E_g = E_c - E_v$ is the energy gap.

Using the thermodynamic relations:

$$\left(\frac{\partial E_g}{\partial n}\right)_{P,T} = \left(\frac{\partial E_g}{\partial V}\right)_{n,T}\left(\frac{\partial V}{\partial n}\right)_{P,T} + \left(\frac{\partial E_g}{\partial n}\right)_{V,T}$$

and:

$$\left(\frac{\partial E_g}{\partial V}\right)_{n,T} = -\frac{1}{\kappa V}\left(\frac{\partial E_g}{\partial P}\right)_{n,T}$$

where κ is the isothermal compressibility, we find:

$$\left(\frac{\partial E_g}{\partial n}\right)_{P,T} = -\frac{1}{\kappa V}\left(\frac{\partial E_g}{\partial P}\right)_{n,T}\left(\frac{\partial V}{\partial n}\right)_{P,T} + \left(\frac{\partial E_g}{\partial n}\right)_{V,T}. \qquad (2.7)$$

Thus, (2.6) and (2.7) yield:

$$\left(\frac{\partial E_g}{\partial n}\right)_{P,T} = -\frac{1}{\kappa}\left(\frac{\partial E_g}{\partial P}\right)^2_{n,T} + \left(\frac{\partial E_g}{\partial n}\right)_{V,T}. \qquad (2.8)$$

We express the energy gap for varying carrier concentration and pressure as:

$$E_g = E_{go} - \beta n - \gamma P. \tag{2.9}$$

Thus:

$$\left(\frac{\partial E_g}{\partial P}\right)_{n,T} = -\gamma. \tag{2.10}$$

Substituting (2.10) in (2.8):

$$\left(\frac{\partial E_g}{\partial n}\right)_{P,T} = -\frac{\gamma^2}{\kappa} + \left(\frac{\partial E_g}{\partial n}\right)_{V,T}. \tag{2.11}$$

But also from (2.9), we see:

$$\left(\frac{\partial E_g}{\partial n}\right)_{P,T} = -\beta. \tag{2.12}$$

Combining (2.11) and (2.12):

$$\beta = \frac{\gamma^2}{\kappa} - \left(\frac{\partial E_g}{\partial n}\right)_{V,T}. \tag{2.13}$$

This is the general thermodynamic expression for β. The first term on the right represents the contribution to β resulting from changes in the volume of the crystal. This term can be evaluated easily from the experimentally measurable quantities, γ, κ, and is always positive. The other contribution to β is an explicit dependence of the gap on carrier concentration at constant volume, and can have either sign.

This thermodynamic argument shows that whenever there is a pressure dependence of the energy gap of a semiconductor, the gap must also depend on carrier concentration. Since the pressure coefficients of the gap in V_2O_3 and VO, two of the materials with which we are especially concerned, are anomalously large, we expect a

relatively large decrease of gap with carrier concentration in these materials. But this argument demonstrates only that E_g depends on the number of excited carriers. It does not say anything about the validity of Eq. (2.1) as n becomes fairly large, nor does it indicate the microscopic reasons for such a variation in energy gap. Therefore, we now turn to specific models for which we can calculate expressions for E_g as a function of n. These calculations will provide us also with expressions for β which can be tested experimentally.

C. Antiferromagnetism

Consider an antiferromagnetic crystal which can be described by Bloch wave functions. Assume that the crystal is an insulator at $T = 0$ because of the splitting of the first Brillouin zone by the doubly-periodic exchange potential. In other words, we have an empty conduction band which begins a distance E_g above the filled valence band, with E_g being a measure of the exchange energy. The lower band refers to wave functions whose amplitudes are large at the sublattice positions of the electron under consideration, whereas the upper band wave functions have large amplitudes at the positions of the sublattice of opposite spin. As the temperature is increased from $T = 0$, the upper band becomes thermally populated. When an electron is excited across the energy gap, the net magnetization on either sublattice decreases, and thus the gap decreases with increasing concentration of carriers. Thus a relationship like Eq. (2.1) can be expected to hold. In this section, we shall determine for how large n Eq. (2.1) remains valid and also calculate the value of β. We shall

begin with a one-dimensional model, since it can be solved in terms of simple band parameters and the solution exhibits quantitatively the points discussed above. We shall then repeat the calculation for the case of a three-dimensional face-centered cubic crystal (such as VO) using the approximation of tight binding. Finally, we shall evaluate β in the limit opposite to that of elementary Bloch theory, employing a virtual crystal approximation.

1. One-Dimensional Model

Consider a one-dimensional antiferromagnetic crystal, with N ions spaced a/2 apart. Assume each ion contains one electron outside the core and take the ion at the origin to have spin up. The exchange potential has periodicity a, and thus the first Brillouin zone is $-\pi/a \leq k < \pi/a$. In accordance with L.C.A.O. theory, the Bloch wave functions are:

$$\psi_1(k,x) = \left(\frac{N}{2}\right)^{-1/2} c_{11}(k) \sum_n e^{ikna}\, a(x - na)\, \alpha + \left(\frac{N}{2}\right)^{-1/2} c_{21}(k) \sum_n e^{ik(n+1/2)a}\, a\left[x - (n+\tfrac{1}{2})a\right] \beta$$

$$\psi_2(k,x) = \left(\frac{N}{2}\right)^{-1/2} c_{12}(k) \sum_n e^{ikna}\, a(x - na)\, \alpha + \left(\frac{N}{2}\right)^{-1/2} c_{22}(k) \sum_n e^{ik(n+1/2)a}\, a\left[x - (n+\tfrac{1}{2})a\right] \beta \,. \qquad (2.14)$$

Assuming the ionic functions do not overlap, the secular equation is:

$$\det\, |H_{mn}(k) - E\ \ \delta_{mn}| = 0 \qquad (2.15)$$

where:

$$H_{11}(k) = \sum_n \cos k n a \int dx\, a(x - na)\, H(x)\, a(x)$$

$$H_{22}(k) = \sum_n \cos k n a \int dx\, a\left[x - (n + \tfrac{1}{2})a\right] H(x)\, a(x - \tfrac{1}{2}a)$$

$$H_{12}(k) = H_{21}(k) \sum_n \cos k (n - \tfrac{1}{2})a \int dx\, a(x - na)\, H(x)\, a(x - \tfrac{1}{2}a) .$$

Let:

$$\alpha_n \equiv \int dx\, a(x - na)\, H(x)\, a(x)$$

$$\hat{\alpha}_n \equiv \int a\left[x - (n + \tfrac{1}{2})a\right] H(x)\, a(x - \tfrac{1}{2}a)$$

$$\beta_n \equiv \int dx\, a(x - na)\, H(x)\, a(x - \tfrac{1}{2}a) .$$

With these definitions, and assuming nearest-neighbor interactions only, (2.15) becomes:

$$O = \begin{vmatrix} \alpha_o - E & 2\beta_o \cos \frac{1}{2} ka \\ 2\beta_o \cos \frac{1}{2} ka & \hat{\alpha}_o - E \end{vmatrix}$$

$$= E^2 - (\alpha + \hat{\alpha})E + \alpha\hat{\alpha} - 4\beta^2 \cos^2 \tfrac{1}{2} ka$$

where we have dropped the subscript o. Solving the secular equation:

$$E(k) = \begin{cases} \dfrac{\alpha + \hat{\alpha}}{2} + \sqrt{\left(\dfrac{\alpha - \hat{\alpha}}{2}\right)^2 + 4\beta^2 \cos^2 \tfrac{1}{2} ka} \\ \dfrac{\alpha + \hat{\alpha}}{2} - \sqrt{\left(\dfrac{\alpha - \hat{\alpha}}{2}\right)^2 + 4\beta^2 \cos^2 \tfrac{1}{2} ka} . \end{cases} \qquad (2.16)$$

Consider an electron with spin down; thus $\alpha > \hat{\alpha}$. Also, consider the narrow band case, where $\beta \ll |\alpha - \hat{\alpha}|$. Then (2.16) may be written:

$$E_c(k) = a + \frac{4\beta^2 \cos^2 \frac{1}{2} ka}{a - \hat{a}}$$

$$E_v(k) = \hat{a} - \frac{4\beta^2 \cos^2 \frac{1}{2} ka}{a - \hat{a}} \qquad (2.17)$$

where $E_c(k)$ refers to the conduction band, $E_v(k)$ to the valence band. From (2.17), we can immediately write down the important band parameters:

$$\text{Energy Gap} \equiv E_g = a - \hat{a}$$

$$\text{Band Width} \equiv 4\beta^2/(a - \hat{a}) = 4\beta^2/E_g \qquad (2.18)$$

$$\text{Effective Mass: } m_e = m_h = m^* = 2\hbar^2/E_b a^2 .$$

In the one-dimensional case, the energy gap is exactly the difference in exchange energy between a spin up and a spin down electron.

Evaluating the wave functions corresponding to electrons in the valence and conduction bands, we obtain:

$$\psi_c = \begin{pmatrix} 1 - \dfrac{2\beta^2 \cos^2 \frac{1}{2} ka}{(a - \hat{a})^2} \\ \dfrac{2\beta \cos \frac{1}{2} ka}{a - \hat{a}} \end{pmatrix} \qquad \psi_v = \begin{pmatrix} \dfrac{2\beta \cos \frac{1}{2} ka}{a - \hat{a}} \\ 1 - \dfrac{2\beta^2 \cos^2 \frac{1}{2} ka}{(a - \hat{a})^2} \end{pmatrix} \qquad (2.19)$$

Equations (2.19) lead to:

$$\langle S_z \rangle_c = \frac{1}{2} - \frac{E_b}{E_g} \cos^2 \frac{1}{2} ka$$

$$\langle S_z \rangle_v = -\frac{1}{2} + \frac{E_b}{E_g} \cos^2 \frac{1}{2} ka \qquad (2.20)$$

Equations (2.20) can be used to give us some insight into antiferromagnetism. If the bandwidth is small compared to the band gap, then the average spin on each sublattice will be close to $\pm 1/2$, and neutron diffraction experiments should show an antiferromagnetic moment near one Bohr magneton per cation. However, as the bandwidth gets to be of the order of magnitude of the energy gap, much lower values for the sublattice magnetization can be obtained.

In connection with this, it is useful to investigate the exact solution, (2.16), rather than the narrow band approximation, (2.17). Although the energy gap remains exactly $E_g = \alpha - \hat{\alpha}$, independent of the bandwidth, the general solution for E_b is:

$$E_b = \frac{E_g}{2}\left[\left(1 + \frac{16\beta^2}{E_g^2}\right)^{1/2} - 1\right].$$

Hence, as β approaches E_g, the real bandwidth is smaller than the value given by (2.18). When $\beta = E_g/4$, $E_b = 0.21\,E_g$; when $\beta = E_g$, $E_b = 1.6\,E_g$.

The exact solution, (2.16), can be most simply discussed in terms of the parameter θ, defined by:

$$\tan\theta = \frac{4\beta\cos\frac{1}{2}ka}{\alpha - \hat{\alpha}}.$$

The exact solutions for ψ_c, ψ_v, $\langle S_z\rangle_c$, and $\langle S_z\rangle_v$ can be expressed:

$$\psi_c = \begin{pmatrix}\cos\frac{\theta}{2}\\ \sin\frac{\theta}{2}\end{pmatrix} \qquad \psi_v = \begin{pmatrix}\sin\frac{\theta}{2}\\ \cos\frac{\theta}{2}\end{pmatrix}$$

$$\langle S_z\rangle_c = \frac{1}{2}\cos\theta \qquad \langle S_z\rangle_v = -\frac{1}{2}\cos\theta$$

Thus, the average value of S_z at the bottom of the conduction band is always exactly 1/2. However, at the top of the conduction band:

$$< S_z > = \frac{1}{2} \left[1 + \frac{16\beta^2}{(a - \hat{a})^2} \right]^{-1/2} .$$

As the ratio of bandwidth to band gap increases, the average value of S_z at the top of the conducting band decreases monotonically. When $E_b = 0.21 E_g$, $< S_z > = 0.34$; when $E_b = 1.6 E_g$, $< S_z > = 0.09$. It is clear that the average values of S_z in the valence band are just the negatives of those in the conduction band in the one-dimensional case.

At $T = 0$, the valence band is exactly filled, the conduction band completely empty. Thus, the magnetization of the sublattice where the spins are down at $T = 0$ is given by the sum of $< S_z >_v$ over all points in k-space:

$$\mu = \sum_k \left[- \frac{1}{2} \cos \theta \right] \mu_B .$$

Clearly, as the bands get wider, the total magnetization on each sublattice decreases considerably. In the limit where the bands are much wider than the gap, the average sublattice magnetization goes to zero. In other words, the antiferromagnetism

BLANK PAGE

becomes undetectable when the exchange energy is much smaller than the overlap between nearest neighbors. We shall return to this point later.

Calculating from (2.20) the change in spin as an electron is excited across the energy gap:

$$\Delta S_z(k) = 1 - \frac{2E_b}{E_g} \cos^2 \frac{1}{2} ka$$

$$= 1 - \frac{E_b}{E_g} (1 + \cos ka) , \qquad (2.21)$$

Integrating (2.21) to find the net change in spin when n electrons have been excited across the gap:

$$\Delta S_z(n) = \frac{a}{\pi} \int_k^{\pi/a} dk \left[1 - \frac{E_b}{E_g} (1 + \cos ka) \right]$$

$$= \frac{n}{N} \left(1 - \frac{E_b}{E_g} \right) + \frac{E_b}{E_g} \frac{\sin \frac{n\pi}{N}}{\pi} \qquad (2.22)$$

since $n/N = 1 - ka/\pi$. Expanding (2.22) in powers of n:

$$\Delta S_z(n) = \frac{n}{N} + \frac{E_b}{E_g} \frac{\pi^2}{6} \left(\frac{n}{N}\right)^3 + \ldots \qquad (2.23)$$

The first term is the major contribution, not only because n/N is usually small, but also because we are considering the situation where $E_b \ll E_g$.

The assumption is now made, in view of the fact that the energy gap is a direct measure of the exchange energy [see (2.18)], that E_g can be expressed in the form:

$$E_g = \frac{1}{2N} n_\beta (n_\beta - 1) U \qquad (2.24)$$

where n_β is the number of down spins and U is an average exchange integral. What (2.24) says is that the exchange energy is porportional to the number of pairs of parallel spins; the assumption here is that each electron sees the spins of all the other electrons in the band, a hypothesis consistent with the spirit of band theory. We can evaluate U by noting that at T = 0:

$$U = 2N E_{go} / [N/2 (N/2 - 1)]$$

$$\approx 8 E_{go} / N.$$

Thus (2.24) becomes

$$E_g = \frac{4E_{go}}{N^2} (n_\beta^2 - n_\beta) . \qquad (2.25)$$

Since $\langle S_z \rangle = (n_\alpha - n_\beta)/2N$ and $N = n_\alpha + n_\beta$, where n_α is the number of up spins, (2.23) and (2.25) show:

$$\Delta E_g = -4E_{go} \left[\frac{n}{N} + \frac{E_b}{E_g} \frac{\pi^2}{6} \left(\frac{n}{N}\right)^3 + \dots \right] \left(1 + \frac{1}{N}\right) \qquad (2.26)$$

$$= -4E_{go} \left[\frac{n}{N} + \frac{E_b}{E_g} \frac{\pi^2}{6} \left(\frac{n}{N}\right)^3 + \dots \right]$$

since $N \sim O(10^{23}) \gg 1$. Equation (2.26) indicates that the energy gap will close down linearly with number of excited carriers for quite a large range of n. In the limit of narrow bands, all terms of higher order in n are negligibly small. Furthermore, even when the band width is of the order of the gap, the first correction term is an order of magnitude smaller than the linear term up to values of n/N = 0.3.

This result tends to justify the use of equation (2.1) in later chapters. From (2.26), the value of β for a one-dimensional antiferromagnet is:

$$\beta = 4 E_{go}/N . \tag{2.27}$$

2. Three-dimensional Model

Much of the calculation of the three-dimensional model is entirely analogous to that of the one-dimensional problem. We return to the use of n and N as concentrations of excited carriers and cations, respectively, and consider the case of a face-centered cubic lattice of magnetic ions with spins antiparallel in alternating (111)-planes. We shall assume that there is one 3d electron per cation outside the core and that this electron can be described by a non-degenerate Wannier function due to a slight distortion of the lattice. This is a good representation of the situation in VO. However, the calculation is virtually unchanged by taking another structure, such as corundum, or by choosing a larger number of 3d electrons per cation in a degenerate band. In the case described, energy gaps due to the exchange potential appear at the surfaces of the reduced part of the first Brillouin zone. Thus, if we take a cation of spin up at the origin and one of spin down at $\vec{\rho} = (110)\, a$, energy gaps appear at the planes $\vec{k} \cdot \vec{\rho} = \pm\pi/2$. In three dimensions, it does not necessarily follow that there is a real energy gap in the density of states, and these materials in principle could exhibit semimetallic rather than semiconducting behavior. It is clear that when overlap is small compared to the exchange energy,

the bands will be narrow and a real gap will occur. But this is not a necessary condition for the existence of a gap. Consider a non-magnetic crystal with no exchange potential, and assume that $E(\vec{k})$ has been calculated for the (double-sized) first Brillouin zone. When the exchange potential is turned on, this zone is split into two. If the original energy levels in the outer half of the large zone were higher than those in the inner half of the zone, then a gap exists even for a relatively small exchange energy. Such a situation could occur for the asymmetric 3d electrons in a low symmetry lattice, as well as in special highly symmetrical lattices, such as body centered cubic. We shall discuss this further in Appendix B, where attempts at energy band calculations will be summarized.

The L.C.A.O. calculation proceeds as in the one-dimensional case. As before, we take one 3d electron per cation. Let $\vec{R}_\alpha$ be the positions of the ions whose 3d electrons have spin up at T = 0, and let $\vec{R}_\beta$ be the positions where the 3d electrons have spin down. Then the Bloch wave functions are:

$$\psi_i(\vec{k}, \vec{r}) = \sqrt{\frac{2}{N}}\, c_{i\alpha} \sum_{\vec{R}_\alpha} e^{i\vec{k}\cdot\vec{R}_\alpha}\, \mu(\vec{r} - \vec{R}_\alpha)\,\alpha + \sqrt{\frac{2}{N}}\, c_{i\beta} \sum_{\vec{R}_\beta} e^{i\vec{k}\cdot\vec{R}}\, \mu(\vec{r} - \vec{R}_\beta)\beta \,. \qquad (2.28)$$

Then:

$$\sum_n \left[H_{mn}(\vec{k}) - E_i(\vec{k})\, \Delta_{mn}(k)\right] c_{ni}(\vec{k}) = 0 \qquad (2.29)$$

where:

$$H_{mn}(\vec{k}) \equiv \sum_{\vec{R}_m} \cos \vec{k} \cdot \vec{R}_m \int d\vec{r}\, \mu_n(\vec{r}) H_{mn}(\vec{r}) \mu_m(\vec{r} - \vec{R}_m)$$

$$\Delta_{mn}(\vec{k}) \equiv \sum_{\vec{R}_m} \cos \vec{k} \cdot \vec{R}_m \int d\vec{r}\, \mu_n(\vec{r}) \mu_m(\vec{r} - \vec{R}_m) \approx \delta_{mn}$$

taking an ion of type n at the origin. Let the origin be the site of a spin up ion, and let $\vec{r} = \vec{\rho}_i$ be the positions of the nearest-neighbor spin down ions. Then, in the nearest-neighbor approximation:

$$H_{11}(\vec{k}) = \alpha_o + \alpha_1 \sum_i \cos \vec{k} \cdot \vec{\rho}_i$$

$$H_{22}(\vec{k}) = \hat{\alpha}_o + \hat{\alpha}_1 \sum_i \cos \vec{k} \cdot \vec{\rho}_i$$

$$H_{12}(\vec{k}) = H_{21}(\vec{k}) = \beta_1 \sum_i \cos \vec{k} \cdot \vec{\rho}_i$$

where $\vec{\rho}_i'$ are the positions of the nearest-neighbor spin up ions, and

$$\alpha_o = \int d\vec{r}\, \mu(\vec{r}) H_{\alpha\alpha}(\vec{r}) \mu(\vec{r})$$

$$\hat{\alpha}_o = \int d\vec{r}\, \mu(\vec{r} - \vec{\rho}) H_{\beta\beta}(\vec{r}) \mu(\vec{r} - \vec{\rho})$$

$$\alpha_1 = \int d\vec{r}\, \mu(\vec{r}) H_{\alpha\alpha}(\vec{r}) \mu(\vec{r} - \vec{\rho}_i)$$

$$\hat{\alpha}_1 = \int d\vec{r}\, \mu(\vec{r} - \vec{\rho}) H_{\beta\beta}(\vec{r}) \mu(\vec{r} - \vec{\rho} - \vec{R})$$

$$\beta_1 = \int d\vec{r}\, \mu(\vec{r} - \vec{\rho}) H_{\beta\alpha}(\vec{r}) \mu(\vec{r} - \vec{\rho} - \vec{\rho}_i') .$$

We do not know where in $\vec{k}$-space the top of the valence band and the bottom of the conduction band are. From our previous discussion it is reasonable to assume that these points are both somewhere on the planes $\vec{k} \cdot \vec{\rho} = \pm\pi/2$. However, this is not necessarily the case. For simplicity, we shall assume the simplest situation: the conduction band minimum and the valence band maximum both

are at $\vec{k} = 0$. Since we are using this calculation primarily to evaluate the average change in spin as electrons are excited across the gap, and since only the zeroth order change will turn out to be significant in the evaluation of β, no error is introduced at this point. The calculation has been repeated using more physical assumptions about the band extrema [conduction band minimum at $\vec{k} = \frac{\pi}{4a}(110)$, valence band maximum at $\vec{k} = \frac{\pi}{4a}(111)$], and it was found that only the higher order terms are affected. Near $\vec{k} = 0$, in the (111) direction, the secular equation (2.29) can be written:

$$O = \begin{vmatrix} a_o + a_1(6 - \frac{8}{3}k^2a^2) - E & \beta_1(6 - \frac{4}{3}k^2a^2) \\ \beta_1(6 - \frac{4}{3}k^2a^2) & \hat{a}_o + \hat{a}_1(6 - \frac{8}{3}k^2a^2) - E \end{vmatrix} \qquad (2.30)$$

As before, we consider an electron with spin down and assume that the bands are narrow compared to the gap. Then the solution of (2.30) is:

$$E_c = a_o + 6a_1 + \frac{36\beta_1^2}{a_o - \hat{a}_o} + \left[-\frac{8}{3}a_1 - \frac{16\beta_1^2}{a_o - \hat{a}_o} \right] k^2a^2$$

$$E_v = \hat{a}_o + 6\hat{a}_1 - \frac{36\beta_1^2}{a_o - \hat{a}_o} - \left[\frac{8}{3}\hat{a}_1 - \frac{16\beta_1^2}{a_o - \hat{a}_o} \right] k^2a^2 . \qquad (2.31)$$

Equations (2.31) show that the assumptions about the band extrema are self-consistent only if a_1 is negative and $\hat{a}_1$ is positive. The band gap is then:

$$E_g = (a_o - \hat{a}_o) + 6(a_1 - \hat{a}_1) + 72\,\beta_1^2/(a_o - \hat{a}_o) .$$

The corresponding wave functions are:

$$\psi_c = \begin{pmatrix} 1 - \dfrac{18\beta_1^2}{(a_o - \hat{a}_o)^2}\left(1 - \dfrac{2}{9}k^2a^2\right) \\ -\dfrac{6\beta_1}{a_o - \hat{a}_o}\left(1 - \dfrac{2}{9}k^2a^2\right) \end{pmatrix} \qquad \psi_v = \begin{pmatrix} \dfrac{6\beta_1}{a_o - \hat{a}_o}\left(1 - \dfrac{2}{9}k^2a^2\right) \\ 1 - \dfrac{18\beta_1^2}{(a_o - \hat{a}_o)^2}\left(1 - \dfrac{2}{9}k^2a^2\right) \end{pmatrix} \tag{2.32}$$

Equations (2.32) lead to:

$$\langle S_z \rangle_c = \frac{1}{2} - \frac{36\beta_1^2}{a_o - \hat{a}_o}\left(1 - \frac{4}{9}k^2a^2\right)$$

$$\langle S_z \rangle_v = -\frac{1}{2} + \frac{36\beta_1^2}{a_o - \hat{a}_o}\left(1 - \frac{4}{9}k^2a^2\right). \tag{2.33}$$

Thus:

$$\Delta S_z(\vec{k}) = 1 - \frac{72\beta_1^2}{(a_o - \hat{a}_o)^2} + \frac{32\beta_1^2}{(a_o - \hat{a}_o)^2}k^2a^2$$

$$\Delta S_z(n) = \frac{1}{N}\int_0^{k(n)} \frac{d\vec{k}}{8\pi^3}\left[1 - \frac{72\beta_1^2}{(a_o - \hat{a}_o)^2} + \frac{32\beta_1^2}{(a_o - \hat{a}_o)^2}k^2a^2\right]$$

$$= \frac{1}{N}\left\{\left[1 - \frac{72\beta_1^2}{(a_o - \hat{a}_o)^2}\right]n + \frac{32(6\pi^2)^{5/3}a^2}{5}\frac{\beta_1^2}{(a_o - \hat{a}_o)^2}n^{5/3}\right\}. \tag{2.34}$$

Using the same assumption about the form of E_g as in the one-dimensional calculation:

$$E_g = \frac{4E_{go}}{N^2}\left(n_\beta^2 - \frac{n_\beta}{V}\right) \tag{2.35}$$

where V is the total volume of the crystal. From (2.34) and (2.35), we

obtain the result:

$$E_g = E_{go} + \Delta E_g$$

$$= E_{go} - \frac{4E_{go}}{N} \left\{ \left[1 - \frac{72\beta_1^2}{(a_o - \hat{a}_o)^2} \right] n + \frac{32(6\pi^2)^{5/3} a^2}{5} \frac{\beta_1^2}{(a_o - \hat{a}_o)^2} n^{5/3} \right\} \tag{2.36}$$

Equation (2.36) shows that β in (2.1) is a constant, independent of n, to within terms of the order of the square of the small quantity, $\beta_1/(a_o - \hat{a}_o)$. The large coefficients of these terms should not be disturbing, since in Appendix B we show that the bandwidth is greater than $12\beta_1$, while the band gap is considerably smaller than $(a_o - \hat{a}_o)$. Thus, the value of $72\beta_1^2/(a_o - \hat{a}_o)^2$ is a good deal less than half the square of the ratio of bandwidth to band gap, which we expect to be itself small in the materials under consideration. Therefore, equation (2.1) will remain valid over a relatively large range of n. The narrower the bands are, the larger the range of n for which (2.1) holds. From (2.36), the value of β is:

$$\beta = 4E_{go}/N . \tag{2.37}$$

Comparing (2.37) with the result of the one-dimensional calculation, (2.27), shows that the value of β is the same. Note that in the limit of narrow bands, $a_1 = \hat{a}_1 = \beta_1 = 0$, and (2.37) is exact within the validity of (2.35).

3. Virtual Crystal Approximation

We shall recalculate β using an entirely different model but maintaining the spirit of the Hartree-Fock approximation. We consider metallic ions with spins ordered antiferromagnetically at $T = 0$. Let an ion with spin down be called type A, a spin-up ion type B. Consider the sublattice where all spins are down when perfect order exists. In the vicinity of an A ion, an electron with spin up sees a potential V_A^+, whereas a spin-down electron sees V_A^-. Similarly, V_B^+ and V_B^- are the potentials in the vicinity of a B ion seen by a spin-up

BLANK PAGE

and a spin-down electron respectively. It is clear that $V_A^+ = V_B^-$ and $V_A^- = V_B^+$. For simplicity, we shall take the case of one 3d electron per cation. Since N is the total density of cations, the density on each sublattice is N/2.

The average potential seen by an electron with spin up on the sublattice under consideration is:

$$V_+' = \frac{2}{N}(n_A V_A^+ + n_B V_B^+)$$

$$= \frac{2}{N}(n_A V_A^+ + n_B V_A^-) \qquad (2.38)$$

where n_A is the number of A ions on the sublattice, n_B is the number of B ions. Similarly, for a spin-down electron:

$$V_-' = \frac{2}{N}(n_A V_A^- + n_B V_B^-)$$

$$= \frac{2}{N}(n_A V_A^+ + n_B V_A^+) . \qquad (2.39)$$

The average exchange energy is then just the difference between (2.38) and (2.39), or:

$$\langle V_{ex} \rangle = \frac{2}{N}(n_A - n_B)(V_A^+ - V_A^-) . \qquad (2.40)$$

For perfect order, $n_A = N/2$, $n_B = 0$, and:

$$\langle V_{ex} \rangle_{T=0} = V_A^+ - V_A^- .$$

For complete disorder, $n_A = n_B = N/4$, and:

$$\langle V_{ex} \rangle = 0 .$$

Since $n_A + n_B = N/2$, and the number of intrinsic carriers is just the number of ions with spin up on the sublattice, (2.40) can be written:

$$\langle V_{ex} \rangle = \langle V_{ex} \rangle_{T=0} (1 - 4n/N) . \qquad (2.41)$$

If we assume that the energy gap is proportional to the average exchange energy, as was found in (2.18), then (2.41) becomes:

$$E_g = E_{go}(1 - 4n/N). \qquad (2.42)$$

Thus $\beta = 4 E_{go}/N$, exactly the same as found in equations (2.27) and (2.37) for one 3d electron per cation. It is clear that if there are z 3d electrons per cation filling the valence band, the result for β in the above approximations would be:

$$\beta = 4 E_{go}/zN .$$

D. Crystalline Structure Distortion

The existence of antiferromagnetism is not a necessary condition for the applicability of (2.1). The relation can also be shown to be appropriate when an energy gap is caused by a crystal structure distortion to lower symmetry. This type of gap can arise from an energy gain due to chemical binding – the lower band may be thought of as a bonding band, the upper an antibonding band. Excitation of an electron across the energy gap decreases the gap because the excited electron no longer contributes to the chemical binding. Thus the situation is analogous to the case of an antiferromagnetic crystal dealt with in section C. However, the evaluation of β is more difficult when the gap is caused by crystalline distortion. In this section, we shall calculate expressions for β, using simple one-dimensional models, but employing as much as possible the physical properties of the vanadium oxides to which we expect the theory to apply.

1. Delta-function Interaction

Consider a one-dimensional crystal with two cations per unit cell at low temperature. Once again, we shall examine the case of one 3d electron per cation in a non-degenerate band; the case of larger concentrations of 3d electrons in degenerate bands is entirely analogous.

In accordance with these assumptions, we place ions at positions:

$$x_{j_1} = \left(j + \frac{1 - 2\epsilon a_j}{4} \right) a$$

$$x_{j_2} = \left(j - \frac{1 - 2\epsilon a_j}{4} \right) a$$

Here ϵ is a parameter which ranges from 0 to 1/2, and reflects the zero temperature deviation from the monionic situation; the a_j are parameters which take on values from 1 to 0 and indicate how the cations change positions with increasing temperature. In the case under consideration, $a_j = 1$ for all j at T = 0, and $a_j = 0$ for all j at high temperature. The crystal is semiconducting due to the extra band gap brought about by the distortion from one cation per unit cell. Each of the assumed conditions is true for V_2O_3, which undergoes a structure change from monoclinic to trigonal at the temperature of the semiconductor-to-metal transition.

To begin with, the simplest interaction we can write down is a delta-function potential:

$$V(x) = V_o \sum_j \left\{ \delta\left[x - \left(j + \frac{1 - 2\epsilon a_j}{4} \right) a \right] + \delta\left[x - \left(j - \frac{1 - 2\epsilon a_j}{4} \right) a \right] \right\} .$$

This is essentially the situation in which the Coulomb interaction is

very strongly screened, which is not too far from the case where an extremely high density of free electrons exists. When the a_j are independent of j, V(x) is periodic and we can solve Schrödinger's equation exactly; when the a_j depend on j, Bloch states are no longer eigenstates, and the problem cannot be solved exactly. Consequently, let us assume $a_j = a$ for all j. Then Schrödinger's equation may be written:

$$-\frac{\hbar^2}{2m}\psi'' + V_o \sum_j \left[\delta(x - ja) + \delta(x - ja - b)\right]\psi = E\psi \qquad (2.43)$$

where $b \equiv (1 - 2\epsilon a)a/2$.

Thus:

$$\begin{aligned} \psi(x) &= A \sin \gamma x + B \cos \gamma x \qquad (0 \leq x < b) \\ \psi(x) &= A' \sin \gamma x + B' \cos \gamma x \qquad (b \leq x < a) \end{aligned} \qquad (2.44)$$

where $\gamma^2 \equiv 2mE/\hbar^2$. Bloch's theorem gives:

$$\psi(x) = e^{ikx}\mu(kx) \qquad (2.45)$$

where:

$$\mu(kx) = \mu\left[k(x + na)\right] .$$

Then:

$$\begin{aligned} \psi(a) &= e^{ika}\mu(0) \\ \psi(b) &= e^{ikb}\mu(kb) . \end{aligned} \qquad (2.46)$$

But from (2.44) and (2.46):

$$\psi(0) = \mu(0) = B$$

$$\psi(b) = A \sin\gamma b + B \cos\gamma b = A' \sin\gamma b + B' \cos\gamma b \qquad (2.47)$$

$$= e^{ikb}\,\mu(kb)$$

$$\psi(a) = A' \sin\gamma a + B' \cos\gamma a = B\, e^{ika}\,.$$

Integrating (2.43) from 0^- to 0^+:

$$\psi'(0^+) - \psi'(0^-) = 2\lambda\,\psi(0) = 2\lambda B \qquad (2.48)$$

where $\lambda = m V_o/\hbar^2$. Similarly, integrating (2.43) from b^- to b^+:

$$\psi'(b^+) - \psi'(b^-) = 2\lambda\psi(b) = 2\lambda\left[A \sin\gamma b + B \cos\gamma b\right]. \qquad (2.49)$$

From (2.44), we see:

$$\psi'(x) = A\gamma \cos\gamma x - B\gamma \sin\gamma x \qquad (0 \leq x < b)$$
$$\qquad (2.50)$$
$$\psi'(x) = A'\gamma \cos\gamma x - B'\gamma \sin\gamma x \qquad (b \leq x < a)$$

while from (2.45):

$$\psi'(x) = e^{-ika}\,\psi'(x + a)\,. \qquad (2.51)$$

Combining (2.48), (2.49), (2.50), and (2.51):

$$\gamma A - e^{-ika}\left[A'\gamma \cos\gamma a - B'\gamma \sin\gamma a\right] = 2\lambda B$$

$$A'\gamma \cos\gamma b - B'\gamma \sin\gamma b - A\gamma \cos\gamma b + B\gamma \sin\gamma b \qquad (2.52)$$

$$= 2\lambda\left[A \sin\gamma b + B \cos\gamma b\right].$$

The secular equation is obtained from (2.47) and (2.52):

$$0 = \begin{vmatrix} \sin\gamma b & \cos\gamma b & \sin\gamma b & -\cos\gamma b \\ 0 & e^{ika} & \sin\gamma a & -\cos\gamma a \\ \gamma\, e^{ika} & -2\lambda\, e^{ika} & \gamma\cos\gamma a & \gamma\sin\gamma a \\ 2\lambda\sin\gamma b + \gamma\cos\gamma b & 2\lambda\cos\gamma b - \gamma\sin\gamma b & \gamma\cos\gamma b & \gamma\sin\gamma b \end{vmatrix}$$

$$= 4\lambda^2 e^{ika}\sin\gamma b\sin\gamma(a-b) + 4\gamma\lambda e^{ika}\cos\gamma a + 2\gamma^2 e^{ika}\cos\gamma a - \gamma^2(1+e^{2ika}). \qquad (2.53)$$

Solving (2.53) for cos ka:

$$\cos ka = \cos\gamma a + \frac{2\lambda}{\gamma}\sin\gamma a + \frac{2\lambda^2}{\gamma^2}\sin\gamma b \sin\gamma(a-b). \qquad (2.54)$$

For greater clarity, let $K = ka$, $y = \gamma a$, $z = \lambda a$; recall $a\epsilon = (a - 2b)/2a$. Then (2.54) becomes:

$$\cos K = \cos y + 2z\frac{\sin y}{y} + 2z^2 \frac{\sin y\left(\frac{1}{2} - \epsilon a\right)}{y} \frac{\sin y\left(\frac{1}{2} + \epsilon a\right)}{y} \qquad (2.55)$$

Equation (2.55) gives the energy band structure of the crystal. We still have two parameters at our discretion, the strength of the interaction, z, and the amount of distortion, ϵ. Since we wish to apply the theory to narrow band materials, we must choose z relatively large. A good choice for ϵ is $\epsilon \sim 0.01$, the distortion present in V_2O_3. The energy band structure at $T = 0$ ($a = 1$) is plotted in Fig. II-1, for $z = -60$, $\epsilon = 0.009$. As can be seen, the bands are narrow. In this case, the relevant energy gap is narrow also, as we might expect in V_2O_3. As a decreases, the gap shrinks. In Fig. II-2, the band structure is plotted for $a = 2/3$; Fig. II-3 shows E(k) for $a = 1/3$. Clearly, the gap must vanish as a goes to zero.

It is important to demonstrate that a decreases with increasing carrier concentration. In the distorted state, the wave functions of electrons in the valence (bonding) band have larger amplitudes in the region where the cations are closely spaced, whereas those of electrons in the conduction (antibonding) band have larger amplitudes in the region of wide spacing. Thus, excitation of an electron across the gap removes charge density from the closely spaced region.

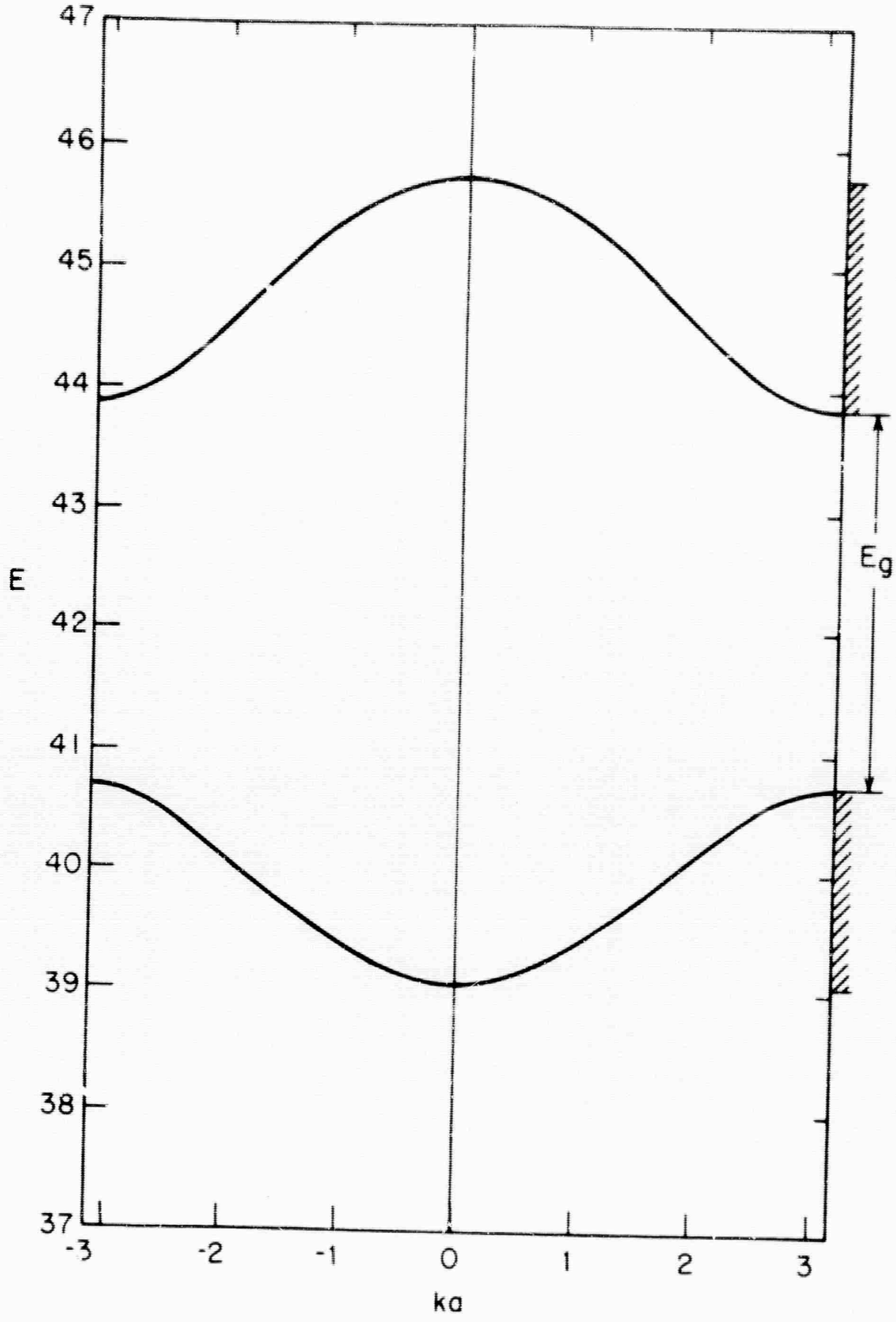

FIG. II-1 ENERGY AS A FUNCTION OF k.
$z = -60$; $\epsilon = .009$; $\alpha = 1$.

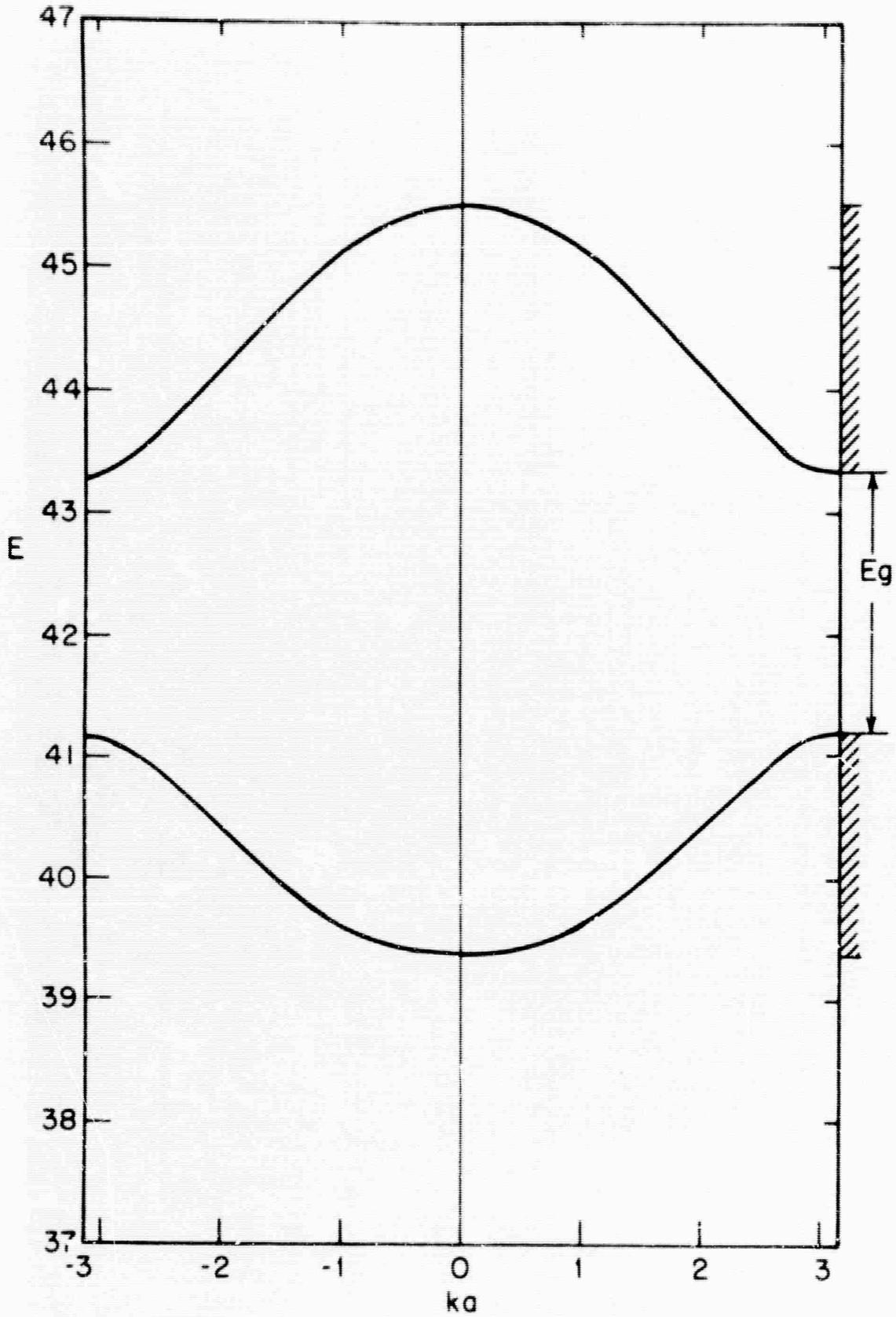

FIG. II-2 ENERGY AS A FUNCTION OF k.
$z = -60$; $\epsilon = .009$; $\alpha = 2/3$

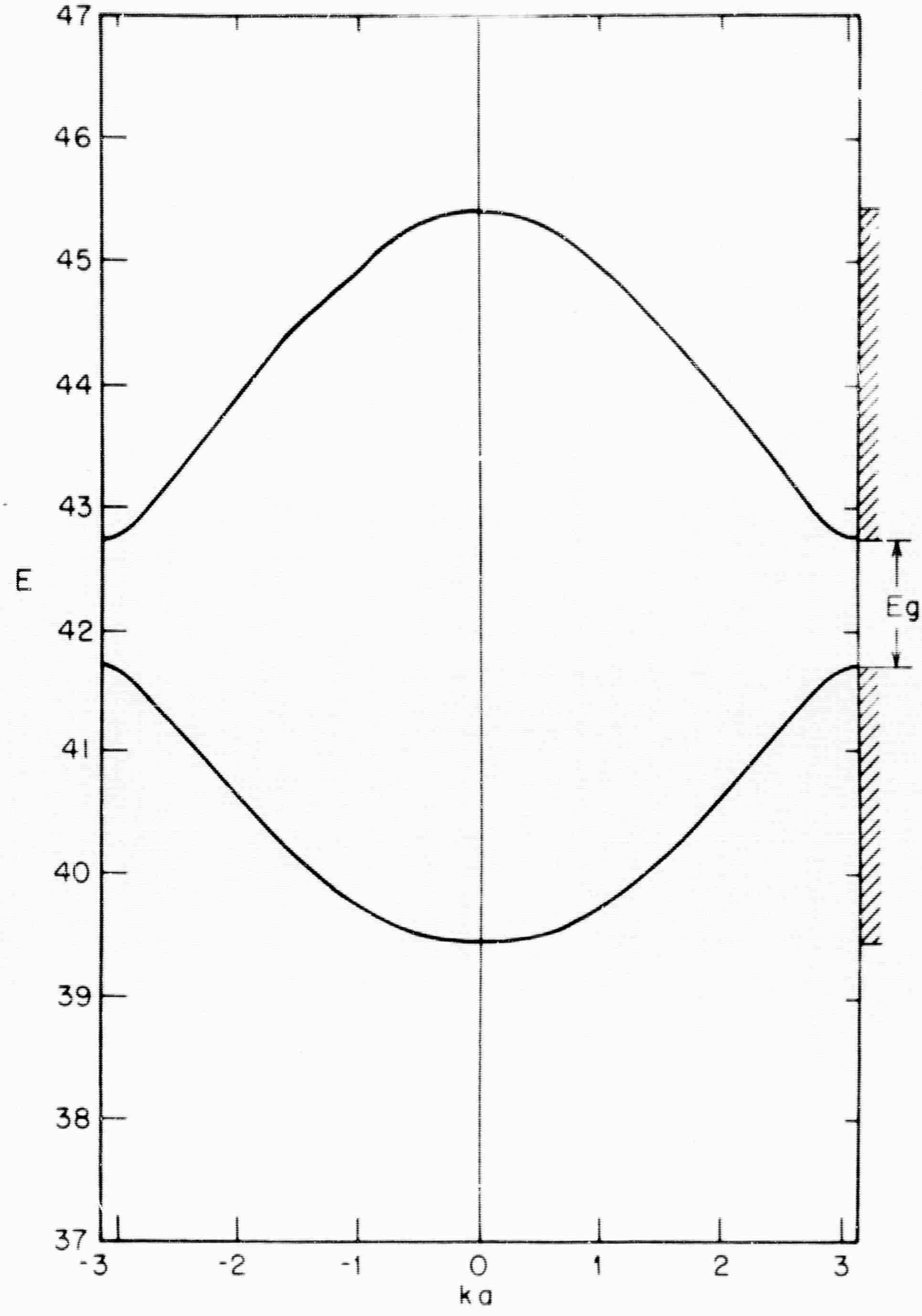

FIG. II-3 ENERGY AS A FUNCTION OF k.

$z = -60$; $\epsilon = .009$; $\alpha = 1/3$.

Consider a hydrogen molecule. With both electrons in bonding orbitals, the equilibrium distance between the hydrogen ions is 0.74 Å; when one electron is removed, we are left with the hydrogen molecular ion, H_2^+, for which the equilibrium distance is 1.06 Å. The ions thus move apart as an electron is removed from a bonding orbital. Of course, the hydrogen molecule is made up of ions and electrons which interact by means of a Coulomb potential, rather than the delta-function potential with which we are dealing. Conceivably this could make an important difference. Consequently, the hydrogen molecule analogy is analyzed in Appendix C using delta-function interactions. It is found that the equilibrium distance of "H_2" is 0.76 of that for "H_2^+", which is roughly the same as the 0.70 ratio for the real molecules. We conclude that a decreases with increasing concentration of free carriers. It is clear that a vanishes after N/2 carriers are excited, since the charge density between all the cations is the same, and thus the cations must be equally spaced. Thus a decreases from 1 to 0 as n increases from 0 to N/2. We shall assume the simplest possible behavior for a, the linear relationship:

$$a = 1 - 2n/N . \tag{2.56}$$

The result of an involved calculation, to first order in n/N, is:

$$E_g = 3.3\ (1 - 3.1\ n/N).$$

The value of β is thus:

$$\beta = 3.1\ E_{go}/N . \tag{2.57}$$

It is worthwhile also to calculate β when the bands are narrow

compared to the energy gap. For this purpose, we investigated the case where $z = -6$, $\epsilon = 0.15$. The band structure is shown in Figs. II-4 through II-7 for $\alpha = 1$, $2/3$, $1/3$, and 0. It can be seen how the energy gap shrinks to zero with decreasing α, while the valence and conduction bands become wider and move toward each other. The result for the variation of E_g is:

$$E_g = 15.2\,(1 - 3.7\,n/N)\,.$$

Hence:

$$\beta = 3.7\,E_{go}/N. \qquad (2.58)$$

In general, β was found to be insensitive to changes in the bandwidth for a constant band gap; however, β was sensitive to changes in the gap, varying from $1.6\,E_{go}/N$ for narrow gaps to $4.9\,E_{go}/N$ for the widest gaps investigated.

Figures II-4 through II-7 can give us some insight into the nature of the distortion. Figure II-7 shows the band structure for the undistorted situation, where there is no gap, but rather a half-filled band. The distortion can be looked at as the band generalization of the Jahn-Teller effect. When the bands are wide, a Jahn-Teller distortion would just introduce a small gap at the ends of the reduced first Brillouin zone, resulting in only a small gain in electronic energy. This gain would quickly be overcome by the loss in strain energy, and the distortion most likely would be sufficiently small so that a real gap in three dimensions would not occur. However, in the narrow band case, the distortion has an effect on all points in k-space, lowering the energy of the entire valence

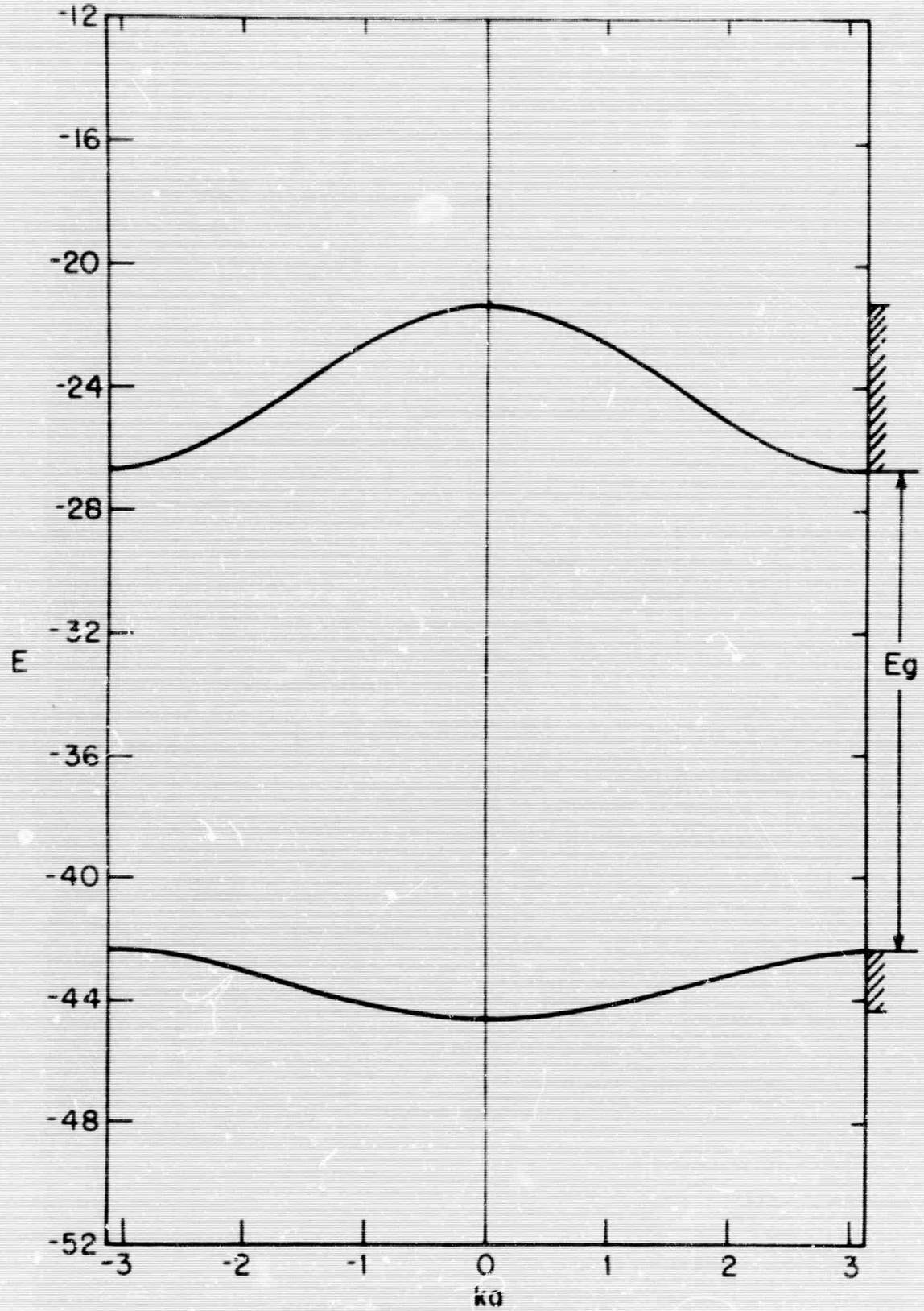

FIG II-4 ENERGY AS A FUNCTION OF k.
$z = -6$; $\epsilon = 0.15$; $\alpha = 1$.

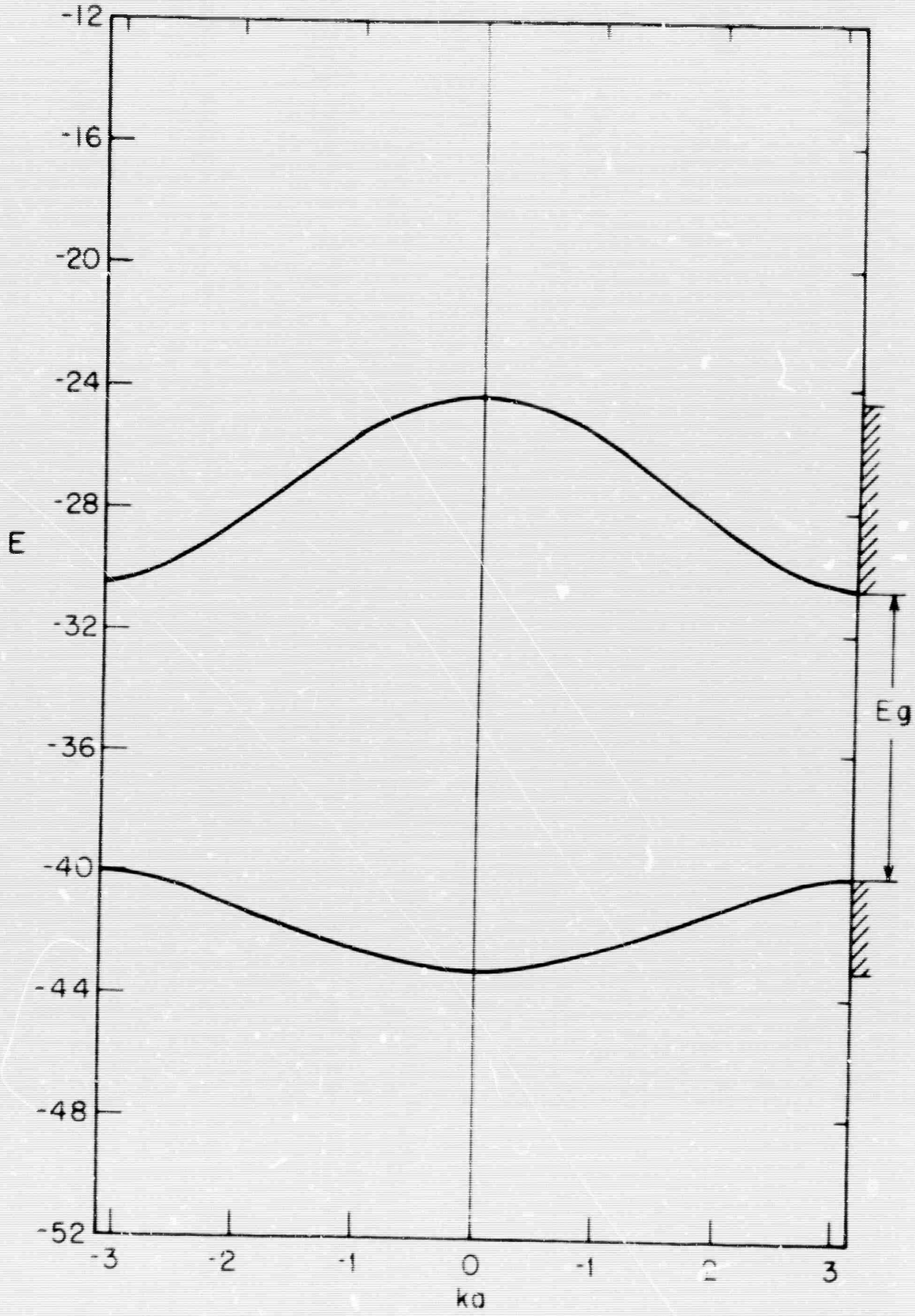

FIG. II-5 ENERGY AS A FUNCTION OF k.
$z = -6$; $\epsilon = 0.15$; $\alpha = 2/3$.

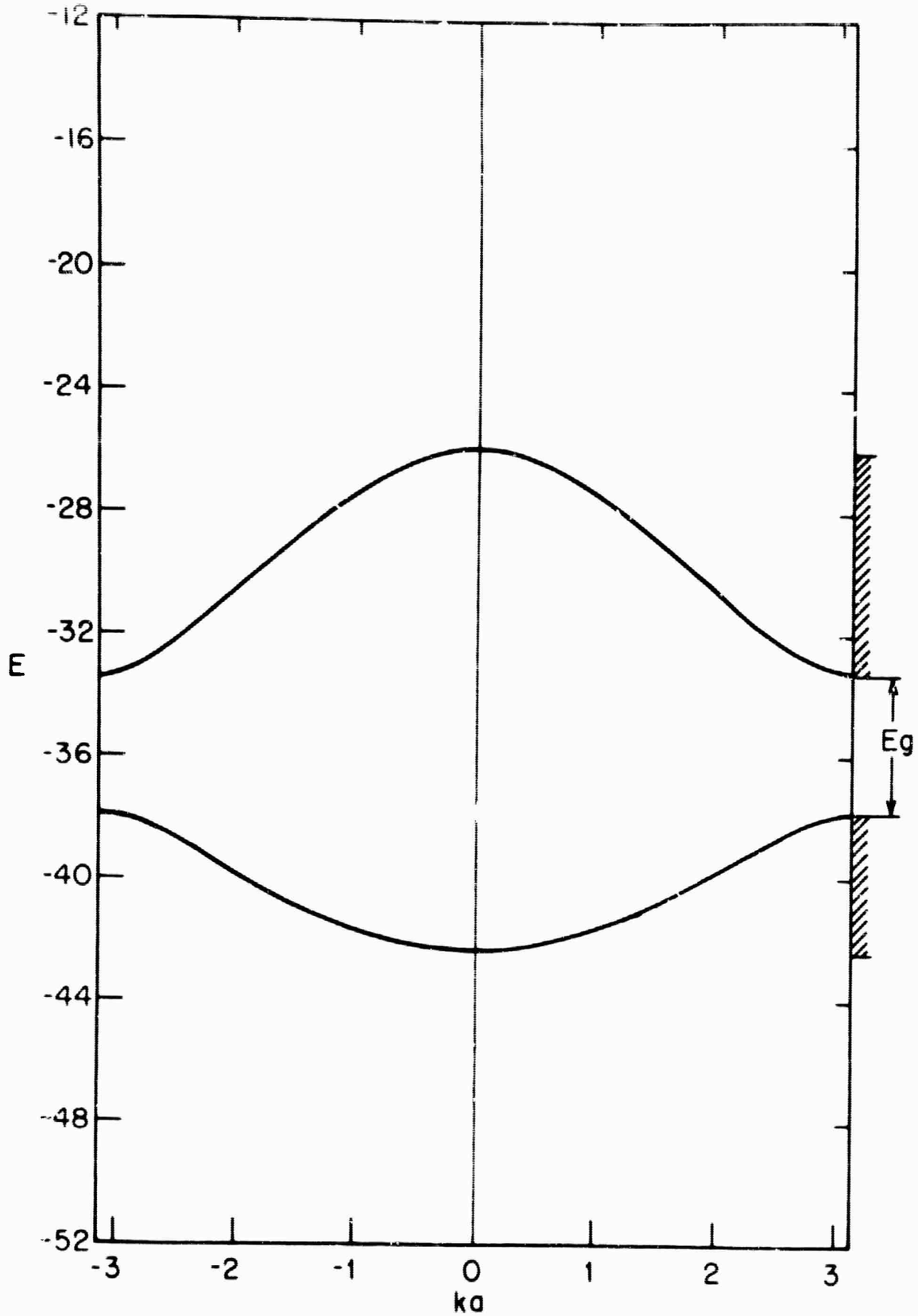

FIG. II-6 ENERGY AS A FUNCTION OF k.
$z = -6$; $\epsilon = 0.15$; $\alpha = 1/3$.

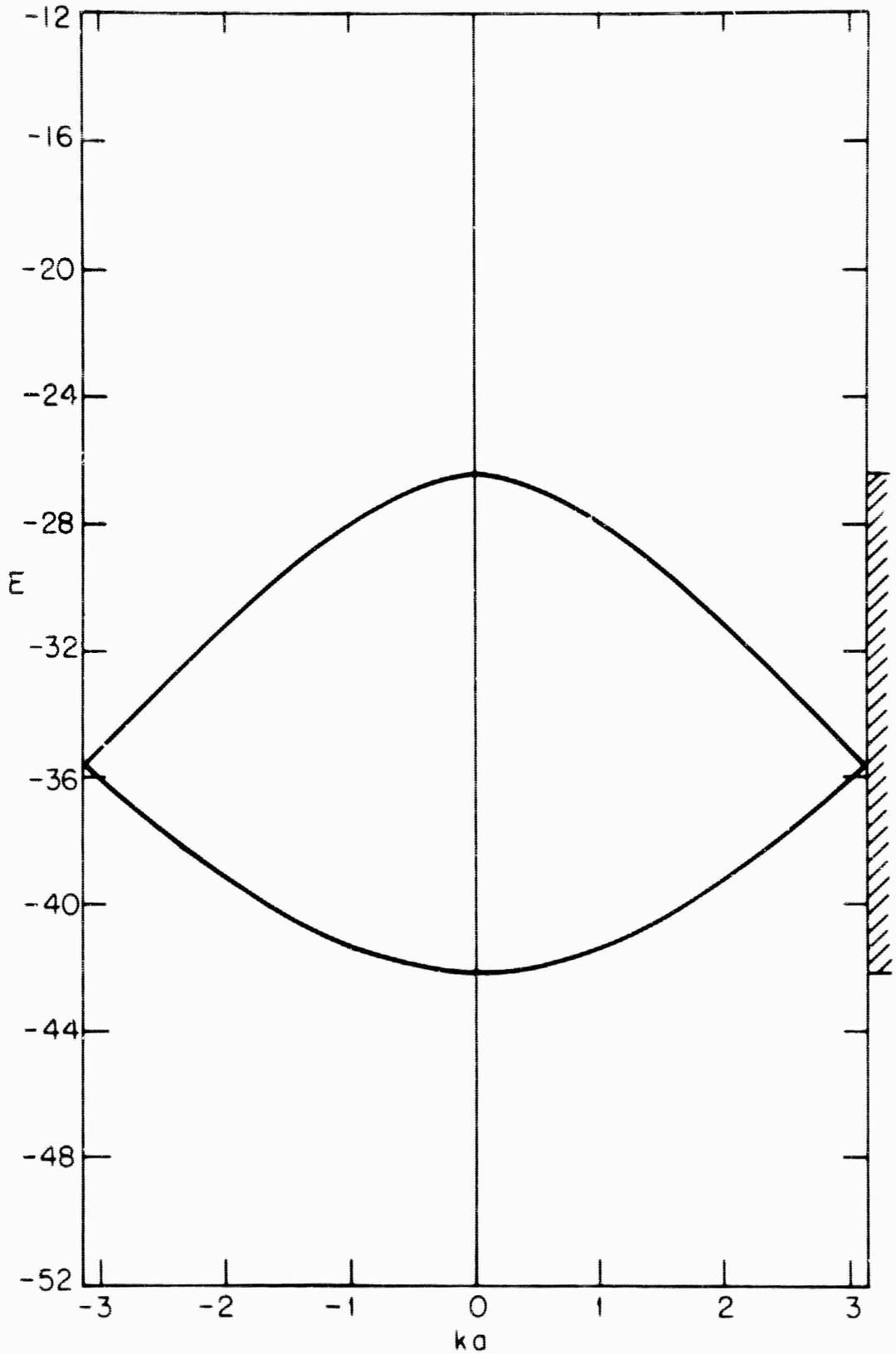

FIG. II-7 ENERGY AS A FUNCTION OF k

$z = -6$, $\epsilon = 0.15$, $\alpha = 0$.

BLANK PAGE

$$z \equiv \frac{\pi x}{a}$$

$$s \equiv \frac{8\pi a^2 V_o}{\pi^2 \hbar^2} \cos \frac{2\pi}{a} x_o \equiv s_o \cos \frac{2\pi}{a} x_o$$

$$\mathcal{E} \equiv \frac{2m a^2}{\pi^2 \hbar^2} E .$$

Then (2.61) can be written:

$$\psi''(z) + \left[\mathcal{E} + \frac{1}{2} s \cos 2z\right] \psi(z) = 0 . \qquad (2.62)$$

Equation (2.62) is just a form of Mathieu's equation, the eigenvalues of which have been tabulated [34]. Take $s_o = 100$, and for simplicity assume that sufficient electrons are present to fill the lowest two bands, leaving all higher bands completely empty. Set $\epsilon = 0.01$, the correct value for V_2O_3. A long calculation shows:

$$E_g = 0.30\left[1 - \frac{3.5n}{N}\right] .$$

Hence:

$$\beta = 3.5\, E_{go}/N . \qquad (2.63)$$

For a Mathieu interaction, the value of β depends somewhat on the number of electrons present and strongly on the amount of distortion ϵ. It was found that β increases for decreasing ϵ. In many ways, the Mathieu interaction is inferior to the delta-function interaction for our purposes. The Mathieu potential is a very weak attraction, and at high temperature actually vanishes, leaving the free electron Schrödinger's equation. This results in a band structure where the bands are wide and the gap is narrow, just the opposite of the physical situation to which we want to apply these results. At

low temperatures, this could be remedied by using extremely large values for s_o; however, no tables of Mathieu functions exist for $s > 100$, so such calculations are not practical at present.

Chapter III

CALCULATION OF CONDUCTIVITY AS A FUNCTION OF TEMPERATURE

The electrical conductivity of a semiconductor can be expressed:

$$\sigma = n e \mu \tag{3.1}$$

where n is the concentration of excited carriers, e is the electronic charge, and μ is the mobility of the carriers. In this chapter, we shall assume that Eq. (2.1) is applicable, and calculate n as a function of temperature. We shall evaluate n(T) in two opposing limits, the effective mass approximation and the limit of narrow bands.

Let us take the bottom of the conduction band as the zero point of energy. The probability that a state with energy E will be occupied by an electron is given by the Fermi function:

$$f_e(E) = \frac{1}{e^{\frac{E-E_F}{kT}} + 1} . \tag{3.2}$$

Clearly, the probability that a state is occupied by a hole is:

$$f_h(E) = 1 - f_e(E)$$

$$= \frac{1}{e^{\frac{E_F-E}{kT}} + 1} . \tag{3.3}$$

Let $\rho_c(E)$ be the number of states per unit volume between energies E and E + dE. Then, using (3.2), the concentration of electrons in the conduction band, n, is given by:

$$n = \int_0^\infty dE\, \rho_c(E)\, \frac{1}{e^{\frac{E-E_F}{kT}} + 1} \quad . \tag{3.4}$$

Similarly, defining $\rho_v(E)$ as the density of states in the valence band, and using (3.3):

$$p = \int_{-\infty}^{-E_g} dE\, \rho_v(E)\, \frac{1}{e^{\frac{E_F-E}{kT}} + 1} \tag{3.5}$$

where p is the concentration of holes in the valence band. For an intrinsic semiconductor, the condition of neutrality requires n = p. This condition determines the Fermi energy, E_F.

A. Effective Mass Approximation

We first consider the situation where the valence and conduction band structure can be well-represented by ellipsoidal constant-energy surfaces. We can then define density-of-states effective masses, m_e for electrons, m_h for holes:

$$m^* = M(m_1\, m_2\, m_3)^{1/3}$$

where m_1, m_2, m_3 are the principal values of the effective mass tensor, and M is the number of equivalent extrema. The densities of states are now given by:

$$\rho_c(E) = \frac{1}{2\pi^2} \left(\frac{2m_e}{\hbar^2}\right)^{3/2} E^{1/2} \tag{3.6}$$

$$\rho_v(E) = \frac{1}{2\pi^2} \left(\frac{2m_h}{\hbar^2}\right)^{3/2} (-E_g - E)^{1/2} \tag{3.7}$$

Equations (3.6) and (3.7) are always true near the band extrema. However, for large values of m_e and m_h, they probably do not remain valid for a very large range of energy. The effective mass approximation assumes that these relations remain applicable for all values of E which have finite probability of occupation at the temperature under consideration. Thus, the effective mass approximation is a good one whenever $|E_F| \gg kT$, and m is not too large. In view of (3.6) and (3.7), (3.4) and (3.5) yield:

$$n = \frac{1}{2\pi^2}\left(\frac{2m_e}{\hbar^2}\right)^{3/2} \int_0^\infty dE \, \frac{E^{1/2}}{e^{\frac{E-E_F}{kT}} + 1} \tag{3.8}$$

$$p = \frac{1}{2\pi^2}\left(\frac{2m_h}{\hbar^2}\right)^{3/2} \int_{-\infty}^{-E_g} dE \, \frac{(-E_g-E)^{1/2}}{e^{\frac{E_F-E}{kT}} + 1} \, . \tag{3.9}$$

We first consider the case where $|E - E_F| \gg kT$, and Boltzmann statistics apply. Then, the exponentials in the denominators are much greater than unity, and (3.8) and (3.9) become:

$$n = \frac{1}{2\pi^2}\left(\frac{2m_e kT}{\hbar^2}\right)^{3/2} e^{\frac{E_F}{kT}} \int_0^\infty dx \, x^{1/2} e^{-x}$$

$$= \frac{1}{4}\left(\frac{2m_e kT}{\pi\hbar^2}\right)^{3/2} e^{\frac{E_F}{kT}} \tag{3.10}$$

$$p = \frac{1}{4}\left(\frac{2m_h kT}{\pi\hbar^2}\right)^{3/2} e^{-\frac{E_F+E_g}{kT}} \, . \tag{3.11}$$

The condition of neutrality gives:

$$m_e^{3/2} \, e^{\frac{E_F}{kT}} = m_h^{3/2} \, e^{-\frac{E_F}{kT}} e^{-\frac{E_g}{kT}}$$

or:

$$E_F = -\frac{E_g}{2} + \frac{3kT}{4} \ln \frac{m_h}{m_e} . \tag{3.12}$$

Defining m^* as the geometric mean of m_e and m_h, (3.10) yields:

$$n = \frac{1}{4} \left(\frac{2m^* kT}{\pi \hbar^2}\right)^{3/2} e^{-\frac{E_g}{2kT}} . \tag{3.13}$$

Letting $A \equiv (2m^* kT/\pi\hbar^2)^{3/2}/4$, (3.13) becomes:

$$n = A \, T^{3/2} \, e^{-\frac{E_g}{2kT}} . \tag{3.14}$$

Substituting (2.1) into (3.14):

$$n = A \, T^{3/2} \, e^{-\frac{E_{go}}{2kT}} e^{\frac{\beta}{2kT} n} . \tag{3.15}$$

Equation (3.15) can be solved explicitly. Let:

$$\tau \equiv \exp\left[\frac{BAT^{1/2}}{2k} \, e^{-\frac{E_{go}}{2kT}}\right] \tag{3.16}$$

$$\eta \equiv \left[\frac{1}{AT^{3/2}} \, e^{\frac{E_{go}}{2kT}}\right] n . \tag{3.17}$$

Substituting (3.16) and (3.17) into (3.15), we are left with the simple equation:

$$\eta = \tau^{\eta} . \tag{3.18}$$

The solution of (3.18) can be written:

$$\eta = \tau^{\tau^{\tau^{\cdot^{\cdot^{\cdot}}}}} \equiv \eta(\tau) \,. \tag{3.19}$$

Equation (3.19) gives n as a function of temperature. The function $\eta(\tau)$, which can be called the infinitely repeating exponential, is a function which will recur often during this analysis. It is not discussed anywhere in applied mathematics literature, and has some unusual properties which are worth detailing at this time. Its behavior is shown in Fig. III-1. η slowly rises from 0 to e as τ increases from 0 to $e^{1/e} = 1.445$. However, at the point $\tau = e^{1/e}$ an essential singularity exists and η increases without limit. Not only does η blow up at this point, but all its derivatives are infinite also. Such a singularity in n(T) completely eliminates the band gap, and brings about a first-order semiconductor-to-metal transition. We can determine the transition temperature easily. At the point of singularity, $\tau_o = e^{1/e}$, and equation (3.16) yields:

$$\frac{\beta A}{2k} T_o^{1/2} = e^{\frac{E_{go}}{2kT_o} - 1} \,. \tag{3.20}$$

Let:

$$Q \equiv \left(\frac{2k}{e\beta A}\right) \frac{1}{T_o}$$

$$R \equiv e^{-\frac{E_{go}}{k}\left(\frac{e\beta A}{2k}\right)^2}$$

Then (3.20) becomes:

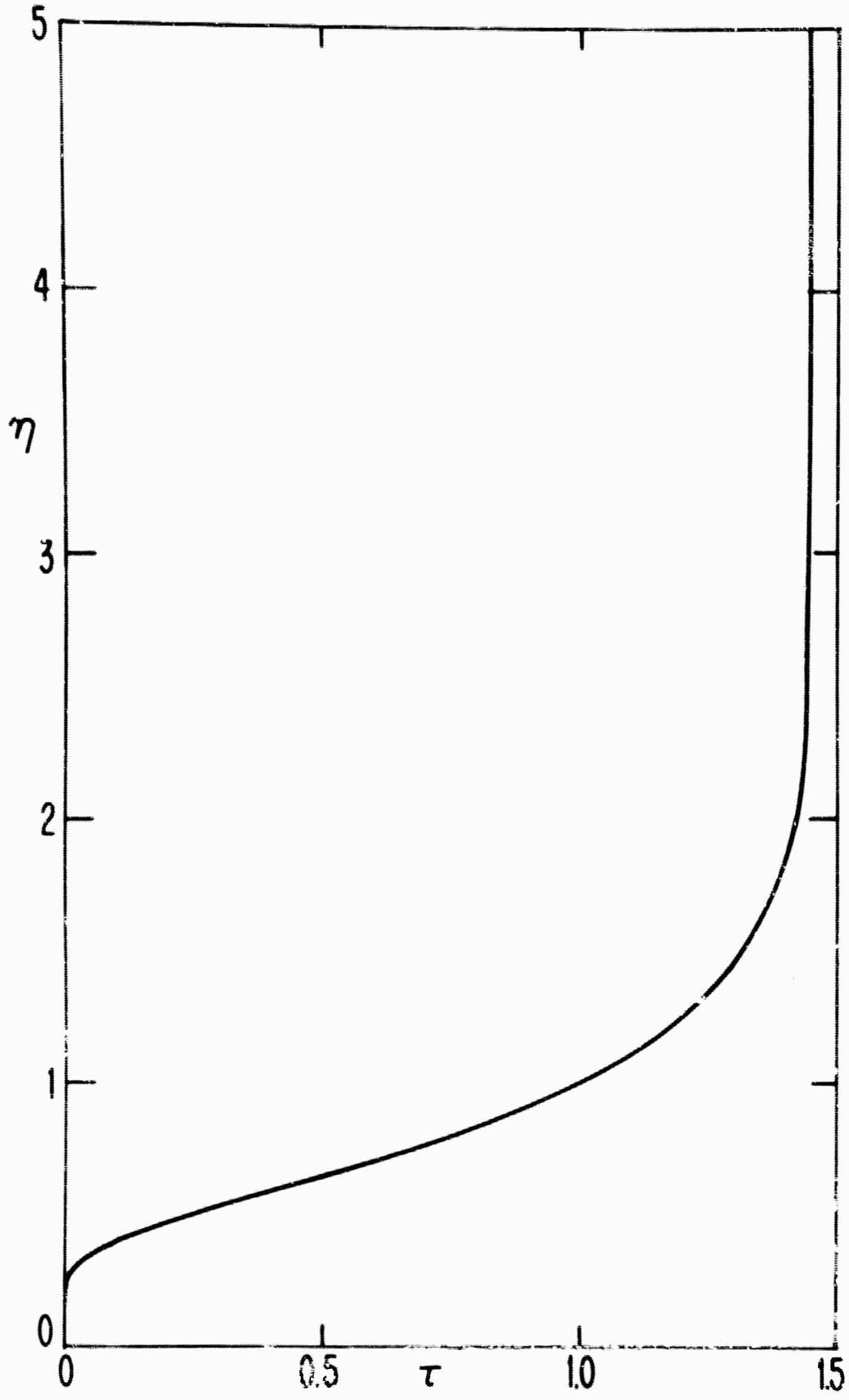

FIG. III-1 THE FUNCTION $\eta(\tau)$

$$Q = R^{Q} = R^{R^{R^{\cdot^{\cdot^{\cdot}}}}} = \eta(R) . \tag{3.21}$$

Equation (3.21) gives the transition temperature, T_o, in terms of the band parameters, E_{go}, β, m^* A transition always occurs in this case, since $R < 1$, and thus (3.21) always has a solution. Using Boltzmann statistics, the number of carriers grows without limit at the transition temperature. We shall be interested in the ratio E_{go}/kT_o, which can be expressed:

$$\frac{E_{go}}{kT_o} = Q \ln\left(\frac{1}{R}\right) = \eta(R) \ln\left(\frac{1}{R}\right) . \tag{3.22}$$

In Chapter II [see equations (2.27), (2.37), and (2.42)], we found that for an energy gap arising from antiferromagnetism:

$$\beta = 4 E_{go}/N . \tag{3.23}$$

In equations (2.57), (2.58), and (2.63), we saw that (3.23) is also a good approximation when the gap is due to a crystalline structure distortion. Let us write:

$$\beta = 4(1 + \delta) E_{go}/N \tag{3.24}$$

where δ vanishes in the case of antiferromagnetism, and is small, probably between -1/4 and 1/4, in the case of crystalline distortion. Then the parameter $\ln(1/R)$, which determines E_{go}/kT , becomes:

$$\ln\left(\frac{1}{R}\right) = 2(1 + \delta)^2 \left[\frac{e}{N}\left(\frac{m^* E_{go}}{\pi\hbar^2}\right)^{3/2}\right]^2 . \tag{3.25}$$

The quantity in brackets in (3.25) is essentially a measure of the

ratio of the band gap to the band width. [In fact, using (2.18), from the one-dimensional theory of antiferromagnetism: $\ln(\frac{1}{R}) = \frac{e^2}{4\pi^3}(1+\delta)^2(\frac{E_{go}}{E_b})^3$.] E_{go}/kT_o is plotted as a function of $\ln(1/R)$ in Fig. III-2. For narrow bands, $\ln(1/R)$ is large, and E_{go}/kT_o is a slowly-varying function of R. Boltzmann statistics are valid for roughly $E_{go}/kT_o > 2$.

The important point is that a semiconductor-to-metal transition can occur in a simple way in a band theory. The resulting behavior of $\ln \sigma$ as a function of $1/T$ is shown in Fig. III-3 for reasonable values of E_{go} and m^*.

Just before the transition, $\eta = e$. Thus, from (3.17), at this point:

$$n(T_o) = e\, A\, T_o^{3/2}\, e^{-\frac{E_{go}}{2kT_o}} . \tag{3.26}$$

But it can be seen from (3.15) that (3.26) implies:

$$n(T_o) = 2kT_o/\beta . \tag{3.27}$$

Substituting (3.24) into (3.27):

$$\frac{n(T_o)}{N} = \frac{1}{2(1+\delta)}\left(\frac{E_{go}}{kT_o}\right)^{-1} . \tag{3.28}$$

From Fig. III-2, we see that for the narrow band situation with which we are most concerned, $E_{go}/kT_o > 5$. Equation (3.28) then shows that the maximum value of n/N before the transition is:

$$\left(\frac{n}{N}\right)_{max} < 0.1 \tag{3.29}$$

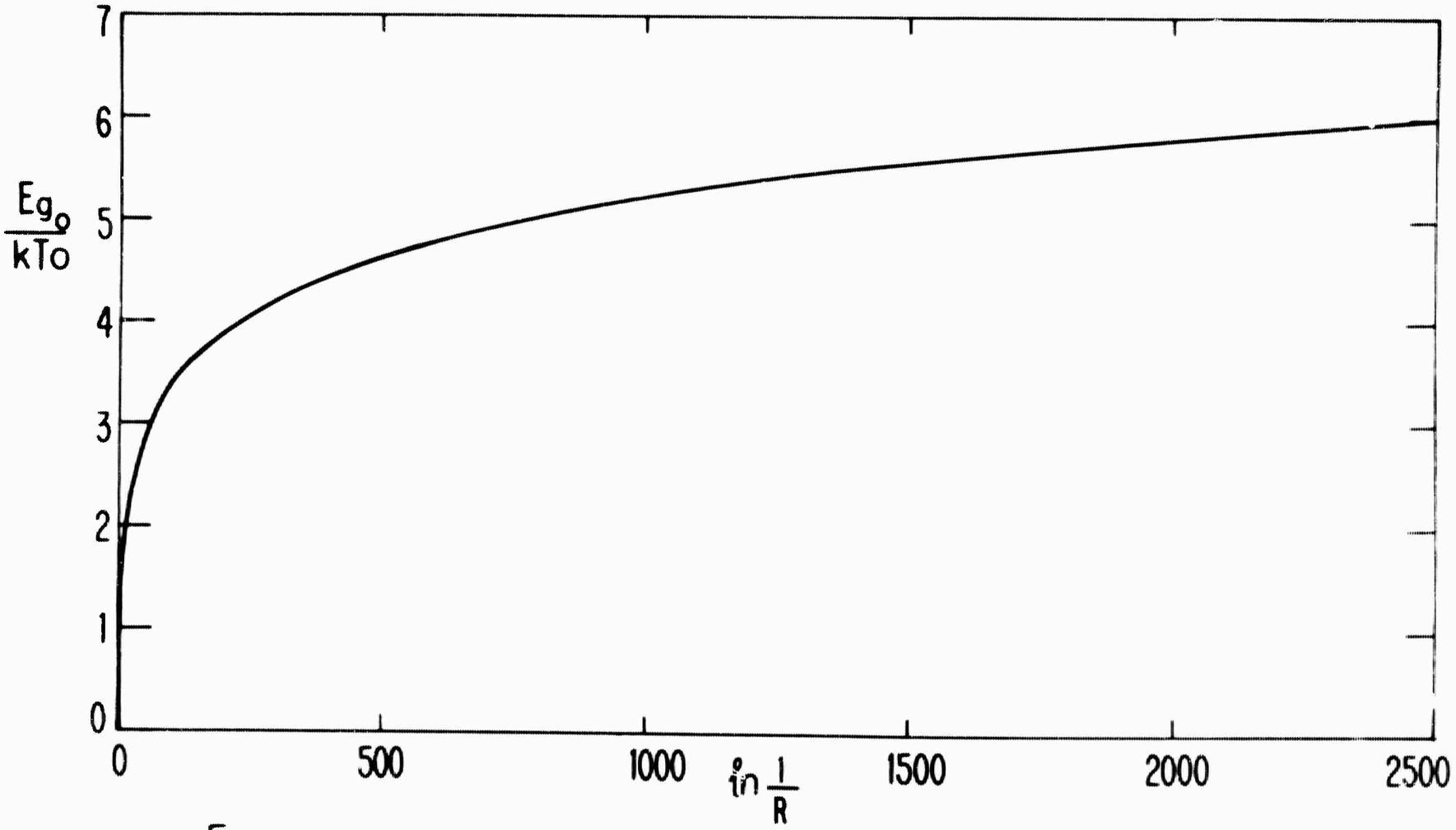

FIG. III-2 $\frac{Eg_o}{kTo}$ vs. $\ell n \frac{1}{R}$ EFFECTIVE MASS APPROXIMATION-BOLTZMANN STATISTICS

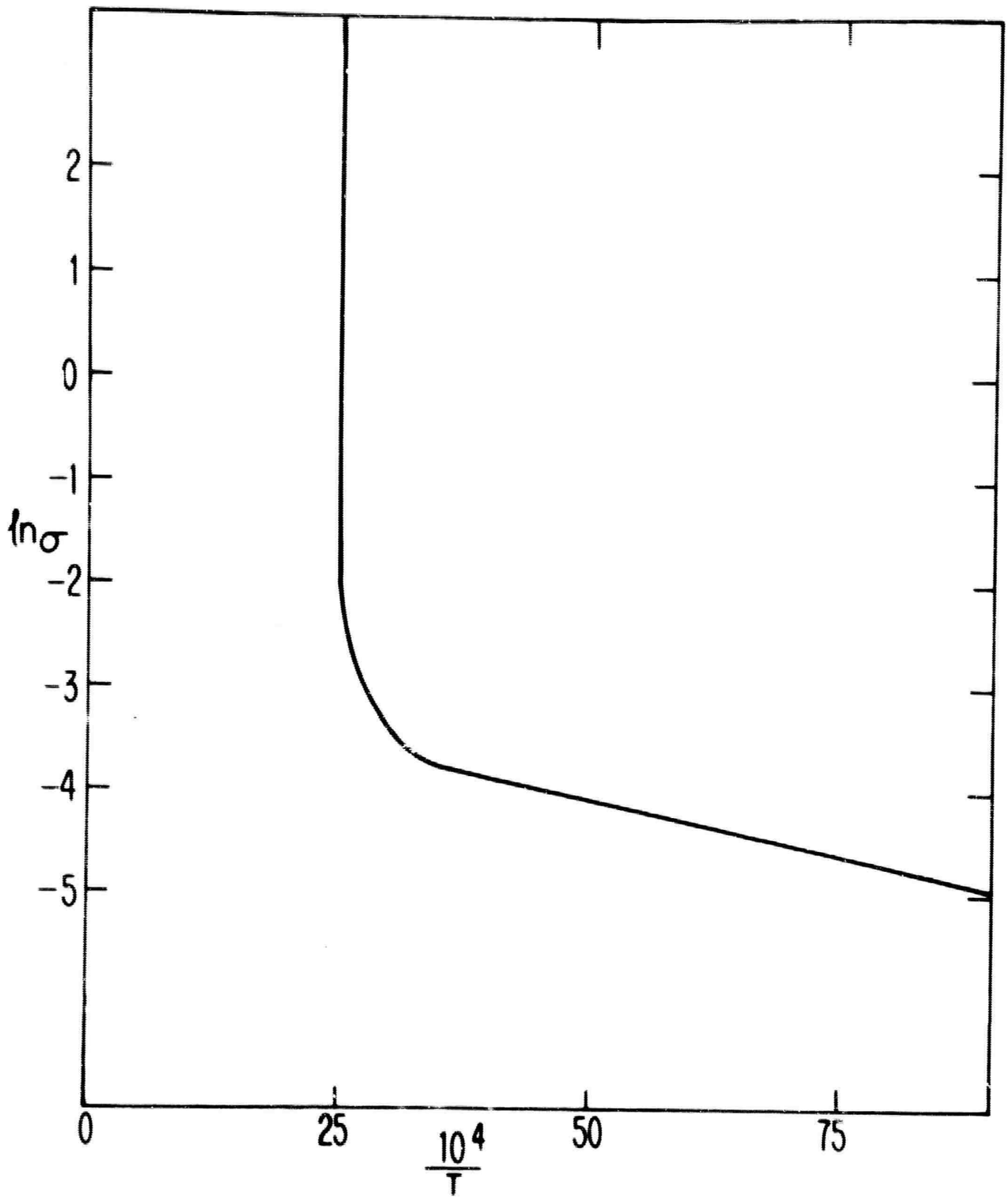

FIG. III-3 CONDUCTIVITY AS A FUNCTION OF TEMPERATURE. EFFECTIVE MASS APPROXIMATION- BOLTZMANN STATISTICS.

Equation (3.29) is a very important result, since it shows that our use of (2.1) for all n up to the transition was valid. Furthermore, if n/N had approached unity before the transition, the value of the effective mass approximation in arriving at (3.8) and (3.9) would have been brought into question. If E_{go}/kT_o is small, and (3.29) does not hold, Boltzmann statistics do not apply and Fermi statistics must be used.

When Boltzmann statistics are invalid, we must return to equations (3.8) and (3.9). We may write these:

$$n = \frac{1}{2\pi^2} \left(\frac{2m_e}{\hbar^2}\right)^{3/2} F_{1/2}\left(\frac{E_F}{kT}\right) \tag{3.30}$$

$$p = \frac{1}{2\pi^2} \left(\frac{2m_h}{\hbar^2}\right)^{3/2} F_{1/2}\left(-\frac{E_F + E_g}{kT}\right) \tag{3.31}$$

where:

$$F_{1/2}(y) \equiv \int_0^\infty \frac{x^{1/2}\, dx}{e^{(x-y)} + 1} \quad .$$

In an approximation valid up to y = +2, or just before the system becomes completely degenerate, Ehrenberg [35] has shown that $F_{1/2}(y)$ can be written:

$$F_{1/2}(y) = \frac{2\sqrt{\pi}}{1 + 4\, e^{-y}} \, . \tag{3.32}$$

This approximation will be valid until the Fermi energy is well into the conduction band, so that we can think of (3.32) as exact in all normal situations involving semiconductors. Then the condition of neutrality gives, from (3.30), (3.31), and (3.32):

$$\frac{M}{1 + 4\, e^{-E_F/kT}} = \frac{1}{1 + 4\, e^{(E_F + E_g)/kT}} \tag{3.33}$$

where $M = (m_e/m_h)^{3/2}$. The solution of (3.33) is:

$$e^{-\frac{E_F}{kT}} = \frac{M - 1}{8} + \sqrt{(\frac{M - 1}{8})^2 + M\, e^{E_g/kT}}\ . \tag{3.34}$$

The concentration of electrons in the conduction band is then:

$$N = (\frac{2m_e kT}{\pi\hbar^2})^{3/2} \frac{1}{1 + 4\, e^{-E_F/kT}} \tag{3.35}$$

For the case $m_e = m_h = m^*$, (3.35) becomes:

$$n = A\, T^{3/2}\, e^{-\frac{E_g}{kT}} \frac{1}{1 + \frac{1}{4}\, e^{-E_g/2kT}} \tag{3.36}$$

This differs from the Boltzmann expression, (3.14), only by a factor of $[1 + \exp(-E_g/2kT)/4]^{-1}$, which is very nearly unity for all ordinary temperatures unless the energy gap is extremely small.

Combining equations (2.1) and (3.36):

$$n = A\, T^{3/2}\, e^{-\frac{E_{go}}{2kT}}\, e^{\frac{\beta}{2kT} n} \frac{1}{1 + \frac{1}{4}\, e^{-\frac{E_{go}}{2kT}}\, e^{\frac{\beta}{2kT} n}}\ . \tag{3.37}$$

Equation (3.37) can be solved analytically only when the initial energy gap is much larger than kT for all temperatures under consideration. In that case, let:

$$\bar{\tau} \equiv \left[e\left(1 - \frac{kT}{2\beta n}\, e^{-\frac{E_{go}}{2kT}}\, e^{\frac{\beta n}{2kT}}\right)\right] \frac{\beta}{2kT} A\, T^{3/2}\, e^{-E_{go}/2kT} \tag{3.38}$$

Equation (3.37) then becomes:

$$\mathcal{N} = \bar{\tau}^{\mathcal{N}} = \bar{\tau}^{\bar{\tau}^{\bar{\tau}^{\cdot^{\cdot^{\cdot}}}}} = \eta(\tau) \qquad (3.39)$$

where $\mathcal{N}$ is defined as in equation (3.17). Thus a transition still occurs with Fermi statistics.

Just before the transition, $\mathcal{N} = e$. Thus the concentration of carriers at the point of transition is the same as the Boltzmann result in terms of T_o:

$$n(T_o) = 2kT_c/\beta. \qquad (3.27)$$

But for Fermi statistics, a different value for T_o is obtained. The transition temperature occurs when $\bar{\tau} = e^{1/e}$, which yields the condition:

$$1 + \ln\left[1 - \frac{k}{2\beta A T_o^{1/2} e} e^{\frac{e\beta A T_o^{1/2}}{2k}} e^{-E_{go}/2kT_o}\right] = \frac{2k}{\beta A T_o^{1/2} e} e^{E_{go}/2kT_o}. \qquad (3.40)$$

Equation (3.40) can be solved graphically for T_o. However, it can be seen that Fermi statistics tend to raise the transition temperature. Since $\exp(-E_{go}/2kT_o)$ is a small parameter, an expansion of (3.40) to first order gives:

$$\frac{e\beta A T_o^{1/2}}{2k} = e^{\frac{E_{go}}{2kT_o}} + \frac{e}{4}. \qquad (3.41)$$

Ignoring the relatively small second term on the right of (3.41), we recapture the Boltzmann relation for T_o, equation (3.20). The presence of the small positive addition to the right-hand side increases T_o by a

small amount. Equation (3.27) then shows that slightly more carriers have been excited at the point of transition than had been when Boltzmann statistics were used.

In the case where the electron and hole effective masses differ, $M \neq 1$, and we must modify equations (3.38) and (3.41). These become:

$$N = A T^{3/2} e^{-\frac{E_{go}}{2kT}} e^{\frac{\beta n}{2kT}} \frac{1}{1 + \frac{1-M}{8\sqrt{M}} e^{-\frac{E_{go}}{2kT}} e^{\frac{\beta n}{2kT}} + \frac{(M-1)^2}{128\,M} e^{-\frac{E_{go}}{kT}} e^{\frac{\beta n}{kT}}} \qquad (3.42)$$

and:

$$\frac{e\beta A T_o^{1/2}}{2k} = e^{\frac{E_{go}}{2kT_o}} + \frac{e(3-M)}{8\sqrt{M}} , \qquad (3.43)$$

Equation (3.43) shows that the transition temperature can be a sensitive function of the mass asymmetry, M. When the electron effective mass is about twice the hole effective mass, T_o is approximately the same as for the Boltzmann case. For greater ratios of m_e to m_h, the transition temperature is lowered, but this lowering is small for normal values of M. As an example, when E_{go} is 6kT, and the electron effective mass is 100 times the hole effective mass, T_o will be decreased by roughly 15%. On the other hand, a large effective mass for holes relative to that for electrons tends to increase T_o somewhat more sharply. When E_{go} is $6kT_o$, and m_h is 100 m_e, T_o increases by about 50%. It is important to bear in mind that (3.43) is valid only for values of E_{go} greater than approximately $4kT_o$.

When E_{go} is not this large relative to kT_o, we must return to

equation (3.38). We cannot solve (3.38) analytically, but we can solve for the transition temperature. Using (3.23):

$$\frac{d \ln n}{dT^2} = \frac{\frac{3}{A} + \frac{\frac{E_{go}}{kT}}{1 + \frac{1}{4} e^{-(E_{go}/2kT)(1 - \frac{4n}{N})}}}{1 - \frac{\frac{E_{go}}{kT} \frac{2n}{N}}{1 + \frac{1}{4} e^{-(E_{go}/2kT)(1 - \frac{4n}{N})}}} \qquad (3.44)$$

From (3.44), we see that the transition occurs when:

$$\frac{E_{go}}{kT} \frac{2n}{N} = 1 + \frac{1}{4} e^{-\frac{E_{go}}{2kT}(1 - \frac{4n}{N})} \qquad (3.45)$$

If we let:

$$\Omega \equiv e^{\frac{e}{4} e^{-E_{go}/2kT_o}}$$

and:

$$\Omega \equiv \frac{1}{\ln \beta} \left[\frac{E_{go}}{kT_o} \frac{2n}{N} - 1 \right]$$

then equation (3.45) becomes:

$$\Omega = B^{\Omega} = B^{B^{B^{\cdots}}} = \hbar(B) . \qquad (3.46)$$

Equation (3.46) can be used to find T_o when the energy gap is small.

A major effect of Fermi statistics is the cutting off of the conductivity anomaly at very high n. This can easily be seen from (3.35). The maximum value for n at the transition temperature, after the

transition, is:

$$n = \left(\frac{2m_h kT_o}{\pi\hbar^2}\right)^{3/2} \tag{3.47}$$

whereas with Boltzmann statistics, n grew without limit after the transition. Such a cut-off is characteristic of Fermi statistics.

Using (3.27) and (3.47), we obtain the jump in carrier concentration at the transition temperature:

$$\Delta n = \left(\frac{2m_h kT_o}{\pi\hbar^2}\right)^{3/2} - \frac{NkT_o}{2E_{go}} .$$

This result, as well as (3.47), is physically meaningful only if the value of n given by (3.47) is significantly less than N, since the effective mass approximation must remain valid in order to use (3.35). If n in (3.47) is greater than N, clearly there can be no more than N carriers per unit volume in the conduction band, and the jump in n at T_o is just:

$$\Delta n = N(1 - kT_o/2E_{go}) .$$

This tells us nothing about the jump in conductivity, since the mobility will change considerably upon transition from a semiconducting to a metallic state. However, this result will enable us to calculate the mobilities before and after the transition from experimental measurements of the conductivity.

B. Narrow Band Limit

The transition metal oxides which exhibit semiconductor-to-metal transitions are characterized by extremely narrow 3d bands.

For such materials, the effective masses of electrons and holes are so large that it is not meaningful to use the approximations in section A. The physical situation is probably closer to the extreme limit of delta function bands. We shall here derive an expression for n(T) in this limit. We assume one 3d electron per cation, although any number can be treated analogously.

We return to equations (3.4) and (3.5) for n and p, but now use the narrow band densities of states:

$$\rho_c(E) = N\,\delta(E) \tag{3.48}$$

$$\rho_v(E) = N\,\delta(E + E_g)\ . \tag{3.49}$$

Substituting (3.48) and (3.49) in (3.4) and (3.5), respectively:

$$n = \frac{N}{e^{-E_F/kT} + 1} \tag{3.50}$$

$$p = \frac{N}{e^{\frac{E_F+E_g}{kT}} + 1}\ . \tag{3.51}$$

The condition of neutrality leads to:

$$E_F = -1/2\ E_g .$$

Hence, the concentration of free carriers is given by:

$$n = \frac{N}{e^{E_g/2kT} + 1}\ , \tag{3.52}$$

Putting (2.1) into (3.52):

$$\frac{n}{N} = \frac{1}{e^{E_{go}/2kT}\ e^{-\beta n/2kT} + 1}\ . \tag{3.53}$$

Using the general expression for β, equation (3.24), (3.53) becomes:

$$\frac{n}{N} = \frac{1}{e^{E_{go}/2kT} \; e^{-\beta n/2kT} + 1} \qquad (3.54)$$

First, we assume $E_{go} \gg kT$ for all ordinary temperatures. This is equivalent to the Boltzmann limit. Then, letting:

$$x \equiv n$$

$$y \equiv E_{go}/2kT ,$$

equation (3.54) can be written:

$$x e^{y} = e^{4(1+\delta)xy} .$$

With the substitutions:

$$Z \equiv x e^{y}$$

$$W \equiv \exp[4(1+\delta)\, y\, e^{-y}] ,$$

this equation becomes:

$$Z = W^{Z} = W^{W^{W^{\cdots}}} = \eta(W) . \qquad (3.55)$$

Once again, we find a transition to the metallic state. The transition occurs at $W_o = e^{1/e}$, where:

$$4(1+\delta)e\, y_o = e^{y_o} = \left[e^{\frac{1}{4(1+\delta)e}}\right]^{4(1+\delta)e\, y_o} \qquad (3.56)$$

Equation (3.56) gives E_{go}/kT_o as a function of δ. The solution is plotted in Fig. III-4. It can be seen that E_{go}/kT_o is not a rapidly varying function of δ over the range of interest. It is important to note that δ is a constant for each material. Thus E_{go}/kT_o will also

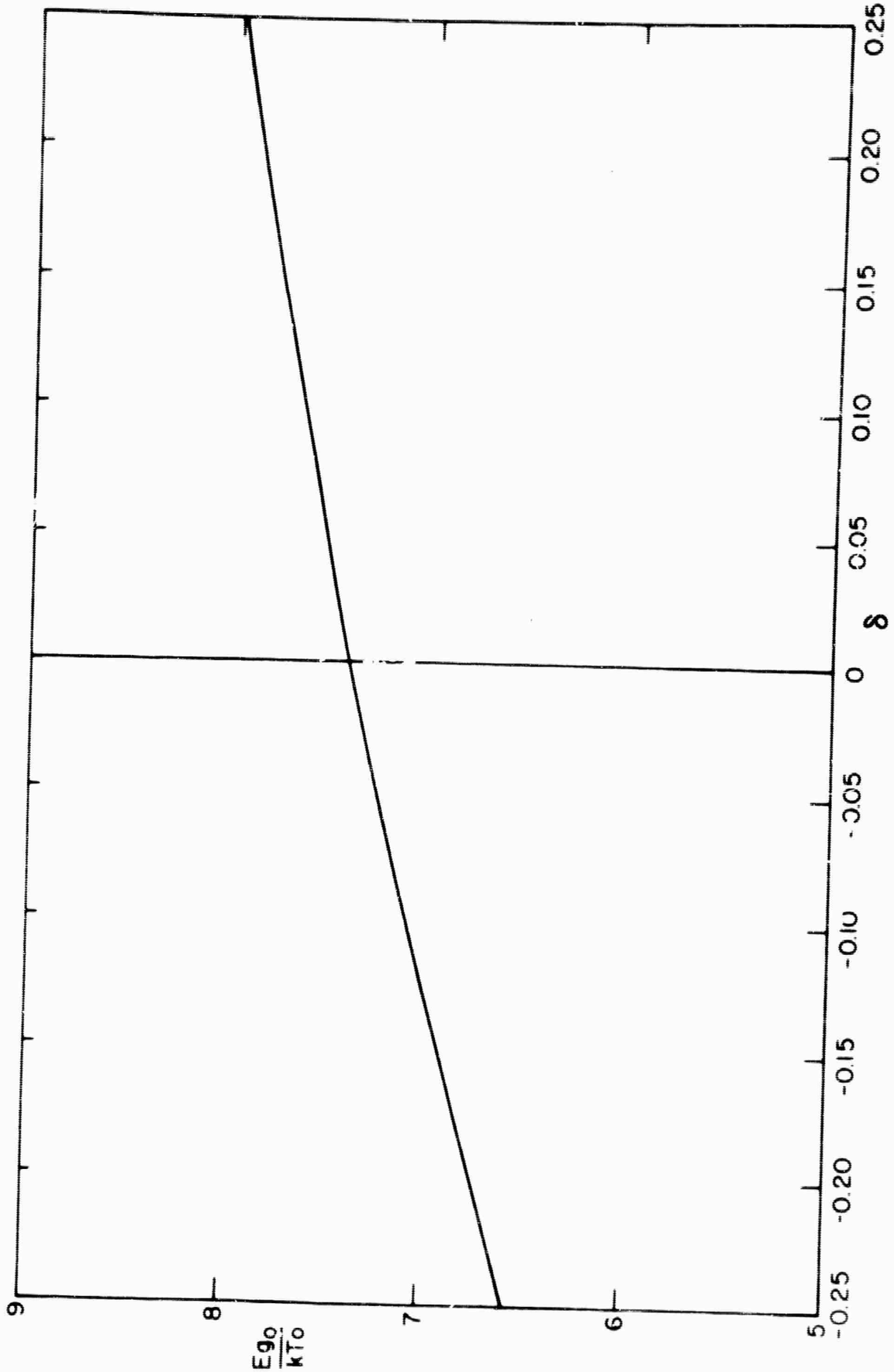

FIG. III-4 $\frac{Eg_0}{kT_0}$ AS A FUNCTION OF δ

be constant. This can be expressed as:

$$\frac{d \ln E_{go}}{dX} = \frac{d \ln T_o}{dX} \tag{3.57}$$

where X is any external parameter, such as pressure. Equation (3.57) can be tested experimentally, and is an important prediction of this theory. In the event the energy gap is of antiferromagnetic origin, $\delta = 0$. Then (3.56) becomes:

$$4e\,y_o = \left[e^{\frac{1}{4e}} \right]^{4e\,y_o} . \tag{3.58}$$

Hence:

$$\frac{E_{go}}{kT_o} = 7.40 . \tag{3.59}$$

Equation (3.59) is true whatever the material, provided it is antiferromagnetism which was responsible for the energy gap. Just before the transition, $Z = e$. At this point, $x_o = e^{(1-y_o)} = 0.067$. Thus the concentration of carriers in the conduction band at the transition point is:

$$\frac{n}{N} = 0.067 . \tag{3.60}$$

This small a value of n justifies the use of (2.1) throughout the semiconducting region.

The approximation $E_g \gg kT$ need not have been made in the narrow band case. The general equation, (3.54) can be solved exactly for the transition temperature, T_o. In terms of x and y, (3.54) becomes:

$$x = \left[e^{y(1-4x)} + 1 \right]^{-1} \tag{3.61}$$

where we have set $\delta = 0$ to investigate the antiferromagnetic situation.

Solving (3.61) for y:

$$y = \frac{1}{1 - 4x} \ln \frac{1 - x}{x} . \tag{3.62}$$

The transition occurs when $dy/dx = 0$, or when:

$$\frac{1 - 4x_o}{4x_o(1 - x_o)} = \ln \frac{1 - x_o}{x_o} . \tag{3.63}$$

The solution to (3.63) is $x_o = 0.08$, which corresponds to $y_o = 3.55$. Hence, the complete Fermi solution is:

$$\frac{E_{go}}{kT_o} = 7.20 . \tag{3.64}$$

As in the effective mass approximation, Fermi statistics tend to raise the transition temperature somewhat.

The solution to equation (3.61) is shown in Fig. III-5. The part of the curve for $x > 1/4$ is unphysical, since the energy gap becomes negative.

Analysis shows that the final result, (3.64), is independent of the number of 3d electrons per cation.

The case of a Gaussian broadening about delta function bands can be solved analytically for Boltzmann statistics, which is a good approximation if the spread is small. Let λ be the parameter which measures the root mean-square deviation in E. Then, for one 3d electron per cation, we write the densities of states:

$$\rho_c(E) = \frac{N}{\sqrt{\pi}\lambda} e^{-\frac{E^2}{\lambda^2}} \tag{3.65}$$

$$\rho_v(E) = \frac{N}{\sqrt{\pi}\lambda} e^{-\frac{(E+E_g)^2}{\lambda^2}} \tag{3.66}$$

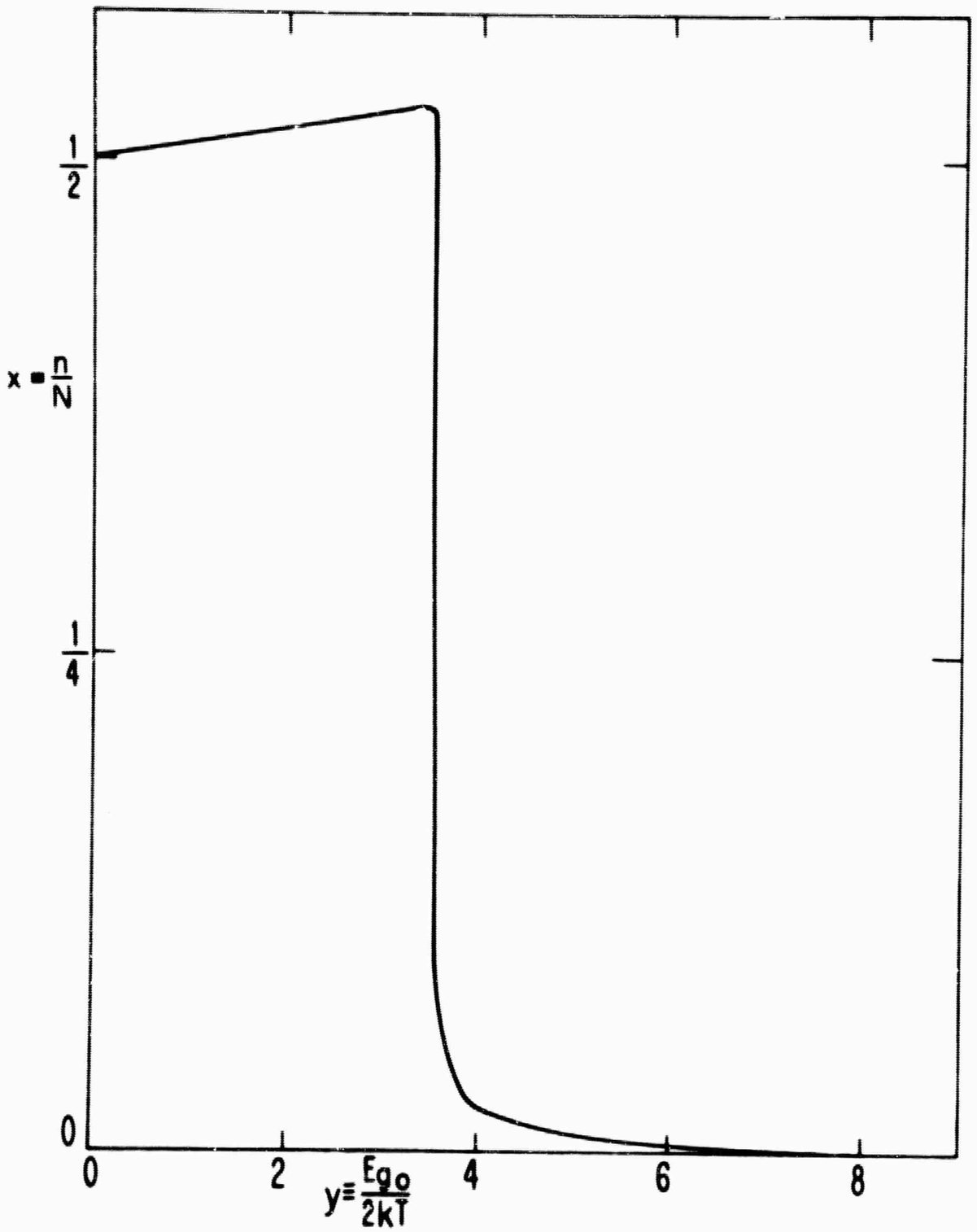

FIG. III-5 CARRIER CONCENTRATION AS A FUNCTION OF TEMPERATURE. NARROW BAND LIMIT-FERMI STATISTICS.

We are assuming both bands are broadened similarly. This can be generalized easily by taking different values of λ for each band.

In the Boltzmann limit, (3.8) becomes:

$$n = \frac{N}{\sqrt{\pi}\lambda} \int_{-\infty}^{\infty} e^{-\left(\frac{E^2}{\lambda^2} + \frac{E}{kT} - \frac{E_F}{kT}\right)} dE$$

$$= N e^{\frac{E_F}{kT}} e^{\frac{\lambda^2}{4k^2T^2}} \qquad (3.67)$$

Similarly, (3.9) can be written:

$$p = N e^{-\frac{E_F + E_g}{kT}} e^{\frac{\lambda^2}{4k^2T^2}} . \qquad (3.68)$$

The condition of neutrality gives:

$$E_F = -1/2\ E_g .$$

Thus, (3.67) shows:

$$n = N e^{\frac{\lambda^2}{4k^2T^2}} e^{-\frac{E_g}{2kT}} \qquad (3.69)$$

Substituting (2.1) and (3.23), and using the previous definitions of x and y, (3.69) becomes:

$$x = e^{-\frac{\lambda^2}{4k^2T^2}} e^{y(1-4x)} . \qquad (3.70)$$

If we let:

$$\overline{Z} \equiv x e^{y} e^{-\frac{\lambda^2}{4k^2T^2}}$$

$$\overline{W} \equiv \exp\left[4y e^{-y} e^{\frac{\lambda^2}{4k^2T^2}}\right]$$

equation (3.70) can be written:

$$\overline{Z} = \overline{W}^{\overline{Z}} = \overline{W}^{\overline{W}^{\overline{W}^{\cdots}}} = \eta(W) . \tag{3.71}$$

The transition occurs at $\overline{W} = e^{1/e}$, where:

$$4y_o e^{-y_o} e^{\left(\frac{\lambda}{2kT_o}\right)^2} = \frac{1}{e} . \tag{3.72}$$

The solution of equation (3.72) is:

$$\frac{E_{go}}{kT_o} = 2 \ln R \; \eta(R) \tag{3.73}$$

where:

$$\ln R \equiv \left\{4e\left[1 + \left(\frac{\lambda}{2kT_o}\right)^2\right]\right\}^{-1} .$$

To second-order in the small quantity, $\lambda/2kT_o$, (3.73) yields:

$$\frac{E_{go}}{kT_o} = 2\left[4e\left(1 + \frac{\lambda^2}{4k^2T_o^2}\right)\right]^{-1} \eta\left\{\exp\left[4e\left(1 + \frac{\lambda^2}{4k^2T_o^2}\right)\right]^{-1}\right\} . \tag{3.74}$$

It can thus be seen that introducing a small spread to the bands tends to raise E_{go}/kT_o somewhat. This means that the transition occurs at a slightly lower temperature than in the zero bandwidth case, as one might intuitively expect. For $\lambda/E_{go} = 0.01$, $E_{go}/kT_o = 7.40$, the same value as when $\lambda = 0$; for $\lambda/E_{go} = 0.05$, $E_{go}/kT_o = 7.44$.

When λ/E_{go} becomes much larger than 0.05, not only does the approximation in (3.74) begin to lose validity, but also we must start to take into account the effective lowering of the real band gap due to the finite bandwidth. The parameter λ is approximately 1/5

the band width, so that we may write the ratio of the band width to the band gap:

$$\frac{\text{Band Width}}{\text{Band Gap}} = \frac{5\lambda}{E_{go} - 5\lambda} .$$

When the bands are about half as wide as the energy gap, then E_{go}/kT_0 7.51. When the band width and energy gap are roughly the same, solution of (3.73) shows that:

$$\frac{E_{go}}{kT_o} = 7.84 . \qquad (3.75)$$

We must bear in mind that (3.73) is valid only for extremely narrow bands, so that we cannot allow λ to become very large. Nevertheless, when the band width and the band gap are both small in absolute magnitude (e.g. of the order of 0.05 eV), equation (3.75) could have meaning.

In the case of antiferromagnetism, the theory presented here gives a behavior for the variation of sublattice magnetization with temperature which differs considerably from that calculated using the ordinary molecular field model of antiferromagnetism. We can evaluate the sublattice magnetization in the narrow band limit, using equations (2.20), (2.22), and (3.55). Equation (2.20), which gives the average value of spin in the valence band, provides the magnetization at T = 0:

$$M_\beta(0) = g\mu_B N \overline{\langle S_z \rangle}$$

$$= g\mu_B N \frac{a}{\pi} \int_0^{\pi/a} dk \left[-\frac{1}{2} + \frac{E_b}{2E_{go}} (1 + \cos ka) \right]$$

$$= -\frac{1}{2} \left(1 - \frac{E_b}{E_{go}}\right) g\mu_B N \qquad (3.76$$

where $M_\beta(0)$ is the magnetization at T = 0 on the sublattice where the spin is primarily down, g is the spectroscopic splitting factor, and $\mu_B = e\hbar/2mc$ is the Bohr magneton. In the limit $E_b = 0$, $M_\beta(0)$ is just the value obtained by the molecular field treatment of antiferromagnetism. For all finite band widths, however, $M_\beta(0)$ is reduced in magnitude.

Equations (2.22) and (3.76) give the sublattice magnetization as a function of the number of free carriers:

$$M_\beta(n) = g\mu_B N\left[\left(1 - \frac{E_b}{E_{go}}\right)\left(-\frac{1}{2} + \frac{n}{N}\right) + \frac{E_b}{E_{go}} \frac{\sin\frac{n}{N}}{\pi}\right]. \qquad (3.77)$$

Finally, equations (3.55) and (3.77) can be used to calculate M as a function of temperature:

$$M_\beta(T) = g\mu_B N\left\{\left(1 - \frac{E_b}{E_{go}}\right)\left[-\frac{1}{2} + x(y)\right] + \frac{E_b}{E_{go}} \frac{\sin[\pi x(y)]}{\pi}\right\} \qquad (3.78)$$

where $y = E_{go}/2kT$ as before, and x(y) is given by (3.55). Equation (3.78) is valid only when $E_b \ll E_{go}$.

We shall investigate the sublattice magnetization for two cases, $E_b = 0$, the narrow band limit, and $E_b = E_{go}/4$, just about the upper limit for the use of (2.20) and (2.22). When $E_b = 0$, the magnetization is given by:

$$M(T) = g\mu_B N\left[-\frac{1}{2} + x(y)\right]. \qquad (3.79)$$

When $E_b = E_{go}/4$, the magnetization is:

$$M(T) = g\mu_B N\left[-\frac{3}{8} + x(y)\right]. \qquad (3.80)$$

From (3.79) and (3.80), the ratios of $M_\beta(T)$ to the magnetization at $T = 0$ are:

$$\frac{M_\beta(T)}{M_\beta(0)} = 1 - 2\,x(y)$$

$$\frac{M_\beta(T)}{M_\beta(0)} = 1 - \frac{8}{3}\,x(y)\ . \tag{3.81}$$

Evaluating (3.81), we find that the ratios remain very close to unity from $T = 0$ until $T \approx 0.7\ T_N$. As T is increased above this point, the ratio begins to fall off, until just below T_N, where:

$$\frac{M_\beta(T_N^-)}{M_\beta(0)} = 0.87 \qquad (E_b = 0)$$

$$\frac{M_\beta(T_N^-)}{M_\beta(0)} = 0.82 \qquad (E_b = E_{go}/4)\ . \tag{3.82}$$

At T_N, the sublattice magnetizations drop sharply from the values given by (3.82) to zero. This behavior for $M_\beta(T)/M_\beta(0)$ contrasts with the Brillouin curve obtained using the molecular field theory of antiferromagnetism in that it remains higher at low temperatures and then drops to zero at T_N much more drastically. As the bands get wider, the ratio $M_\beta(T)/M_\beta(0)$ approaches the molecular field behavior more closely; however, as we have seen, the magnitude of $M_\beta(0)$ is greatly reduced from the zero band width, and thus the molecular field case.

Chapter IV

COMPARISON OF THEORY WITH EXPERIMENTAL RESULTS

In this chapter, we shall present the results of experiments performed on the four materials known to exhibit semiconductor-to-metal transitions, and compare the results to the predictions of the theory given in Chapters II and III.

A. V_2O_3

V_2O_3 will be of primary interest to us since it is the material which has been studied experimentally in the greatest detail. At room temperature, V_2O_3 has corundum structure, with rhombohedral symmetry. The lattice parameters are most easily expressed in terms of a hexagonal unit cell, consisting of 6 molecules. As measured by Warekois [36] at 300°K, the hexagonal c-axis, $c_H = 14.00$ Å, whereas the basal plane lattice parameter, $a_H = 4.95$ Å. The c-axis contracts with increasing temperature as:

$$\frac{d \ln c_H}{dT} = -5.8 \times 10^{-6} \ (^\circ K)^{-1}$$

while the a-axis expands as:

$$\frac{d \ln a_H}{dT} = 22.9 \times 10^{-6} \ (^\circ K)^{-1} .$$

Thus the thermal expansion coefficient is:

$$\frac{d \ln V}{dT} = 40.0 \times 10^{-6} \ (^\circ K)^{-1} .$$

In the vicinity of 150°K, a phase transformation occurs. At lower temperatures, V_2O_3 has monoclinic symmetry. As also

measured by Warekois [36] at 77°K, the monoclinic unit cell, consisting of 12 molecules, can be expressed as:

$a = 8.57$ Å

$b = 4.98$ Å

$c = 13.88$ Å

$\beta = 91.6°$.

A simplified diagram of both structures of V_2O_3 is shown in Fig. IV-1.

The monoclinic distortion can be thought of as a shifting of pairs of cations in the hexagonal basal plane towards one another, resulting in an effective tilting of the c-axis. From the above data at 77°K, the parameter ϵ, defined in Chapter II, can be evaluated as:

$$\epsilon = \frac{\frac{c \sin(\beta - \pi/2)}{12}}{\frac{a}{3}} = \frac{0.0323 \text{ A}}{2.86 \text{ A}}$$

$$= 0.011 .$$

Dilatometric data by Foëx [16] showed that there is a sharp contraction of volume at the transition temperature. Recent experiments by Minomoru and Nagasaki [37] have shown that this contraction is about 3.5%.

The presence of antiferromagnetism has never been established in V_2O_3. Carr and Foner [38] measured $\chi_{\parallel}$ and $\chi_{\perp}$ with respect to the c-axis, and found both components the same order of magnitude and essentially constant down to 4°K. Paoletti and Pickart [39] performed neutron diffraction experiments which placed an upper limit on the antiferromagnetic moment of 0.5 Bohr magneton per cation.

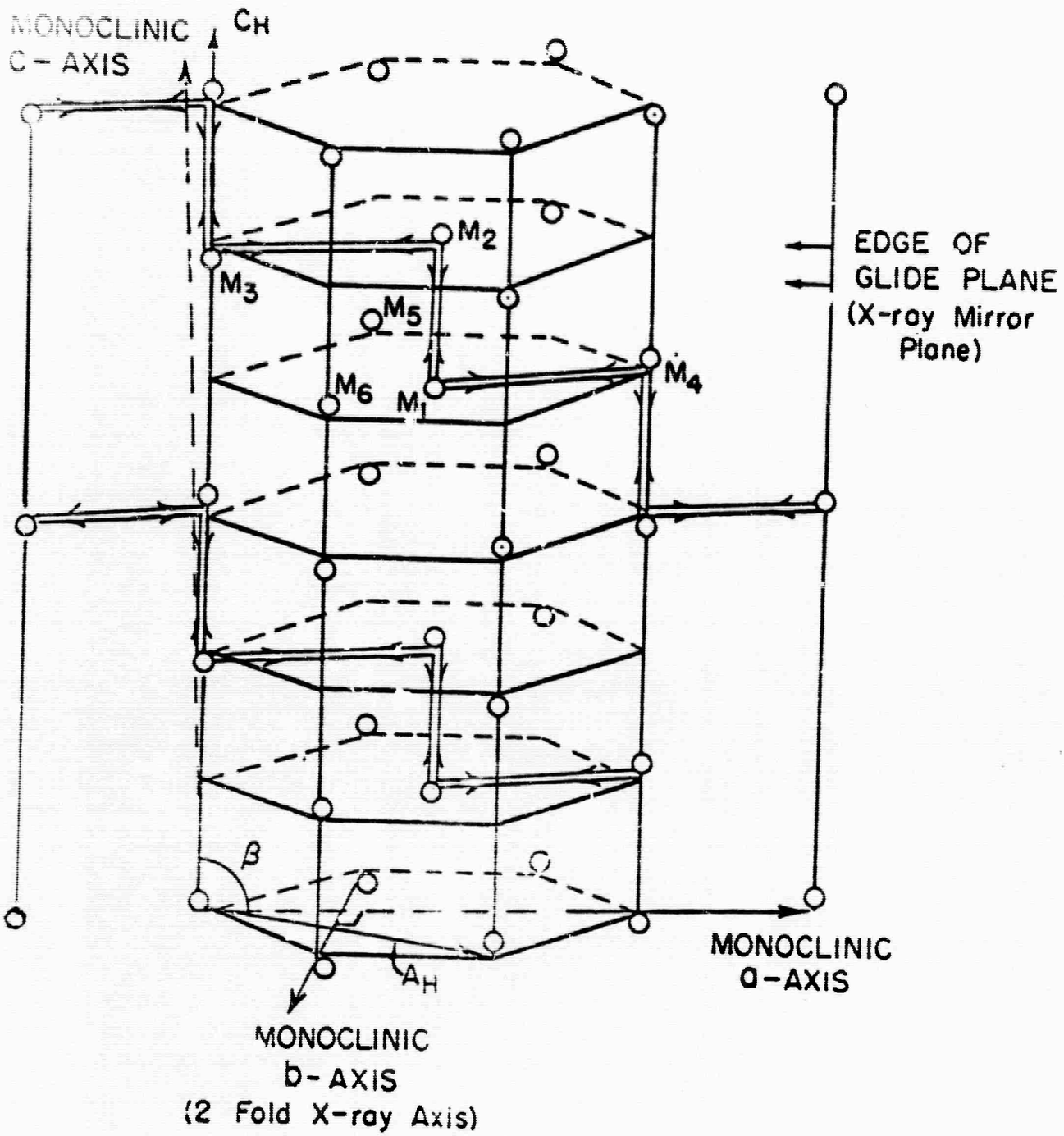

FIG. IV-1 SIMPLIFIED STRUCTURE OF V_2O_3 SHOWING ONLY V^{3+} ION POSITIONS

Abrahams [23] was able to detect antiferromagnetism in Ti_2O_3 by means of neutron diffraction, and found a moment of 0.2 Bohr magneton per cation, so antiferromagnetism is certainly not as yet ruled out. Wucher [40] and later Teranishi and Terama [41] have interpreted their magnetic susceptibility measurements to infer that V_2O_3 is antiferromagnetic clear through the transition, up until the vicinity of 525°K; we shall refer to this point as the high-temperature transition.

Transport measurements on V_2O_3 have been done by many workers. Foëx [16] found that at the same temperature as the dilatometric anomoly, there was a semiconductor-to-metal transition. Below the transition temperature, the resistivity increased exponentially with 1/T, the activation energy being 0.20 eV. Above the transition and up to the high-temperature anomaly at 525°K, the resistivity increased linearly with T, and was metal-like. There was a jump in conductivity of a factor of 10^6 at the transition. Foex found that above 525°K, the resistivity decreased exponentially once again, with an activation energy of 0.04 eV.

Morin's experiments [20] (see Fig. I-1) confirmed most of Foex's results. In Morin's samples, the jump in conductivity was also a factor of 10^6, and his measured activation energy in the semiconducting region was 0.17 eV. MacMillan [42] prepared a number of samples of stoichiometry varying from $V_2O_{2.90}$ to $V_2O_{3.05}$, and found virtually identical conductivity behavior for all samples. The activation energy was 0.13 eV, independent of the composition. Recently, Feinleib [21] performed measurements on single crystals

of V_2O_3, found to be within 0.3% of stoichiometry. He found a jump of 10^8 in conductivity at the transition temperature, measured to be:

$$T_o = 152^oK . \tag{4.1}$$

The magnitude of the activation energy varied from 0.12 to 0.18 eV. Other electrical conductivity work has been done on V_2O_3, by Austin [43], and by Goodman [44]. All experiments confirm that a semiconductor-to-metal transition occurs with T_o near or at 152^oK, that it is a sharp transition with jumps in σ of 10^6-10^8, that above T_o the behavior is metallic, and that below T_o the conductivity is thermally activated, with activation energy in the range 0.11 to 0.20 eV. These results show that V_2O_3 is a material to which the theory developed in Chapters II and III may be applicable, and they provide the value of T_o, equation (4.1). Where there is a choice, we shall use the results of Feinleib [21], since his data were taken on single crystals, and his material was closest to stoichiometric. The values obtained for the activation energy conceivably could give us some information about the size of the energy gap. In particular, if the mobility were independent of temperature, our previous results would give:

$$\sigma = n e \mu$$

$$= \sigma_o e^{-\frac{E_{go}}{2kT}(1 - \frac{4n}{N})} \tag{4.2}$$

Since we have shown that n/N does not become very large before the transition, (4.2) would imply:

$$E_A = E_{go}/2 \ , \qquad (4.3)$$

However, it is unrealistic to assume a temperature-independent mobility. For example, if polar scattering is important, then the mobility would be thermally activated, giving a negative contribution to the measured activation energy of approximately $k\,\Theta_D$, where Θ_D is the Debye temperature. Since the Debye temperature is in the vicinity of $500^{\circ}K$ [15], this would modify (4.3) to give:

$$E_A = E_{go}/2 - 0.04 \text{ eV}.$$

Other types of scattering may be present, such as spin-disorder scattering or impurity effects. Also, if polaron formation is important as we expect in the case of narrow bands, there may be a polaron contribution to the apparent activation energy. In general, the most we can say is:

$$E_A = E_{go}/2 + E_x \qquad (4.4)$$

where E_x contains all contributions besides that of the energy gap, and may depend on the particular sample being investigated. Only if lattice scattering dominates can E_x be negative, all other contributions are positive or zero. If we assume E_x is positive, the measured range of activation energies of 0.11 eV to 0.20 eV gives us an upper limit for E_{go}:

$$E_{go} < 0.22 \text{ eV} \ . \qquad (4.5)$$

In order to find the exact value of E_{go}, Feinleib [24] performed optical experiments on V_2O_3 at temperatures above and below the transition. No transmission was observed in the room temperature

metallic region between 0.05 eV and 6 eV. However, in the semiconducting region, at 77°K, transmission was obtained between 0.1 eV and 0.4 eV. The transmission changed by several orders of magnitude in this range, and clearly indicated the presence of an absorption edge at approximately 0.1 eV. Since at 77°K, $T = 1/2\ T_c$, and we have shown that n/N is negligible at this point, this value can be taken as E_{go} for V_2O_3:

$$E_{go} = 0.10 \text{ eV} . \tag{4.6}$$

From (4.1) and (4.6), we find:

$$\frac{E_{go}}{kT_o} = 7.6 \tag{4.7}$$

For V_2O_3, we expect the narrow band analysis of section III B to be appropriate. If the energy gap in V_2O_3 were of antiferromagnetic origin, equation (3.59) should apply. The result, (4.7), agrees with this well within experimental error. If the gap were due to a crystalline distortion, then as we have seen, (3.59) still remains approximately true. We can then use the experimental result (4.7) to evaluate β. This can be done directly from (3.56), or from Fig. III-4. The result is:

$$\beta = 4.4\ E_{go}/N . \tag{4.8}$$

There is no evidence that V_2O_3 is antiferromagnetic. The presence of a phase transformation of the correct type at T_o is strong evidence that the gap arises from a crystalline distortion. If so, the theory of Chapters II and III would account for the phase transformation as well as for the semiconductor-to-metal transition. We can gain

further insight into the nature of the transition from the result of the thermodynamic argument in section II B:

$$\beta = \frac{\gamma^2}{\kappa} - \left(\frac{\partial E_g}{\partial n}\right)_{V,T} . \tag{2.13}$$

Feinleib [21] has measured the total pressure coefficient, γ_F:

$$\gamma_F = -\frac{dE_g}{dP}$$

$$= -\left(\frac{\partial E_g}{\partial P}\right)_{n,T} - \left(\frac{\partial E_g}{\partial n}\right)_{P,T} \frac{dn}{dP} . \tag{4.9}$$

Assuming Boltzmann statistics apply, the concentration of carriers is:

$$n = n_o e^{-\frac{E_{go}}{2kT}} . \tag{4.10}$$

Recall:

$$E_g = E_{go} - \beta n - \gamma P . \tag{2.9}$$

Substituting (2.9) into (4.10):

$$n = n_o e^{-\frac{E_{go}}{2kT}} e^{\frac{\beta n}{2kT}} e^{\frac{\gamma P}{2kT}} \tag{4.11}$$

Thus:

$$\frac{dn}{dP} = n\frac{\gamma}{2kT} + n\frac{\beta}{2kT}\frac{dn}{dP} . \tag{4.12}$$

Solving (4.12) for $\frac{dn}{dP}$:

$$\frac{dn}{dP} = \frac{n\gamma}{2kT - n\beta} . \tag{4.13}$$

But from (2.9):

$$\frac{dE_g}{dP} = -\gamma - \beta \frac{dn}{dP} . \qquad (4.14)$$

Substituting (4.13) and (4.14) into (4.9):

$$\gamma_F = \gamma \left[\frac{1}{1 - \beta n / 2kT} \right] . \qquad (4.15)$$

At $T = 132^{\circ}K$, Feinleib measures $\gamma_F = 2.2 \times 10^{-6}$ eV bar^{-1}. Hence, from (4.15):

$$\gamma = 1.8 \times 10^{-6} \text{ eV bar}^{-1} . \qquad (4.16)$$

Unfortunately, the isothermal compressibility has not been measured for V_2O_3. But the value $\kappa = 0.58 \times 10^{-6}$ bar^{-1} has been found for the very similar materials Fe_2O_3 and $FeTiO_3$ [45], and the compressibility of V_2O_3 will undoubtedly not be much different. Using this value for κ in equation (2.13) yields:

$$\beta = \frac{3.6\, E_{go}}{N} - \left(\frac{\partial E_g}{\partial n}\right)_{V,T} \qquad (4.17)$$

Thus the measured value for β, equation (4.8), is almost entirely accounted for by the variation of E_g due to explicit volume changes. In fact, with just a very slight band spread, such as that due to spin disorder broadening (see Chapter VI), this variation alone is sufficient to obtain the experimental value (4.7). This result, taken together with the measurement of a finite volume change at T_o by Minomura and Nagasaki [37], is another indication that the transition is due to crystalline structure effects rather than antiferromagnetism.

No matter what the cause of the gap, the theory predicts that the ratio E_{go}/kT_o will remain constant. We have expressed this as:

$$\frac{d \ln E_{go}}{dX} = \frac{d \ln T_o}{dX} . \qquad (3.57)$$

In order to test equation (3.57), Feinleib [21] varied both E_{go} and T_o by applying hydrostatic pressure and uniaxial stress. His results were as follows. The transition temperature varied with pressure as:

$$\frac{d \ln T_o}{dP} = -2.6 \times 10^{-5} \text{ bar}^{-1} \qquad (4.18)$$

where P is the hydrostatic pressure. With uniaxial stress applied parallel to the corundum structure's b-axis, the relation between transition temperature and stress was determined to be:

$$\frac{d \ln T_o}{dS} = -2.8 \times 10^{-5} \text{ bar}^{-1} \qquad (4.19)$$

where S is the stress. With stress applied along the c-axis, the uniaxial stress coefficient was at least an order of magnitude smaller:

$$\frac{d \ln T_o}{dS} < 0.3 \times 10^{-5} \text{ bar}^{-1} . \qquad (4.20)$$

The pressure and uniaxial stress coefficients for the energy gap were determined from the stress dependence of the activation energy for electrical conductivity. These results can be expressed, in the case of hydrostatic pressure, as:

$$\frac{d \ln E_{go}}{dP} = -2.2 \times 10^{-5} \text{ bar}^{-1} \qquad (4.21)$$

whereas with uniaxial stress along the b-axis:

$$\frac{d \ln E_{go}}{dS} = -3.0 \times 10^{-5} \text{ bar}^{-1} . \qquad (4.22)$$

In Chapter VI, we show that the pressure coefficient of contributions

to the activation energy from polaron effects and non-stoichiometry are of the order of 10^{-6} bar^{-1}, and thus these contributions do not affect the results (4.21) and (4.22).

A comparison of (4.21) with (4.18) and (4.22) with (4.19) shows that equation (3.57) is indeed satisfied within experimental error. Thus the two major predictions of the theory, equations (3.57) and (3.59) are verified by Feinleib's results. There is no a priori reason for the validity of (3.57) and (3.59), and no other model heretofore suggested predicts these relations. Therefore the agreement with experiment must be considered as good evidence for the applicability of the model of Chapters II and III.

The anisotropy in variation of T_o with uniaxial stress found in (4.19) and (4.20) provides still another indication that it is crystal structure changes which bring about the energy gap. The distortion which doubles the number of cations in each unit cell is entirely in the basal plane of the corundum structure. Therefore the variations of E_{go} and T_o with stress applied along the c-axis should not be very great, as is borne out by (4.20). However, the changes in E_{go} and T_o with stress applied along the a-axis or b-axis are strikingly large, as we would expect.

Feinleib [21] also investigated the high-temperature anomaly, measuring resistivity vs. temperature from 300°K to 800°K. He found that resistivity increases linearly with temperature with the same slope both below and above the high-temperature transition. However, in the vicinity of 550°K, the resistivity undergoes a rather sharp anomalous increase. In the region $T_o < T < 500°K$, the

measured resistivity can be expressed:

$$\rho_L(T) = 4.3 \times 10^{-4} \text{ ohm-cm } (0.51 + 0.49\ T/T_o). \qquad (4.23)$$

If we write for the total resistivity up to 800°K:

$$\rho(T) \equiv \rho_L(T) + \rho_A(T) \qquad (4.24)$$

where $\rho_L(T)$ is an extrapolation of (4.23), and $\rho_A(T)$ is the anomalous resistivity, then $\rho_A(T)$ is a function which is zero up to 500°K, then sharply rises to a value of 12×10^{-4} ohm-cm by 600°K, above which temperature it remains constant. Such behavior for $\rho_A(T)$ bears a striking resemblance to the spin-disorder resistivity calculated by De Gennes and Friedel [46], and therefore suggests a magnetic ordering temperature of 600°K. As we have mentioned, Wucher [40] and Teranishi and Terama [41] have concluded that this is the Néel temperature of V_2O_3. We shall return to this point later.

B. VO

The experimental results for VO are quite similar to those for V_2O_3. VO has (cubic) rock salt structure above T = 126°K. At this temperature, there is a crystalline structure distortion to orthorhombic symmetry. The exact low temperature crystal structure has not as yet been reported. Little is known about the magnetic properties of VO as well. Neutron diffraction and magnetic susceptibility measurements have not been performed.

What we do know about VO is its electrical properties. Morin [20] (see Fig. I-1) found that there is a sharp semiconductor-to-metal transition at:

$$T_o = 126^{\circ}K . \tag{4.25}$$

The jump in conductivity at T_o was measured to be a factor of 10^6. Below T_o, the activation energy was $E_A = 0.14$ eV. Above T_o, the resistivity increases linearly with T and is metal-like. It can be seen from Fig. I-1 that the electrical properties of VO greatly resemble those of V_2O_3.

Austin [43] has performed pressure experiments on VO, and has observed the effects of quasi-hydrostatic pressure on the electrical properties of single crystals of variable composition. From measurements of resistivity as a function of pressure at $94^{\circ}K$, Austin obtained:

$$\frac{dE_g}{dP} = -2.9 \times 10^{-6} \text{ eV bar}^{-1}. \tag{4.26}$$

Since no direct measurement of the energy gap has been made in the case of VO, we cannot do more than assume the gap is the same as that of V_2O_3 as a first approximation, and perform a self-consistent calculation using (2.13) and (3.56) to obtain a better value. Thus, we begin with:

$$E_{go} = 0.10 \text{ eV} . \tag{4.27}$$

We use this value to calculate the contribution to β of the volume term in (2.13). In the case of V_2O_3, this term was sufficient to give the correct ratio of E_{go} to T_o. If VO is completely analogous to V_2O_3, as Fig. I-1 suggests, we should obtain good results in this manner. From (4.26):

$$\gamma_F = 2.9 \times 10^{-6} \text{ eV bar}^{-1} .$$

Using (4.15):

$$\gamma = 2.7 \times 10^{-6} \text{ eV bar}^{-1}. \tag{4.28}$$

For the isothermal compressibility, the best value available is that for ZnO [45]:

$$\kappa = 0.78 \times 10^{-6} \text{ bar}^{-1} . \tag{4.29}$$

Substituting (4.28) and (4.29) into (2.13), we can evaluate the contribution due to explicit volume changes as:

$$\beta = \frac{6.9 \, E_{go}}{N} . \tag{4.30}$$

Using this value for β in the general expression for narrow bands, equation (3.56), we find:

$$\frac{E_{go}}{kT_o} = 8.9 . \tag{4.31}$$

But (4.31) implies that $E_{go} = 0.10$ eV, as was assumed in (4.27). Thus we see that this assumption is self-consistent, and that, just as for V_2O_3, the volume term in (2.13) and narrow band theory give the correct ratio of E_{go} to T_o.

However, now we can use Austin's results for dT_o/dP to check the validity of (3.57). This relationship provides an important test of the theory. From (4.26) and (4.27), we can express Austin's measurements on the pressure variation of the energy gap as:

$$\frac{d \ln E_g}{dP} = -29 \times 10^{-6} \text{ bar}^{-1} . \tag{4.32}$$

As we mentioned before, we shall show in Chapter VI that the pressure coefficients of contributions to E_A from polaron effects and non-stoichiometry are of the order of 10^{-6} bar^{-1}, so that (4.32) probably

does represent only the variation of the energy gap.

At 94°K, Austin found:

$$\frac{dT_o}{dP} = -3 \times 10^{-3}\ ^{o}K\ bar^{-1}.$$

Hence:

$$\frac{d \ln T_o}{dP} = -32 \times 10^{-6}\ bar^{-1}. \qquad (4.33)$$

Comparison of (4.32) with (4.33) demonstrates that (3.57) is satisifed within experimental error.

We conclude that it appears likely that the energy gap in VO arises from a crystalline structure distortion and has a value of about 0.10 eV, approximately the same as that of V_2O_3. The lower transition temperature of VO seems to be due to a greater change in volume at T_o. This is reflected in a larger value for β in equation (2.1). Outside of the slightly lower transition temperature, the behavior of VO and V_2O_3 seems identical.

C. VO_2

The crystalline structure of VO_2 is relatively simple and well-known. Above T = 340°K, the structure is that of rutile, the cations occupying the positions of a body-centered tetragonal lattice. Below 340°K, the symmetry is monoclinic, the structure being that of MoO_2. The low temperature phase is just a distorted rutile structure – the cations which in the rutile phase were collinear and separated by 2.87 Å, are slightly non-collinear and spaced alternately 2.65 Å and 3.12 Å apart [47]. This is an almost classic example of the model of section II D – the unit cell is doubled by a distortion of the lattice

in one dimension, alternate cations pairing. The parameter ϵ, defined in II D, is:

$$\epsilon = \frac{1}{2} - \frac{2.65\ \text{Å}}{5.77\ \text{Å}}$$

$$= 0.04 .$$

The details of the transformation have been studied by Minomura and Nagasaki [37]. They find that at T_o the monoclinic a-axis contracts from 5.77 Å to 5.70 Å, twice the rutile structure's c-axis; simultaneously, the monoclinic b-axis expands from 4.50 Å to 4.54 Å, the rutile a-axis, while the monoclinic c-axis contracts from 5.39 Å to 5.24 Å $2/\sqrt{3}$ of the rutile a-axis. They found no measurable total volume change at the transition point, just a change in the slope (thermal expansion coefficient). They concluded that the transformation was of second order. Jaffray and Dumas [18] measured a volume contraction of 0.08% on powdered VO_2, which is consistent with the lattice constant measurements of Minomura and Nagasaki. In any event, the volume change is more than an order of magnitude smaller than that which occurs in V_2O_3.

Magnetic susceptibility data have been taken on VO_2 by Rudorff et al [48] and by Kawakubo and Nakagawa [49]. Both sets of experiments found susceptibility independent of temperature both above and below 340°K, with a jump in χ_m at 340°K of a factor of roughly 7. They conclude that the low temperature susceptibility can be accounted for by temperature independent paramagnetism, and that there is no evidence for antiferromagnetism. Similarly, Kasper [50] found no magnetic scattering in neutron diffraction measurements below 340°K.

The electrical conductivity behavior of VO_2 was also studied by Morin [20] (see Fig. I-1), who found a sharp semiconductor-to-metal transition at:

$$T_o = 340^oK \tag{4.34}$$

the temperature at which the phase transformation takes place. Below T_o, the activation energy was 0.13 eV. The jump in conductivity at T_o was a factor of 10^2. Neuman, Lawson, and Brown [51] found the same value for T_o, but obtained a jump in σ at T_o of 10^4 and an activation energy of 0.44 eV.

The energy gap has not as yet been measured. The narrow band limit appears to have given good results in the cases of V_2O_3 and VO; we expect it should be at least as appropriate for VO_2, since the cations are V^{++++}, which are smaller in spatial extent than are V^{+++} and V^{++}. It can be concluded that the cause for the higher transition temperature in VO_2 is most likely a larger value for E_{go}. This can be easily explained by the four times larger value obtained for the distortion parameter ϵ in the case of VO_2, which should certainly produce a much larger gap. In our analysis of section II D, we found that using a delta function potential, the larger the initial gap, the larger the value obtained for β. The most reasonable conclusion is that the final E_{go}/kT_o ratio for VO_2 is probably somewhat larger than it is for V_2O_3. As a rough estimate, we shall take:

$$E_{go} \sim 10\, kT_o$$

$$\sim 0.3 \text{ eV} .$$

Pressure measurements on VO_2 have been carried out by

Minomura and Nagasaki [37] and by Neuman et al [51]. Minomura and Nagasaki measured the variation of T_o with pressure and found:

$$\frac{d \ln T_o}{dP} = - 1.4 \times 10^{-6} \text{ bar}^{-1} . \qquad (4.35)$$

This is a very small value and contrasts strikingly with the pressure coefficients of V_2O_3 and VO [see (4.18), (4.19), and (4.33)], which are an order of magnitude larger. Neuman et al could not find a shift of T_o with pressures up to 6 kilobars within the 0.5^oK scatter in T_o itself. Thus they find a still smaller value for $d \ln T_o/dP$ than is given in (4.35).

Neuman et al also measured the change in activation energy with pressure. Their experiments show:

$$\frac{dE_A}{dP} = - 5.0 \times 10^{-7} \text{ eV bar}^{-1} . \qquad (4.36)$$

From their measured value of $E_A = 0.44$ eV, (4.36) yields:

$$\frac{d \ln E_A}{dP} = - 1.1 \times 10^{-6} \text{ var}^{-1} .$$

This is also an order of magnitude smaller than the values for V_2O_3 and VO, given in equations (4.21), (4.22), and (4.33). However, in this case we cannot use (4.36) to evaluate $d \ln E_{go}/dP$ in order to compare with (4.35) and check the validity of (3.57). For equation (4.4) gives:

$$\frac{dE_A}{dP} = \frac{1}{2} \frac{dE_{go}}{dP} + \frac{dE_x}{dP} . \qquad (4.37)$$

In the cases of V_2O_3 and VO, the measured values of dE_A/dP were so large that we could neglect dE_x/dP in (4.36). As we mentioned previously, we show in Chapter VI that dE_x/dP is normally of the

order of 10^{-7} eV/bar. But, in the case of VO_2, this is just the order of magnitude measured for dE_A/dP in (4.36). A further complication in the results of Neuman et al is the extremely high value found for E_x. Since we expect $E_{go} \sim 0.3$ eV, (4.4) shows that $E_x \sim 0.3$ eV, much larger than in V_2O_3 or VO. Therefore, for VO_2, we can only use (3.57) and (4.35) to conclude:

$$\frac{d \ln E_{go}}{dP} = - 1.4 \times 10^{-6} \text{ bar}^{-1} . \qquad (4.38)$$

Using the approximate value, $E_{go} \sim 0.3$ eV, (4.38) shows:

$$\frac{dE_{go}}{dP} \sim - 4 \times 10^{-7} \text{ eV bar}^{-1} .$$

We can use this approximation and equation (2.13) to calculate the contribution to β from volume changes. Since the volume change at the transition is so small in VO_2, we expect this term also to be very small. Taking for the compressibility the value measured [45] for the rather similar material, TiO_2, $\chi \sim 0.59 \times 10^{-6}$ bar^{-1}, equation (2.13) gives:

$$\beta = 0.05 \, E_{go}/N - (\partial E_{go}/\partial n)_{V, T} .$$

Therefore, the contribution due to explicit changes in volume is negligible, as we expected. The transition in VO_2 seems to be due to a crystalline distortion with little or no accompanying volume change. Thus hydrostatic pressure is actually a poor variable to use in the study of this material. It should be much more advisable to study the changes in electrical conductivity with uniaxial stress.

D. Ti_2O_3

In crystal structure, Ti_2O_3 appears to resemble V_2O_3 considerably. Pearson [19] studied Ti_2O_3 from 300°K to 650°K and found that the structure was that of corundum, as in V_2O_3. At 300°K, the lattice parameters are c_H = 13.64 Å, a_H = 5.15 Å. The c-axis expands and the a-axis contracts with increasing temperature, slowly, except in the neighborhood of 450-550°K. At 650°K, the lattice parameters of Ti_2O_3 and V_2O_3 are virtually the same. Abrahams [23] examined the structure of Ti_2O_3 down to 4.2°K and found the lattice constants to be within 0.5% of those at 300°K. Thus there is no phase transformation in Ti_2O_3, and the symmetry is rhombohedral at all temperatures. The only region resembling an anomalous one is the range 450-550°K, where the thermal expansion parameters sharply increase.

The magnetic structure of Ti_2O_3 is known unambiguously. Abrahams [23] performed neutron diffraction experiments over the temperature range 1.4°K. to 711°K and found that antiferromagnetism was present until a Néel temperature in the vicinity of 600°K. The magnetic structure was monoclinic, strikingly resembling the low temperature crystal structure of V_2O_3. Abrahams determined that the c-axis pairs were antiferromagnetically aligned, whereas the basal plane spins were all parallel. The spins were perpendicular to the c-axis, thus reducing the symmetry to monoclinic. The magnitude of the antiferromagnetic moment was about 0.2 Bohr magneton per cation.

Pearson [19] and Foëx and Wucher [52] have measured magnetic

found a jump in conductivity of a factor of 40 at about 550°K, approximately the experimental Néel temperature. The variation in T_o is unique to Ti_2O_3, and prevents us from deciding on an exact value for T_o. The most we can say is:

$$T_o = 450\text{-}550^{\circ}K . \qquad (4.4)$$

Since there is no crystalline distortion in the case of Ti_2O_3, it must be the antiferromagnetism which is responsible for the energy gap. Thus the theory of section II C is applicable. We must also decide whether the effective mass approximation or the narrow band limit is more appropriate. Theoretically, we expect the bands to be wider in Ti_2O_3 than in V_2O_3, since the overlap between Ti^{+++} ions should be significantly greater than that between the smaller V^{+++} ions. Furthermore, the c-axis pairs are 3% closer in Ti_2O_3, which would tend to increase the overlap, and hence the band width, in the t_o band, which we shall show in Chapter V is the band of interest in the case of Ti_2O_3. Experimentally, the presence of antiferromagnetism with such a small moment as 0.2 μ_B per cation is an indication of some degree of band width, as we noted in the discussion following equations (2.20). Application of the exact one-dimensional theory of section II C shows that a band width equal to three times the energy gap leads to a sublattice magnetization of 0.2 μ_B per cation. [We would expect in three dimensions that a smaller band width to band gap ratio could suffice for the same sublattice magnetization, since the density of states in the center of the Brillouin zone (low spin region) is far greater compared to that at the zone edges than in the one-dimensional case.] A band width considerably wider than the energy gap would seem to preclude use of the narrow band limit.

BLANK PAGE

An additional point is the low value of E_x found in equation (4.40), as compared with the $E_x > 0.6$ eV in V_2O_3. We can take this as evidence that polaron effects are not as important in Ti_2O_3 as in V_2O_3, as we shall discuss in Chapter VI. But this is still one more indication that the bands are relatively wide in Ti_2O_3. Finally, we note from our discussion of the Jahn-Teller effect in section II D that a lack of observable crystalline distortion is a wide band characteristic. Thus we conclude that it is probably more accurate to use the effective mass approximation than the narrow band limit for Ti_2O_3.

Unfortunately, the presence of an extra parameter, m^*, affords

a m a greater degree of freedom in the calculation of the transition temperature in this case than in the narrow band limit. Frederikse [53] measured the effective mass of the bottom of the lowest 3d band in TiO_2, and obtained:

$$\frac{m^*}{m} = 25 . \tag{4.42}$$

We shall use this value as the best available approximation, noting that the ratios of nearest neighbor cation-cation and cation-anion distances to cationic radii, probably the best single measures of overlap available, are virtually the same in TiO_2 and Ti_2O_3. Using (4.39) for E_{go}, the solution of equations (3.22) and (3.23) is:

$$\frac{E_{go}}{kT_o^*} = 0.6.$$

This shows that Boltzmann statistics are invalid, as might be expected with such a small energy gap. The general Fermi equations, (3.37) and (3.46) must be used. In the case of Ti_2O_3, the solution of (3.37) and (3.46), using (4.39) and (4.42), is:

$$\frac{E_{go}}{kT_o^*} = 1.4. \tag{4.43}$$

Equations (4.39) and (4.43) predict for the transition temperature:

$$T_o = 490^{\circ}K . \tag{4.44}$$

A comparison of (4.44) with (4.41) shows that this value is within the experimental range.

For this solution, the jump in carrier concentration at the transition is much smaller than those for the oxides of vanadium.

Furthermore, the wider bands of Ti_2O_3 should give a larger value for the mobility in the semiconducting state. These points should be reflected in the larger conductivity in the semiconducting region and a smaller jump in conductivity at the transition in the case of Ti_2O_3. As can be seen in Fig. I-1, this is indeed the experimental situation. Connected with this, however, is the fact that, for this solution, a large percentage of the available carriers have been excited before the transition. This probably means that the effective mass approximation begins to break down below T_o, and that (3.6) and (3.7) should be modified by introducing the details of the band structure. One possible way around this is to allow the effective mass in (3.35) to depend on temperature. If we add to the effective mass a small negative contribution linear in T, we find that the sharpness of the transition disappears, and the transition to the metallic state takes place over a small range of temperature. But this is just the peculiar characteristic of the transition in Ti_2O_3 which we noted previously. Furthermore, small deviations from stoichiometry could now cause large variations in T_o, and this may be the explanation of the wide range of experimental values of T_o, as given in (4.4).

Chapter V

MODELS FOR BAND STRUCTURE

In this chapter, we take the results of Chapter IV, togethe what is known about the structure of the various materials, and try to piece together the approximate band structure of each. Since some critical information is missing about every one of these materials, the band models presented here contain some guesswork. But they are all consistent with both the symmetry and the electrical properties of the crystals.

As we discuss in detail in Appendix B, little information can be gained from actual band structure calculations. For the sake of this chapter, we are primarily interested in the bands arising from the overlap of the 3d wave functions of the magnetic ions. We shall use the point of view presented in Appendix B to discuss these bands. In short, we begin with the tight binding approximation, taking the ionic wave functions to approximate the Wannier functions of the crystal. We also adopt the outlook of Anderson [8], in which the Wannier functions localized around the cations contain contributions due to overlap between the cations and all the ligands. These functions are primarily 3d ionic electron orbitals, but they contain finite amplitudes on the surrounding anions. For example, for a cation at the origin:

$$\psi(\vec{r}) = \psi_{3d}(\vec{r}) + \sum_i A_i \, \phi_{2p\,i}(\vec{r} - \vec{R}_i) \qquad (5.1)$$

where $\vec{R}_i$ are the positions of the oxygen ions. For our purposes, this enables us to proceed by ignoring the anions, assuming that they are

taken into account in some effective way by using functions such as (5.1). Functions of the form (5.1) can have finite overlap even when the cation wave functions $\psi_{3d}(\vec{r} - \vec{R}_m)$ have negligible overlap, since they can have finite amplitude on the same anion. We shall label the functions (5.1) by the type of ionic orbital of which they mainly consist.

We first note that since the ligands are large oxygen ions and are doubly charged, the octahedral crystal field is undoubtedly very large, and accordingly we expect a large separation of the t_{2g} and e_g bands. Experimentally, this splitting seems to be of the order of 1.5 eV or more. In these materials, where the 3d bands are relatively very narrow, this means that we can neglect the interaction between t_{2g} and e_g bands. For all the transition metal oxides, each cation is surrounded by an octahedral array of 0^{--} ligands. The negative charge clouds of the e_g orbitals are directed at these negative ligands, and therefore the e_g orbitals have a higher electrostatic energy than do the t_{2g} orbitals, which are directed between the ligands. Thus the t_{2g} bands are lower than the e_g bands. Since none of the oxides of titanium and vanadium have more than 6 3d electrons, we need not consider the e_g bands at all.

The t_{2g} bands contain 6N states per unit volume, which are not split any further by a pure cubic field. Tetragonal and trigonal fields split the t_{2g} band into two sub-bands, one with a concentration of 2 states per cation, the other with 4 states per cation. Monoclinic fields produce three sub-bands with 2 states per cation in each. The presence of antiferromagnetism or of a unit cell which consists of two cations can bring about a splitting in half of all the t_{2g} bands.

A. V_2O_3

For the corundum phase of V_2O_3, the trigonal field will split the t_{2g} band into a t_o and a $t_\pm$ band. The t_o band is associated with orbitals directed along the c-axis, the $t_\pm$ band with orbitals primarily in the basal plane. Below 150°K, the crystal has monoclinic symmetry, and the $t_\pm$ band is split into two sub-bands, which we shall call the t_a band and the t_b band. The c-axis pairs form the closest cation-cation distances, and these cations are in octahedral arrays of anions which share a common face. We should therefore expect a relatively large bonding-antibonding splitting of the t_o band. The monoclinic distortion, as we have demonstrated in Chapter IV leads to the pairing of cations in the basal plane, albeit with a somewhat larger cation-cation distance than along the c-axis. Thus the bonding-antibonding splitting of the t_a and t_b bands is relatively small. We infer that the t_o bonding band is lowest for V_2O_3, and that it is separated from the t_o antibonding band by an energy E_{g2}. The t_a bonding band is next lowest, and it is separated from the t_a antibonding band by an energy E_{g1}. We assume the situation is as given in Fig. V-1(a). Since the narrow band limit appeared to give good results for V_2O_3, we have drawn the bands as quite narrow, and thus there is no overlap. We shall give an order-of-magnitude estimate of the band width below. Each of the six sub-bands contains one state per cation. Thus, for V_2O_3, with two 3d electrons per V^{+++} ion, the bottom two bands are exactly filled at T = 0, while the top four bands are completely empty. The material is thus a narrow band semiconductor with

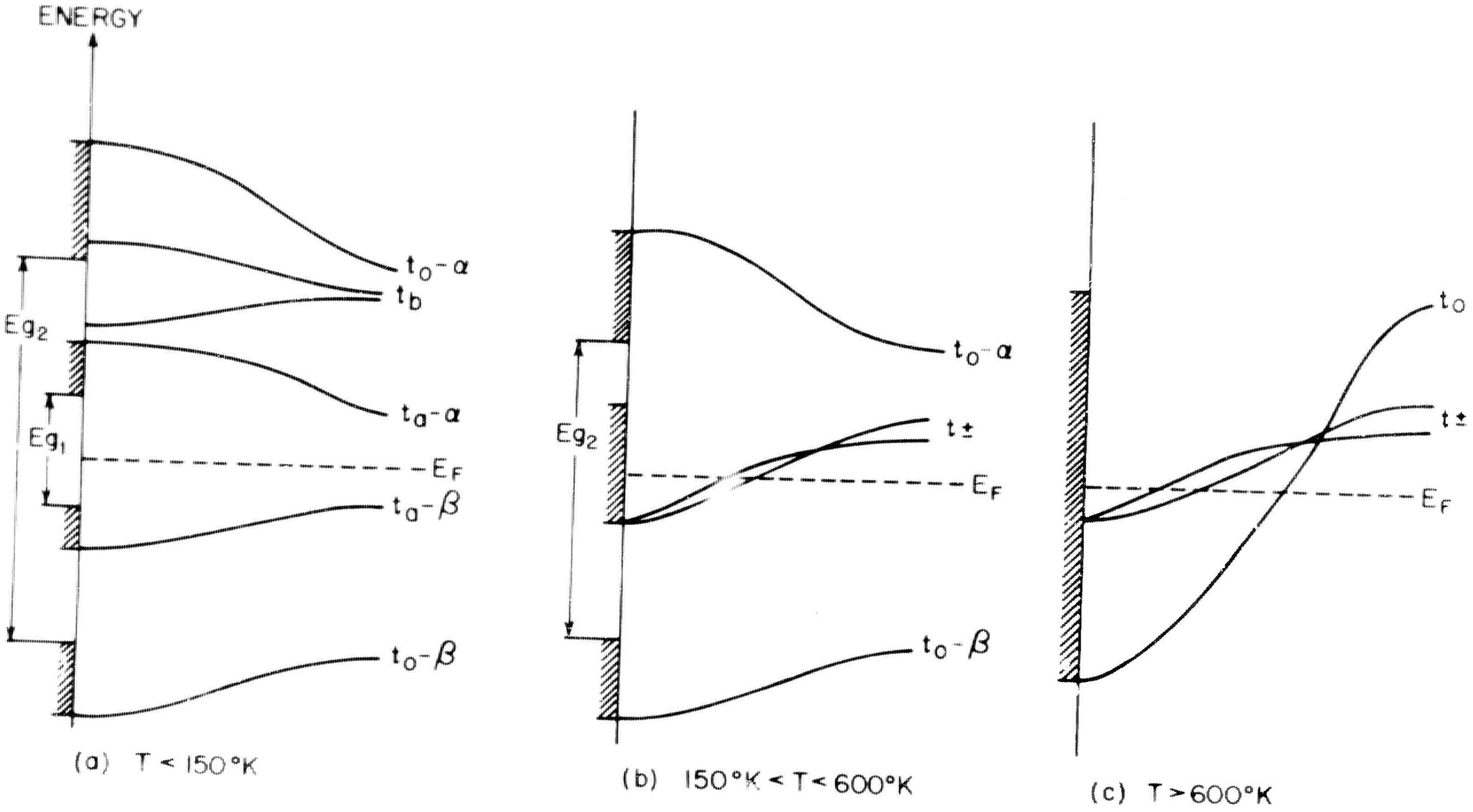

FIG. V-1 SUGGESTED BAND SCHEME FOR V_2O_3. THE SYMBOL α REFERS TO ANTIBONDING, β TO BONDING BANDS.

an energy gap E_{g1}. We determined in Chapter IV that $E_{g1} = 0.10$ eV. The theory presented there shows that at $T_o = 150^oK$, a phase transformation occurs due to the breaking up of the basal plane pairs, changing the crystal structure to the higher symmetry rhombohedral phase.

As a very rough estimate, we can use equations (2.18) to determine the band widths for V_2O_3. Since these equations were obtained from a one-dimensional model, we must consider these estimates as order-of-magnitude approximations at best. From (2.18):

$$E_b \sim \frac{2\hbar^2}{m^* a^2}. \tag{5.2}$$

For the t_o bands, the lattice parameter of interest is the c-axis pair distance of 2.70 Å, which yields:

$$(E_b)_{t_o} \sim 0.03 \text{ eV}. \tag{5.3}$$

For the $t_\pm$ bands, a ~2.88 Å, giving:

$$(E_b)_{t_\pm} \sim 0.02 \text{ eV}. \tag{5.4}$$

We have used for the effective mass the value calculated in section VI-E for the semiconducting state of V_2O_3: $\frac{m^*}{m} = 70$.

From 150^oK to 600^oK, the situation is now as shown in Fig. V-1(b). In this temperature range, V_2O_3 is a metal, the $t_\pm$ band being 1/4 filled. Thus T_o is also the temperature at which a semiconductor-to-metal transition occurs, as is experimentally observed. However, the theory of Chapters II and III now can be applied to the energy gap E_{g2} between the t_o bonding and the t_o antibonding bands. The application

of the final results of Chapter III is not immediately obvious in this case, since there are now electrons present in the gap between the two bands of interest. The situation is analogous to that of a normal semiconductor containing a large percentage of impurities. However note that we are concerned with the thermal excitation of electrons from the $t_o - \beta$ band to the $t_o - \alpha$ band, for it is this excitation which reduces the bonding and thus tends to close down the gap. The concentration of electrons in the $t_o - \alpha$ band is still given by (3.50), and the concentration of holes in the $t_o - \beta$ band is given by (3.51), with $E_g = E_{g2}$. But now the position of the Fermi level depends on the intermediate partially-filled band. If this band is approximately half-way between the $t_o - \beta$ and the $t_o - \alpha$ bands, $E_F = -E_g/2$, and the final result, (3.64), follows exactly as in Chapter III. If the intermediate band is nearer one or the other t_o band, the theory must be modified somewhat. Equation (2.1) should be generalized to:

$$E_g = E_{go} - \beta_n n - \beta_p p$$

since n and p are no longer equal. The results of Chapter II indicate that $\beta_n \approx \beta_p \approx \frac{\beta}{2}$. With this modification, it can be shown that (3.64) remains approximately true, even when the intermediate band is very close to one of the t_o bands.

Thus another transition is predicted at a temperature $T_t \sim 7E_{g2}/k$, at which point E_{g2} shrinks to zero, leaving one t_{2g} band 1/3 filled. The behavior, of course, is still metallic, and no striking change in conductivity will be observed at T_t. However, this transition changes the shape of the Fermi surface and could account for an

anomalous resistivity change such as the high temperature transition discussed in Chapter IV. From the temperature of this anomaly, $T_t = 600^\circ K$, we can estimate:

$$E_{g2} \sim 0.4 \text{ eV} .$$

Recall that the anomaly in resistivity at T_t resembled the additional resistivity due to spin-disorder scattering [see the discussion following equation (4.23)]. If V_2O_3 is antiferromagnetic at $T = 0$, then antiferromagnetism would contribute to the t_o band splitting. In particular, the antiparallel spin arrangement of c-axis pairs is just the magnetic configuration found by Abrahams [23] in Ti_2O_3. We would expect the same spin configuration in V_2O_3 as in the structurally similar Ti_2O_3, so this is a reasonable hypothesis. Then the theory predicts the breakdown of long-range order (i.e. the Néel point) to occur at $T_t = 600^\circ K$, and the high temperature anomaly of V_2O_3 is easily explained. We shall return to this point when we consider spin-disorder scattering resistivity in Chapter VI.

B. Ti_2O_3

In the case of Ti_2O_3, which has corundum structure at all temperatures, the trigonal field results in a splitting of the t_{2g} band into t_o and $t_\pm$ sub-bands. Experimentally as well as theoretically, the t_o band turns out to have lower energy than the $t_\pm$ band [54]. Since the structure of Ti_2O_3 below $500^\circ K$ is the same as that of V_2O_3 between $150^\circ K$ and $600^\circ K$, we might expect similar band schemes in these temperature ranges. However, as we demonstrated in Chapter IV, the bands in Ti_2O_3 are much wider than those in V_2O_3. The same

estimate which led to (5.3) and (5.4) can be used with the values $\frac{m^*}{m} = 25$, $a = 2.59$ Å to calculate the band widths in Ti_2O_3:

$$(E_b)_{t_o} \sim 0.10 \text{ eV}. \tag{5.5}$$

We know the energy gap due to the antiferromagnetism of c-axis pairs is 0.06 eV. Thus the ratio of band width to band gap is drastically different in Ti_2O_3 and V_2O_3. Note that the cation separation in the basal plane, which determines the bandwidth in (5.2) is considerably larger in Ti_2O_3 (3.02 Å) than in V_2O_3 (2.88 Å), whereas the separation of the c-axis pairs is in the opposite order for the two materials. Thus (5.2) estimates the $t_\pm$ bandwidth for Ti_2C_3 as:

$$(E_b)_{t\pm} \sim 0.06 \text{ eV}. \tag{5.6}$$

The band scheme for Ti_2O_3 below T_o is given in Fig. V-2(a). Since there is only one 3d electron present per cation, the t_o - β band, which corresponds to electrons primarily with spins on their own sublattice (analogous to the bonding bands in V_2O_3), is exactly filled, while all higher t_{2g} bands are completely empty. In this temperature range, Ti_2O_3 is therefore a semiconductor, with a gap of $E_g = 0.06$ eV, brought about by c-axis antiferromagnetism. The theory then predicts a semiconductor-to-metal transition at about $T_o = 500^\circ K$. Above $500^\circ K$, the band situation is given in Fig. V-2(b). In this range, the t_{2g} bands are 1/6 filled, and the material is metallic.

The details of the band structure presented here offer an alternative explanation for the spread-out nature of the transition in Ti_2O_3. This is the effect on the transition of the probable overlap of

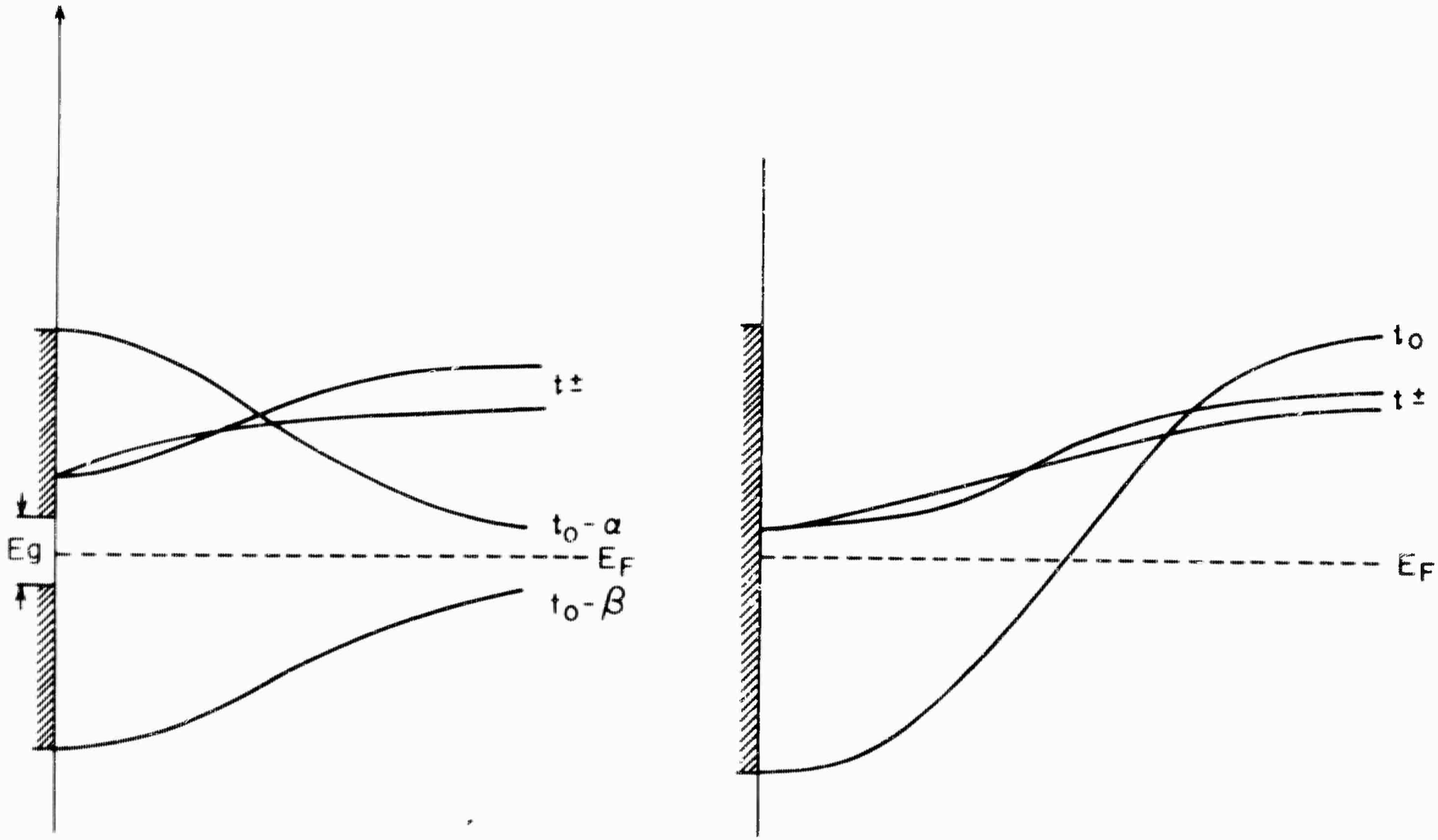

(a) T < 500°K

(b) T > 500°K

FIG. V-2 SUGGESTED BAND SCHEME FOR Ti_2O_3.

the $t_{\pm}$ band with the t_o - a (conduction) band. Since the transition in Ti_2O_3 does not occur until the conduction band is relatively well thermally populated, the significant change in density-of-states due to the $t_{\pm}$ band will clearly be important.

It should be noted that the main difference between Ti_2O_3 and V_2O_3 is the number of 3d electrons present per cation. V_2O_3 would be semiconducting up until the high-temperature transition were it not for the additional 3d electron on each V^{+++} ion. Then the conductivity would greatly resemble that of Ti_2O_3, despite the smaller gap and wider bands of the latter. Further evidence for this picture will be given in Chapter VI.

C. VO and TiO

Below 126°K, VO undergoes a distortion to orthorhombic symmetry, so that the t_{2g} bonding and antibonding bands are each split into three sub-bands, which we call t_x, t_y, t_z. The exact low temperature structure is as yet unknown, so that we cannot make any statement about the relative positions of these sub-bands. We arbitrarily take the orthorhombic lattice parameters to be smallest along the x-axis, largest along the z-axis. In the case of VO, we expect the bands to be wider than in V_2O_3, but probably not so wide as in Ti_2O_3, since the V^{++} ion is smaller in extent than is the Ti^{+++} ion. Whether or not there is overlap between the sub-bands is irrelevant in VO, as long as there is a real gap between the t_x bonding and the t_x antibonding bands. From experiment, we know that this gap exists and is about 0.10 eV. The band structure of VO below

126°K is sketched in Fig. V-3(a). There are three 3d electrons per cation, and so the lower three sub-bands are just filled, while the upper three sub-bands are completely empty. Thus VO is a semiconductor, whose gap of 0.10 eV is brought about by a crystalline distortion. The theory predicts a transition at T_o = 126°K to the situation as shown in Fig. V-3(b). Above T_o, VO has a 1/2 filled t_{2g} band and is metallic.

Note that TiO retains rock salt structure down to at least 4°K. The presence of antiferromagnetism has not been established, but since TiO contains only two 3d electrons per Ti^{++} ion, it must exhibit metallic behavior at all temperatures. As can be seen from the results of Morin's work [20] (see Fig. I-1), this is the case down to at least 1.5°K.

D. VO_2

The rutile phase of VO_2 has tetragonal symmetry, and splits the t_{2g} band into a t_a sub-band with 4 states per cation and a t_c band with 2 states per cation. Since c is considerably smaller than a in rutile VO_2, we expect the t_c band to be well below the t_a band. At low temperatures, the crystal undergoes a distortion to monoclinic symmetry, the c-axis cations of the rutile structure pairing and puckering somewhat. This monoclinic distortion has two effects. The t_a band is split into sub-bands, which we shall call the t_{a1} and the t_{a2} bands. But, more important, the t_c band is split into bonding and antibonding sub-bands by the pairing along the c-axis, which is a classic example of the theory of crystalline distortion given in

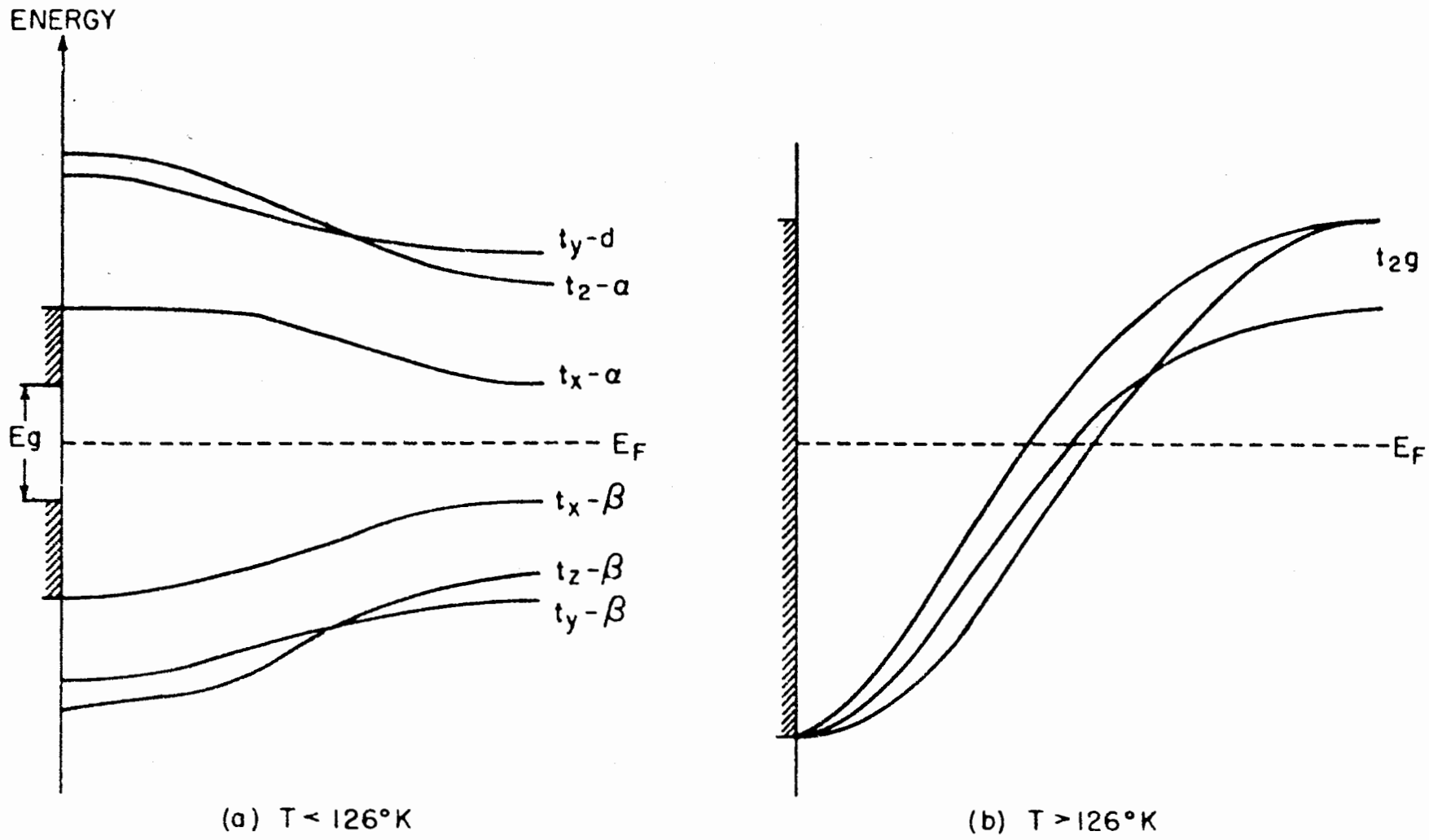

FIG. V-3 POSSIBLE BAND SCHEME FOR VO.

section II D. The distortion parameter ϵ is rather large, which tends to bring about a large energy gap, estimated in Chapter IV to be 0.3 eV. The band structure below $T_o = 340^oK$ is outlined in Fig. V-4(a). Since there is just one 3d electron per V^{++++} ion, the $t_c - \beta$ band is completely filled, and all higher bands are empty. The theory predicts a transformation at T_c to rutile structure. Above 340^oK, the band structure is given in Fig. V-4(b). It can be seen that the t_c band is 1/2 filled, resulting in a semiconductor-to-metal transition at 340^oK, as is observed.

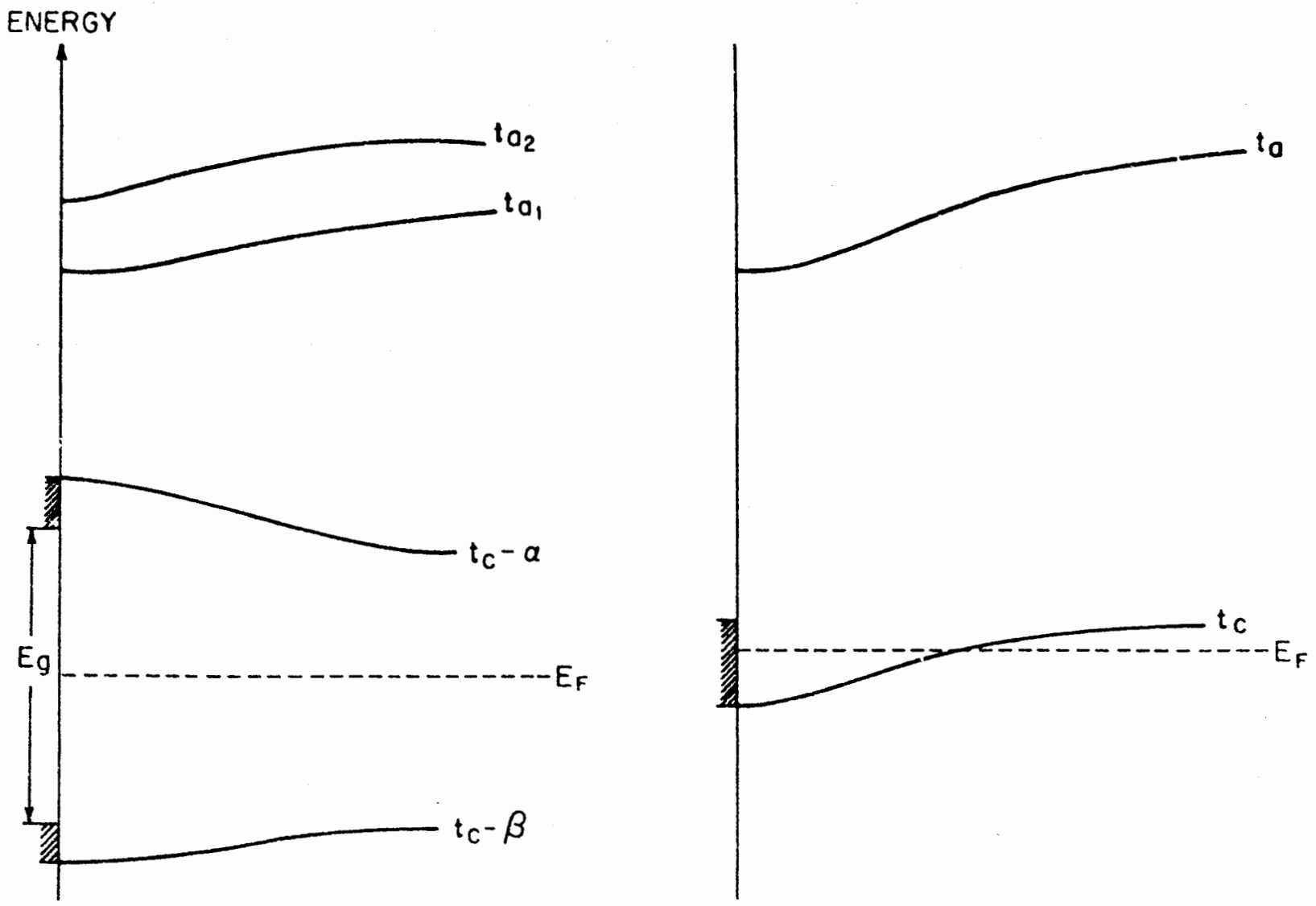

FIG. V-4 SUGGESTED BAND SCHEME FOR VO_2.

Chapter VI

DISCUSSION

A. The Metallic State of V_2O_3

Primarily because of the exhaustive work of Feinleib [21], much more is known about V_2O_3 than about any of the other materials which exhibit semiconductor-to-metal transitions. Therefore, much can be gained by considering V_2O_3 in more detail.

In view of the recent accurate measurements of the lattice parameter changes at the transition [37], we shall recalculate the latent heat of transformation and the Fermi energy from Feinleib's pressure measurements [21]. The Clausius-Clapeyron equation gives:

$$L = \frac{\Delta V}{V} \times V \times T_o \Big/ \frac{dT_o}{dP}$$

$$= \frac{.035 \times 30.8 \ \frac{cm^3}{mole} \times 152^oK}{3.86 \times 10^{-9} \ \frac{^oK \ \ cm^2}{dyne}}$$

$$= 1020 \ \frac{cal}{mole} = 0.044 \ \frac{eV}{molecule} \qquad (6.1)$$

We can use the value of latent heat to approximate the Fermi energy, as was done by Feinleib [55]. We assume no spin changes occur at the transition. The difference in free energy between the semiconducting and metallic states at the transition point can then be expressed:

$$0 = \Delta G = \Delta E - T_o \left(\Delta S_{electronic} + \Delta S_{lattice}\right)$$

$$\approx \Delta E - \frac{1}{2} \frac{\pi^2 k^2 T_o^2}{E_F} - kT_o \ . \qquad (6.2)$$

According to the model we presented in Chapter V, two 3d electrons per V_2O_3 molecule (one 3d electron per cation) contribute to the metallic band. Setting ΔE in (6.2) equal to half the value of the latent heat per molecule found in (6.1), we obtain:

$$E_F \approx \frac{\pi^2 k^2 T_o^2}{L - 2k T_o}$$

$$\approx 0.09 \text{ eV} . \qquad (6.3)$$

This is a reasonable magnitude for E_F, consistent with the orders of magnitude assumed in Chapter V for the band parameters in V_2O_3. With this value for E_F, the band width in the metallic state can be estimated as $E_b \sim 0.18$ eV. Note that $E_F = 7\ kT_o$, so that the usual statistical approximations are valid.

We can now use (6.3) to calculate the effective mass of electrons in the metallic state. In the effective mass approximation for metals [56]:

$$E_F = \frac{\hbar^2}{2m^*} (3\pi^2 N)^{2/3} . \qquad (6.4)$$

Hence:

$$\frac{m^*}{m} = \frac{\hbar^2}{2m} \frac{(3\pi^2 N)^{2/3}}{E_F}$$

$$= 50 . \qquad (6.5)$$

This order of magnitude effective mass is roughly what we would expect for V_2O_3. We can approximate the effective mass in the metallic state in another way, to check (6.5). Feinleib [57] has estimated the plasma frequency from optical data on the metallic state of V_2O_3 as:

$$\omega_p = 1.2 \text{ eV} .$$

But from the usual expression for the plasma frequency [58]:

$$\frac{m^*}{m} = \frac{4\pi N e^2}{m\omega_p^2}$$

$$= 45 .$$

This is in agreement with the approximation (6.5).

We can now use this value for the effective mass to calculate the relaxation time in the metallic state. From (4.22), we get for the conductivity just above the transition:

$$\sigma(T_o^+) = 4.6 \times 10^3 \text{ ohm}^{-1} \text{ cm}^{-1} . \tag{6.6}$$

Hence, the mobility is:

$$\mu = \frac{\sigma}{N e}$$

$$= 0.72 \text{ cm}^2/\text{volt-sec.} \tag{6.7}$$

The relaxation time, in view of (6.5), is:

$$\tau = \frac{\mu m}{e} \times \frac{m^*}{m}$$

$$= 2.0 \times 10^{-14} \text{ sec.} \tag{6.8}$$

This is a typical magnitude of relaxation time for a good metal. It is clear that the difference in mobility between metallic V_2O_3 and metals such as copper is solely due to the large effective mass in V_2O_3. This means that the carriers are moving much more slowly than they are in copper. Thus, although the average time between collisions, (6.8), is the same for V_2O_3 and copper, the average distance between collisions, or mean free path, is much lower for

V_2O_3. Using (6.3), we evaluate the velocity of carriers at the Fermi surface as:

$$u_F = \frac{2E_F}{m^*}$$

$$= 0.03 \times 10^8 \text{ cm/sec} . \qquad (6.9)$$

From (6.8) and (6.9), we find for the mean free path:

$$\Lambda = \tau u_F$$

$$= 6 \text{ Å} . \qquad (6.10)$$

Therefore, the mean free path is about $2\frac{1}{2}$ lattice constants in V_2O_3, as opposed to about 100 lattice constants in copper. All these values are consistent with the picture of a partially filled narrow band resulting in the observed metallic conductivity. However, we are approaching a borderline situation, since if the mean free path gets much below one lattice constant, the carriers are essentially localized and the bands can be considered to be washed out.

As the temperature is increased above T_o, kT increases, until at 600°K, it is almost half the Fermi energy, as given by (6.3). At this point, the statistical variations in Fermi energy begin to become important, and we are entering another borderline region. But here the high temperature transition helps retain metallic behavior. For at $T_t = 600^\circ$K, the t_g- β and the t_g- α bands merge, and above this temperature, there is essentially one relatively wide t_{2g} band, 1/3 filled. This means that the number of free electrons contributing to the metallic conductivity has doubled. Assuming the

effective mass remains the same, the doubling of N serves to increase the Fermi energy to:

$$E_F = 0.14 \text{ eV}. \tag{6.11}$$

We conclude that the experimental data on V_2O_3 above 150°K can be satisfactorily explained by the model presented in Chapters IV and V. However, the bands can probably not get much narrower and still maintain metallic conductivity. We shall add one more supporting argument in section B, where we consider spin-disorder scattering.

B. Spin-Disorder Scattering

The theory of spin-disorder scattering has been given by De Gennes and Friedel [46]. There are two main effects of this type of scattering, which we completely ignored in Chapter III. Firstly, there is a contribution to the resistivity, which is small when the spins are highly ordered (i.e. below T_N), but adds a term independent of temperature after long range order disappears. Secondly, there is the effect of the broadening of the bands due to spin disorder. This broadening will affect the relations developed between E_{go} and T_o.

If our hypothesis about V_2O_3 presented in Chapter V is correct, we can calculate the spin-disorder resistivity above T_N = 600°K, and compare it to the experimental jump in resistivity at T_t measured by Feinleib [21] [see discussion below equation (4.24)].

We first apply the theory of sections II C and III B to estimate the antiferromagnetic energy gap from T_N. Since we expect

narrow band theory to be applicable, equation (3.59) is the appropriate relation for E_{go}, and we find:

$$E_{go} = 0.4 \text{ eV} \tag{6.12}$$

as we already estimated in Chapter V (where we referred to this gap as E_{g2}). The energy gap is due to the coherent scattering arising from the exchange potential. But it is the incoherent scattering caused by this same potential which gives rise to the spin-disorder resistivity. Using the Born approximation and the extreme simplifications of spherical energy surfaces and quasi-free electrons, the spin-disorder resistivity above T_N can easily be calculated in terms of the energy gap.

Under the assumption of quasi-free electrons, the energy gap can be expressed as twice the Fourier component of the exchange potential:

$$E_{go} = 2 V_{\vec{k}\vec{k}'} \equiv 2 \int d\vec{r}\, \psi^*_{\vec{k}'}(\vec{r})\, V_{ex}(\vec{r})\, \psi_{\vec{k}}(\vec{r}) \tag{6.13}$$

where $\vec{k} - \vec{k}'$ is twice the Fermi momentum, $\vec{k}_F$. For the case of V_2O_3, using the value for E_{go} calculated in equation (6.12):

$$V_{\vec{k}\vec{k}'} = 0.2 \text{ eV} . \tag{6.14}$$

For spherical energy surfaces, the resistivity can be expressed [59]:

$$\rho_{SO} = \frac{3}{16\pi\, \hbar\, e^2 v^2 N} \int\int d\Omega\, d\Omega'\, |V_{\vec{k}\vec{k}'}|^2\, (1 - \cos\theta) . \tag{6.15}$$

Performing the integrations, (6.15) can be written:

$$\rho_{SO} = \frac{3\pi}{8} \left(4 - \frac{\pi^2}{4}\right) \frac{m(V_{\vec{k}\vec{k}'})^2}{\hbar e^2 N E_F} \left(\frac{m^*}{m}\right) . \tag{6.16}$$

But for the high temperature phase of V_2O_3, using (6.5), (6.11), and (6.14), equation (6.16) gives for the spin-disorder resistivity:

$$\rho_{SO} = 12 \times 10^{-4} \text{ ohm-cm.} \qquad (6.17)$$

This is just the value of $\rho_A(T)$ measured by Feinleib for the anomalous resistivity increase in V_2O_3 above 600°K. Although the values of Fermi energy and of the effective mass used in (6.16) are just rough approximations, they can both be arrived at by two different methods and we thus do not expect too much variation. Therefore, the agreement between theory and experiment can be considered quite good. However, we cannot prove the existence of antiferromagnetism in V_2O_3 by such arguments, since the agreement could be accidental.

If V_2O_3 were non-magnetic at all temperatures, there would be a contribution to resistivity from the spin-disorder scattering. In order to estimate this contribution from (6.15), we must use the appropriate values of E_F, N, and m^* for the range 150°K < T < 600°K, and we must approximate $V_{k\bar{k}'}$ in some way. One possibility is to assume that the exchange energy is the same for V_2O_3 as for Ti_2O_3. Then we can use the value of E_{go} in Ti_2O_3 to obtain:

$$V_{k\bar{k}'} = 0.03 \text{ eV}.$$

Evaluating (6.15) in this case gives:

$$\rho_{SO} = 1.4 \times 10^{-4} \text{ ohm-cm.} \qquad (6.18)$$

But the temperature independent part of the metallic resistivity as measured by Feinleib [21] and given in (4.23) is:

$$\rho_{T\text{-indep}} = 2.2 \times 10^{-4} \text{ ohm-cm.}$$

Thus (6.18) shows that spin-disorder scattering could account for almost 2/3 of the temperature independent part of the resistivity above T_o. The remaining 1/3 could be due to the effects of impurities, imperfections, or, as we shall see in section C, polaron formation. Clearly, spin-disorder resistivity, being of the order given by (6.18), is completely negligible in the semiconducting region.

It is also important to estimate the amount of broadening of the bands brought about by spin-disorder. Using the same assumptions as in equation (6.13), the perturbing potential due to spin disorder can be expressed as half the change in energy gap:

$$\langle V_{pert} \rangle = \frac{1}{2} (E_{go} - E_g) . \qquad (6.19)$$

Using equation (2.42) for the change in energy gap, we obtain from (6.19):

$$\langle V_{pert} \rangle = \frac{2n}{N} E_{go} . \qquad (6.20)$$

Thus, the mean square deviation in energy due to spin disorder is:

$$(\Delta E)^2 = E_{go}^2 \left(\frac{2n}{N}\right)^2 . \qquad (6.21)$$

Equation (6.21) shows that the effect of spin-disorder broadening is similar to the modifications brought about by a Gaussian spread around delta function bands in the narrow band limit, except that the spread is no longer constant, but depends on the amount of spin disorder, and thus on n. We have already worked out the case of a Gaussian spread in detail in section III B. Using (6.21) as the value for λ in equation (3.70), we obtain:

$$x = e^{-4y^2x^2} e^{y(1-4x)} , \tag{6.22}$$

Solving (6.22) gives:

$$\frac{E_{go}}{kT_o} = 7.6 . \tag{6.23}$$

Thus, spin-disorder broadening lowers the transition temperature somewhat, as we would expect.

C. Polaron Effects

A second effect which has not been considered thus far is polaron formation. It is clear from the extremely narrow band widths that only "small" polarons are involved in these materials. Holstein [10] has calculated the conductivity in the two cases where transport occurs in a polaron band and where an electron hops to a neighboring site. Conduction in a polaron band, which should dominate at very low temperatures, is characterized by an exponential decrease with increasing temperature. This is certainly not the situation in the oxides of vanadium and titanium. For thermally activated hopping, the experimentally observed temperature dependence is obtained. The activation energy in the temperature range where polaron hopping is the dominant mode of conduction is [10]:

$$(E_A)_{pol} = \frac{K}{\pi} \int_0^{\pi} \frac{dk(1 - \cos k)}{\omega_k^2} \tag{6.24}$$

where K is a constant depending on the masses of the ions and the strength of the electron-phonon interaction, and ω_k are the optical

phonon frequencies. Assuming a narrow-band vibrational spectrum (Einstein model), which is a good approximation for optical phonons:

$$\omega_k = \omega_o ,$$

we obtain from (6.24):

$$(E_A)_{pol} = \frac{K}{\omega_o^2} . \tag{6.25}$$

Although the mean phonon frequency can be expected to increase somewhat with pressure, the likelihood is small that it would change sufficiently to account for the decrease in activation energy by a factor of 2 at pressures of 20 kilobars, as measured by Feinleib [21] for V_2O_3 and by Austin [43] for V_2O_3 and VO. Thus it is unlikely that thermally activated hopping of polarons is the major contributor to the conductivity.

However, we can estimate the contribution of polaron effects to the pressure coefficient of the total activation energy from (6.25). Equation (6.25) implies:

$$\frac{d \ln (E_A)_{pol}}{dP} = - \frac{2 \, d \ln \omega_o}{dP} . \tag{6.26}$$

But Gruneisen's relation [60] shows:

$$\frac{d \ln \omega_o}{d \ln V} = - \frac{\alpha}{\rho \kappa c_v} \tag{6.27}$$

where α is the thermal expansion coefficient, ρ is the density, κ is the isothermal compressibility, and c_v is the specific heat at constant volume. Solving (6.27) for the pressure coefficient of ω_o:

$$\frac{d \ln \omega_o}{dP} = \frac{\alpha}{\rho c_v} \tag{6.28}$$

The values appropriate to V_2O_3 are $\alpha = 40 \times 10^{-6}\ (^\circ K)^{-1}$, $c_v = 6.7 \times 10^6$ dyne-cm/g-$^\circ$K, and $\rho = 5.0\ g/cm^3$. Substituting in (6.28), we find:

$$\frac{d \ln \omega_o}{dP} = 1.2 \times 10^{-6}\ bar^{-1} . \qquad (6.29)$$

Combining (6.26) and (6.29):

$$\frac{d \ln (E_A)_{pol}}{dP} = -2.4 \times 10^{-6}\ bar^{-1} . \qquad (6.30)$$

Comparing (6.30) to (4.21) and (4.22), we see that the contribution to the pressure coefficient from polaron effects is an order of magnitude smaller than the total observed value. We were therefore justified in neglecting polaron effects in the case of V_2O_3. A similar comparison for VO shows that the polaron contribution is a negligible part of (4.32). However, for VO_2, this is not the case. As we pointed out in section IV C, the polaron contribution to (4.36) is quite significant. In (4.36), we found:

$$\frac{dE_A}{dP} = -5.0 \times 10^{-7}\ eV\ bar^{-1} . \qquad (6.31)$$

Using (3.57), (4.35), and our estimate of $E_{go} \sim 0.3$ eV, we conclude:

$$\frac{1}{2} \frac{dE_{go}}{dP} = -2.1 \times 10^{-7}\ eV\ bar^{-1} . \qquad (6.32)$$

Putting (6.31) and (6.32) into (4.37):

$$\frac{dE_x}{dP} = -2.9 \times 10^{-7}\ eV\ bar^{-1} . \qquad (6.33)$$

Since $E_x \sim 0.3$ eV, (6.33) shows:

$$\frac{d \ln E_x}{dP} \sim -1.0 \times 10^{-6}\ bar^{-1} . \qquad (6.34)$$

Evaluating (6.28) for VO_2, we obtain:

$$\frac{d \ln (E_A)_{pol}}{dP} = -1.2 \times 10^{-6} \text{ bar}^{-1} . \qquad (6.35)$$

A comparison of (6.34) and (6.35) shows that polaron effects could be responsible entirely for the E_x obtained by Neumann et al [51] in VO_2. We expected VO_2 to be the material with the narrowest bands of those we considered. Consequently, we would expect the largest polaron effects in VO_2. It is significant that the value of $E_x \sim 0.3$ eV for VO_2 was indeed largest. For V_2O_3, which should have slightly wider bands than VO_2 has, $E_x \sim 0.07$ eV to 0.15 eV. For VO, $E_x \sim 0.1$ eV, similar to V_2O_3. Finally, for Ti_2O_3, where the effective mass approximation was found to give better results than the narrow band limit, (4.40) shows that $E_x \sim 0.01$ eV. It seems reasonable to conclude that polaron effects are responsible for at least a large part of E_x in these materials.

It is worth noting that the decrease in resistivity as a function of pressure in NiO, CoO, CuO, and MnO, as measured by Minomura and Drickamer [61], are considerably less sharp than they are in V_2O_3 and VO. For the former materials, the calculated changes in ω_o with pressure by means of (6.28) can completely account for the experimental pressure coefficients of E_A. Thus, for these transition metal oxides, the model of conduction by means of polaron hopping may indeed apply. Since we would expect the bands to be still narrower in these materials than in V_2O_3, which was, as we have seen, almost a borderline case, it is not surprising that they are non-conducting at all temperatures.

Polaron effects can also manifest themselves in the metallic region. For example, if there were a weak activation energy, so that

resistivity were of the form:

$$\rho \sim T\, e^{\frac{A}{kT}}$$

$$\sim T + \frac{A}{k}$$

then the activation energy would contribute to the temperature independent term in (4.23). As we showed in (6.18), spin-disorder scattering could account for at most 2/3 of this term. It is possible that polaron effects are responsible for the remaining 1/3.

D. Effects of Non-Stoichiometry

It is also important to consider the effects of deviations from stoichiometry, both in the form of impurities and imperfections, particularly in the materials under consideration, which are difficult to obtain in their pure form. For simplicity, we shall consider the case where there is a given number, N_d, of donor levels per unit volume. The case where acceptor levels are present follows analogously. Let n_i be the concentration of intrinsic carriers excited into the conduction band. At extremely low temperatures, it is possible to have electrons partly trapped on the donor sites; however, such temperatures are not reached in practice, so we shall ignore this region. At higher temperatures, the donors become completely ionized, and saturated extrinsic conductivity dominates. Here the concentration of carriers in the conduction band is given by:

$$n = N_d + \frac{N^2 e^{-E_g/2kT}}{N_d} \quad . \tag{6.36}$$

In this temperature region, the conductivity will not vary strongly with

temperature, but will vary with composition. As the temperature is increased, n_i becomes comparable with N_d, and the general expression for n must be used:

$$n = \frac{1}{2} N_d \left[1 + \left(1 + \frac{4n_i^2}{N_d^2} \right)^{1/2} \right] . \tag{6.37}$$

At still higher temperatures, intrinsic conductivity dominates, and n can be approximated by:

$$n = N e^{-E_g/2kT} + \frac{1}{2} N_d . \tag{6.38}$$

In this region, conductivity will exhibit an exponential temperature dependence, but be nearly independent of composition. In order to determine the extent of the intrinsic region, the experiments of MacMillan [42] are particularly useful. MacMillan obtained V_2O_3 samples by reducing V_2O_5 in hydrogen at different temperatures. He was thus able to vary the composition from $V_2O_{2.90}$ to $V_2O_{3.04}$. In measurements down to 100°K, it was found that conductivity, activation energy, and transition temperature were all independent of composition. This is strong evidence that conductivity is primarily intrinsic in this temperature range, and that equation (6.38) should be used to evaluate n.

The effect of donor and acceptor levels on the theory can now be determined. Equation (3.61) must be modified in the following way:

$$x = \left[e^{y(1 - 4x)} + 1 \right]^{-1} + \frac{1}{2} x_d \tag{6.39}$$

where $x_d \equiv N_d/N$. We are dealing with concentrations of impurities such that $N_d \ll N$, and thus $x_d \ll 1$. Solution of equation (6.39) shows

that the transition is moved only slightly: x_o is decreased and y_o is increased. The fractional increase in y_o is $2.8\, x_d$, or $2.8\, N_d/N$. Thus donor levels decrease the transition temperature. A similar calculation performed in the next section, shows that acceptor levels also tend to decrease T_o, in the same proportion as do donors.

Since the experimental results quoted in Chapter IV seem to be in the intrinsic conductivity region, the observed activation energies must still contain contributions of $1/2\ E_g$. Then, since the solution of (6.39) maintains the proportionality of E_{go} to T_o, equation (3.57) remains valid for small amounts of non-stoichic etry.

A major effect of small deviations from stoichiometry is the contribution of the corresponding scattering to the mobility. The mobility due to scattering by ionized impurities is given by the Conwell-Weisskopf formula [62]:

$$\mu_I = K \frac{(\frac{T}{T_I})^{3/2}}{|\ln(\frac{T}{T_I})|} \tag{6.40}$$

where K and T_I are constants which depend on the number of impurities and the dielectric constant of the material. Thus, if impurity scattering dominates, (6.40) shows that the contribution to the observed activation energy is:

$$(E_A)_I = \frac{3}{2} kT + \frac{kT}{|\ln(\frac{T}{T_I})|} \quad . \tag{6.41}$$

Since the number of impurities is small, $T_I \ll T$, and the first term of (6.41) is the important one. The activation energy due to

ionized impurities is thus small and somewhat temperature dependent. Since there is no pressure dependence of the activation energy given by (6.41), ionized impurity scattering cannot account for the pressure variation of the observed activation energies in V_2O_3, VO, or VO_2. Furthermore, we were justified in neglecting in Chapter IV the pressure dependence of the contributions to E_A from this type of scattering.

Scattering by neutral impurities or by dislocations are temperature independent, and are small except at very low temperatures [63]. Thus there is no contribution to E_x from these sources.

As we already pointed out, the transition temperatures observed in the oxides of vanadium do not seem to change with small deviations from stoichiometry. However, the measured T_o in Ti_2O_3 does seem to vary, although the fact that the transition is not very sharp makes it difficult to decide on an exact value for T_o in this case. It appears that the effects of non-stoichiometry can be important only in Ti_2O_3. Some supporting evidence for such a conclusion comes from the work of Yahia and Frederikse [22], who found that the Hall mobility in Ti_2O_3 obeys a Conwell-Weisskopf law below 150°K. Between 200°K and 450°K, polar scattering appears to predominate. All this is consistent with the idea that the relatively wide bands of Ti_2O_3 cause polaron effects to be negligible, whereas in the narrow bands of V_2O_3, VO, and VO_2, polaron effects are quite important.

E. The V_2O_3-Ti_2O_3 System

The models for V_2O_3 and Ti_2O_3 presented in Chapters IV and V taken together with the discussion of non-stoichiometry in section

VI-D enable us to make predictions about the electrical conductivity properties of the V_2O_3-Ti_2O_3 syste: . Substitution of Ti^{+++} for V^{+++} introduces holes in the valence band, since a Ti^{+++} ion has only one 3d electron and consequently acts like an acceptor.

Let x_a be the fractional amount of Ti^{+++} introduced into a crystal of V_2O_3. Thus $x_a = N_a/N$, where N_a is the concentration of acceptors. In general, we know:

$$p - n = N_a$$

$$np = n_i^2$$

so that:

$$p = \frac{1}{2} N_a \left[1 + \left(1 + \frac{4n_i^2}{N_a^2} \right)^{1/2} \right] . \tag{6.42}$$

In the narrow band limit, (6.42) becomes:

$$x = \frac{1}{2} x_a \left[1 + \left(1 + \frac{4}{x_a^2} e^{-E_g/2kT} \right)^{1/2} \right] \tag{6.43}$$

where $x \equiv p/N$ is the fractional amount of holes in the valence band. For small $x_a \ll 1$, equation (6.43) becomes:

$$x = e^{-E_g/2kT} + \frac{1}{2} x_a \tag{6.44}$$

which is the relation for acceptors analogous to (6.38). Introduction of (2.1) into (6.44) gives:

$$x = e^{-y(1-4x)} + \frac{1}{2} x_a \tag{6.45}$$

where $y = E_{go}/2kT$ as before. The solution of (6.45) shows that a small percentage of acceptors lowers the transition temperature by a

small amount. For example, when 1% Ti^{+++} is introduced into V_2O_3, the transition temperature determined by (6.45) decreases by 3%. The approximation leading to (6.45) is valid in the case of V_2O_3 up until 2% Ti^{+++} concentration.

As x_a gets large, we must return to the general relation, (6.43). When $N_a \gg n_i$, (6.43) can be written:

$$x = x_a + \frac{1}{x_a} e^{-E_g/kT} . \tag{6.46}$$

Introduction of (2.1) into (6.46) yields:

$$x = x_a + \frac{1}{x_a} e^{-2y[1-4(x-x_a)]} . \tag{6.47}$$

Using the notation:

$$X \equiv \frac{x_a(x - x_a)}{e^{2y}}$$

$$Y \equiv \exp\left[\frac{8y}{x_a} e^{2y}\right]$$

equation (6.47) becomes:

$$X = Y^X = Y^{Y^{Y^{\cdot^{\cdot^{\cdot}}}}} = \eta(Y) . \tag{6.48}$$

The transition occurs at:

$$y_o = \frac{x_a}{8e} \left(e^{-x_a/4e}\right) . \tag{6.49}$$

For values of x_a where (6.47) is valid, (6.49) shows that the transition temperature is extremely low. For $x_a = 0.1$, the transition occurs at $y_o = 33$, or, in the case of V_2O_3, at a temperature, $T_o = 18^\circ K$. Thus, substitution of 10% or more Ti^{+++} for V^{+++} in V_2O_3 lowers the transition

temperature sufficiently to produce metallic behavior at almost all normal temperatures. We found that for 2% or less Ti^{+++} in the crystal, the transition temperature is changed only slightly. When between 2% and 10% Ti^{+++} is introduced into V_2O_3, we are in an intermediate region, and the general expression, (6.43), must be used without further approximations. It can be shown that the predicted transition temperature begins to drop sharply when the Ti^{+++} concentration exceeds 8%.

Since we have considered only the extreme narrow band limit, we can solve only for the transition temperature, at which point the two bands overlap. We cannot find out if the large number of holes present in the valence band at low temperature are sufficient to produce a metal even below the transition point, since the zero width bands cannot give metallic behavior. The Fermi energy in this limit approaches the valence band as:

$$E_F = E_v + kT \ln \frac{1}{x_a}$$

for $0.1 < x_a < 1$. Since E_F cannot get lower than the top of the valence band, the holes can never become degenerate. But this is only because of the zero bandwidth assumption. Since we have some idea of the effective mass of carriers in V_2O_3 from the discussion in sections A and B, we can look at the effective mass approximation to investigate the degeneracy of the valence band holes.

In the effective mass approximation, metallic behavior sets in when:

$$N_a = \frac{1}{4} \left(\frac{2m_h kT}{\pi \hbar^2} \right)^{3/2} .$$

For greater acceptor concentration, the Fermi energy is below the top of the valence band. Using the value of $m^*/m = 50$, estimated in section A for metallic V_2O_3, we find:

$$N_a = \frac{1}{4}\left(\frac{50 \times 9 \times 10^{-4}}{3.14}\right)^{3/2} \times \left(\frac{T}{T_o}\right)^{3/2} \times \frac{N}{.0048}$$

$$= .10\left(\frac{T}{T_o}\right)^{3/2} N . \qquad (6.50)$$

Thus, for Ti^{+++} concentrations of 10% or more, metallic behavior should occur at all temperatures. At $T = 100^{\circ}K$, the holes in the valence band will be degenerate for concentrations of Ti^{+++} greater than 6%.

MacMillan [42] studied the $Ti_{2x}V_{2(1-x)}O_3$ system in detail. He found that substitution of Ti^{+++} in V_2O_3 in small amounts monotonically depressed the transition temperature. This effect was measured for concentrations up to 2%, and is just as predicted above. MacMillan also measured conductivity as a function of temperature for 10% and 50% Ti^{+++} concentrations. For 10% Ti^{+++}, the conductivity was metallic below $100^{\circ}K$, decreased slowly about a factor of 10^2 as the temperature was raised to $140^{\circ}K$, and then increased to its previous value somewhat more sharply. This is what is predicted by (6.50) for a concentration of 6%, and thus indicates that an effective mass of 70 free electron masses for holes in V_2O_3 in the semiconducting state is more appropriate than the value of 50 used in (6.50). Since $m^*/m = 50$ was the value estimated for metallic V_2O_3, we should expect a larger m^*/m for the narrower

bands of the semiconducting state.

For 50% Ti^{+++} concentration, MacMillan found a temperature-independent metallic conductivity, just as we would predict from the above theory. In this case, the t_a - β band is half-filled.

F. Thermally Activated Hopping Theories

Some authors [64] have suggested that the origin of the conductivity in the semiconducting state is thermally activated electron hopping. Then the observed activation energy should be totally associated with the mobility, and the concentration of carriers should be temperature independent. There is now much experimental evidence against this hypothesis. The direct measurement of the energy gap in V_2O_3 by Feinleib [24] and the measurement of the Hall coefficient in Ti_2O_3 by Yahia and Frederikse [22] strongly indicate the presence of a normal semiconducting energy gap with thermal activation of free carriers. Furthermore, a theory which ascribes conduction to a diffusion of charge predicts an increase in activation energy with pressure [5, 65]. Such an increase has been observed by Young et al. [65] in CoO, CuO, and Cu_2O. However, in the cases of V_2O_3, VO, VO_2, and Ti_2O_3, the activation energy decreases with pressure [21, 43, 51].

G. Theories which Postulate a Critical Lattice Parameter

The theory of Mott [4, 26, 27] assumes that there exists a critical lattice constant, R_c, above which there is insufficient overlap to obtain physically meaningful bands. Mott suggested that materials whose lattice parameters exceed R_c must be non-conducting, and all

the electrons have to be considered as localized on individual ions rather than spread throughout the crystal. One immediate difficulty with theories based on this hypothesis is the explanation of the conductivity below the transition. If thermally activated hopping is considered to be the conduction mechanism below T_o, all the objections of the previous section apply. It is hard to think of any other model employing localized electrons which can account for the considerable ($\sigma \approx 10$ ohm-cm) conductivity in the insulating states of VO_2 and Ti_2O_3. Other objections emerge from the details of the transition in Ti_2O_3 and in VO_2. At T_o in Ti_2O_3, the c-axis actually expands. Thus, the nearest neighbor cation distance is larger above T_o than it is below T_o. This is difficult to reconcile with the idea of a critical lattice spacing being exceeded at low temperatures but not at high temperatures. Furthermore, below T_o in VO_2, the c-axis cations pair up. Thus, the nearest neighbor cation distance is much smaller in the non-conducting state than it is in the conducting state. But also, the linear thermal expansion is such that at very high temperatures all cation-cation distances are greater than the distance between the more-separated c-axis cations at low temperatures. Thus, even a theory based on an average R_c also seems to fail.

As a final point, the transport properties of the $Ti_{2x}V_{2(1-x)}O_3$ system, discussed in section E, are not consistent with a theory which ascribes the transition to a critical value of the lattice parameter. In particular, $TiVO_3$, which has a structure with lattice constants very close to V_2O_3, is metallic even below 150°K, where both V_2O_3 and Ti_2O_3 are semiconducting.

H. Theories which Ascribe Lack of Conductivity to Direct Cation-Cation Interaction

Goodenough [28, 29, 30] has postulated that direct interactions between cations lead to the formation of homopolar bonds, and therefore a non-conducting state can occur if all the 3d electrons are used up in such bonds. As with Mott's theory, models based on this principle have great difficulty in explaining the low temperature conductivity and its behavior under pressure. There is also some independent experimental evidence which seems to contradict this particular hypothesis. In VO_2, the pairing of the c-axis cations is not in a straight line, but the pairs are puckered below T_o; yet in the high temperature rutile structure, all these cations are collinear. If cation-cation interaction was the dominant reason for the pairing, it is hard to see why the V^{++++} ions would not move directly towards one another. A more serious objection is the lack of anisotropy in conductivity of V_2O_3 between 150°K and 600°K. Goodenough's theory predicts that the conductivity should be almost entirely in the basal plane in this temperature range, the t_o electrons being tied up in homopolar bonds along the c-axis. As Feinleib [21] has shown, this is not in agreement with experiment.

Appendix A

CORRECTION FOR THE αT CONTRIBUTION TO THE ENERGY GAP

In section IIA, we wrote for the energy gap:

$$E_g = E_{go} - \alpha T - \beta n \tag{A.1}$$

where E_{go} is the gap at $T = 0$, $\alpha \equiv -(\partial E_g/\partial T)_n$, and $\beta \equiv -(\partial E_g/\partial n)_T$. In our fundamental equation, (2.1), we dropped the term linear in T. In this appendix, we shall show that this omission does not lead to any serious errors in the evaluation of conductivity as a function of temperature, which was carried out in Chapter III.

We shall calculate the effects of the term $-\alpha T$ in the case of V_2O_3. Consequently, we can specialize to the regions where the narrow band limit is applicable and Boltzmann statistics are valid. Then, equation (3.52) in the Boltzmann limit becomes:

$$n = N e^{-E_g/2kT} . \tag{A.2}$$

From equation (A.1):

$$\frac{dE_g}{dn} = -\beta - \alpha \frac{dT}{dn} \tag{A.3}$$

$$\frac{dE_g}{dT} = -\alpha - \beta \frac{dn}{dT} . \tag{A.4}$$

But, equation (A.2) shows:

$$\frac{dn}{dT} = n \left[\left(\frac{E_g}{2kT^2} \right) - \frac{1}{2kT} \frac{dE_g}{dT} \right] . \tag{A.5}$$

Using equation (A.4) in (A.5):

$$\frac{dn}{dT} = \frac{n}{2kT}\left[\frac{E_g}{T} + \alpha + \beta\frac{dn}{dT}\right] . \qquad (A.6)$$

Solving equation (A.6) for dn/dT:

$$\frac{dn}{dT} = \frac{n}{2kT}\,\frac{\frac{E_g}{T} + \alpha}{1 - \frac{\beta n}{2kT}} \qquad (A.7)$$

Substituting (A.7) into (A.3), we find:

$$\frac{dE_g}{dn} = -\beta - \frac{\alpha}{n}\,\frac{2kT - \beta n}{\frac{E_g}{T} + \alpha} . \qquad (A.8)$$

We may rewrite (A.8) as:

$$\frac{dE_g}{dn} = -\beta\left[1 + \frac{\alpha T}{\beta n}\,\frac{2kT - \beta n}{E_g + \alpha T}\right] . \qquad (A.9)$$

Thus, the fractional error in equation (2.1) is just:

$$\frac{\alpha T}{E_g + \alpha T}\left[\frac{2kT}{\beta n} - 1\right] .$$

For the cases of V_2O_3 and VO, when we evaluated β from thermodynamics, we found that virtually the entire contribution to β came from the term which gave the change in energy gap due to changing volume. We can assume that the same will be true in evaluating α. A thermodynamic argument [66], similar to that which led to equation (2.13), gives:

$$\alpha = \frac{\lambda}{\kappa}\left(\frac{\partial E_g}{\partial P}\right)_T - \left(\frac{\partial E_g}{\partial T}\right)_V$$

where λ is the thermal coefficient of volume expansion, and κ is the isothermal compressibility. Since we are taking the entire contribution to α to be the first term, we have:

$$\alpha = -\frac{\lambda}{\kappa}\gamma \qquad \text{(A. 10)}$$

where $\gamma \equiv -(\partial E_g/\partial P)_T$, as defined in equation (2. 10).

For V_2O_3, we use the experimental values given in section IV A:

$$\lambda = 40.0 \times 10^{-6}\ (^\circ K)^{-1}$$

$$\kappa = 0.58 \times 10^{-6}\ \text{bar}^{-1}$$

$$\gamma = 1.8 \times 10^{-6}\ \text{eV bar}^{-1}\ .$$

Then, (A. 10) yields:

$$\alpha = -1.2 \times 10^{-4}\ \text{eV}/^\circ K\ . \qquad \text{(A. 11)}$$

Thus, from (A. 9), the correction to β near the transition temperature is of the order of 2%. Thus, the dropping of the term in αT in equation (2. 1) introduces an error of the order of a few per cent, which is certainly negligible. Note that since α is negative in V_2O_3, equation (A. 9) shows that β is slightly reduced. This implies that the calculated ratio of E_{go} to kT_o obtained in Chapter IV should be a few per cent lower. Thus the transition temperature is increased a small amount, as we would expect, having introduced a slight increase, linear in temperature, to the gap.

Appendix B

ENERGY BAND CALCULATIONS

The spreading of localized ionic energy levels into energy bands is a consequence of the overlap between the wave functions corresponding to the ions which make up the crystal. We can easily show by perturbation theory that as long as there is some overlap, there must be some spreading of the localized levels, and thus a finite band width. It would be most desirable to be able to determine the energy band structure of given materials from first principles, but to date such calculations are long, laborious, and grossly in error. This has been particularly true in the case of transition metal compounds, where, for example, careful energy band calculations on NiO have led to conclusions that one of the best known insulators is a good metal [67] or that it forms a crystal consisting of neutral atoms [68]. One of the reasons for the general worthlessness of such calculations seems to be the inability to obtain correctly even order of magnitude estimation of overlap. Better results have been acquired for the band structure of crystals when overlap is treated as an experimental parameter.

What we are really interested in finding out is whether, in the real three-dimensional case, the exchange splitting in antiferromagnetic crystals or the splitting due to lower symmetry in distorted crystals is sufficient to produce true energy gaps in the densities of states. In an attempt to ascertain some information about this, we

shall outline an energy band calculation for VO. We shall consider the rock salt phase of VO, assume the crystal is an antiferromagnet, and try to determine how strong the exchange energy must be to obtain a true energy gap. The reason for choosing VO, although we do not believe VO to be antiferromagnetic, is purely the simplicity of its structure; a similar calculation for corundum Ti_2O_3 would be much more difficult. However, we expect that the orders of magnitude involved will be about the same in all the oxides of titanium and vanadium.

We shall adopt the point of view of the tight binding approximation, in which the Wannier functions of the crystal are approximated by the ionic functions of the component cations and anions. However, we shall make a further approximation, consistent with the spirit of the perturbation theory described by Anderson [8]. We shall take as the Wannier functions of the cations the V^{++} wave functions plus a small part of the wave functions at the surrounding oxygen sites. Then we shall use these wave functions to calculate the cation-cation overlap. By this method, we can neglect the anions after it is decided what percentage of O^{--} wave function to add to the V^{++} function at each cation site. As has been observed by Anderson [8], this method eliminates the distinction between direct cation-cation overlap and indirect cation-anion-cation overlap.

In an attempt to learn something about the real problem, we first look at a very simple model, a linear chain of alternating V^{++} and O^{--} ions. For further simplicity, we shall deal with only one state from each ion. Actually, there should be three states making

up the t_{2g} triplet. We place V^{++} ions with spin down at $x = (4n-1)a$, and V^{++} ions with spin up at $x = (4n+1)a$. The O^{--} ions are then put at $x = 2na$.

First, we neglect the O^{--} ions completely. There are V^{++} ions at $x = \pm a$. Let $\vec{\rho} \equiv (a\,0\,0)$. The wave functions are:

$$\phi_\alpha(\vec{r} - \vec{\rho}) = yz\,F(|\vec{r} - \vec{\rho}|)\,\alpha$$
$$\phi_\beta(\vec{r} + \vec{\rho}) = yz\,F(|\vec{r} + \vec{\rho}|)\,\beta \qquad \text{(B.1)}$$

where $F(r)$ is the appropriate radial function. Applying Schrödinger's equation, we obtain the secular equation:

$$0 = \begin{vmatrix} a - E & 2\beta\cos 2ka \\ 2\beta\cos 2ka & \hat{a} - E \end{vmatrix} \qquad \text{(B.2)}$$

where:

$$a \equiv \int d\vec{r}\,\phi_\alpha^*(\vec{r} - \vec{\rho})\,H_{\alpha\alpha}(\vec{r})\,\phi_\alpha(\vec{r} - \vec{\rho})$$
$$\hat{a} \equiv \int d\vec{r}\,\phi_\beta^*(\vec{r} + \vec{\rho})\,H_{\beta\beta}(\vec{r})\,\phi_\beta(\vec{r} + \vec{\rho})$$
$$\beta \equiv \int d\vec{r}\,\phi_\alpha^*(\vec{r} - \vec{\rho})\,H_{\alpha\beta}(\vec{r})\,\phi_\beta(\vec{r} + \vec{\rho})\,.$$

Solving (B.2):

$$E = \frac{a + \hat{a}}{2} \pm \sqrt{\left(\frac{a - \hat{a}}{2}\right)^2 + 4\beta^2\cos^2 2ka}\,. \qquad \text{(B.3)}$$

This solves the problem in terms of the physical quantities a and $\hat{a}$, and the non-physical quantity, β, which is the effective cation-cation overlap. Since a and $\hat{a}$ are intraionic integrals, they can be evaluated from the Hartree-Fock ionic wave functions. However, we must find

a way of approximating β.

We now redo the same problem, only taking this time as the V^{++} wave functions the above functions plus a small part of the O^{--} 2p functions. Then we can use perturbation theory to second order, neglecting all but the physical $V^{++} - O^{--}$ overlap, to evaluate both the mixing parameter and the effective cation-cation overlap, β.

Let:

$$\psi_\alpha(\vec{r} - \vec{\rho}) = \phi_\alpha(\vec{r} - \vec{\rho}) + \epsilon\left[\phi_{O^{--},1}(\vec{r}) + \phi_{O^{--},2}(\vec{r} - 2\vec{\rho})\right]$$
$$\psi_\beta(\vec{r} + \vec{\rho}) = \phi_\beta(\vec{r} + \vec{\rho}) + \epsilon\left[\phi_{O^{--},1}(\vec{r}) + \phi_{O^{--},2}(\vec{r} + 2\vec{\rho})\right]. \qquad \text{(B.4)}$$

The secular equation for this problem is, to first order in ϵ:

$$0 = \begin{vmatrix} a + 2\epsilon(\gamma + \gamma') + \epsilon^2(a' + \hat{a}') & 2\left[\epsilon(\gamma + \gamma')\right]\cos 2ka \\ 2\left[\epsilon(\gamma + \gamma')\right]\cos 2ka & \hat{a} + 2\epsilon(\gamma + \gamma') + \epsilon^2(a' + \hat{a}') \end{vmatrix} \qquad \text{(B.5)}$$

where:

$$\gamma \equiv \int d\vec{r}\ \phi_\alpha^*(\vec{r} - \vec{\rho})\, H(\vec{r})\, \phi_{O^{--},1}(\vec{r})$$

$$\gamma' \equiv \int d\vec{r}\ \phi_\alpha^*(\vec{r} - \vec{\rho})\, H(\vec{r})\, \phi_{O^{--},2}(\vec{r} - 2\vec{\rho})$$

$$a' \equiv \int d\vec{r}\ \phi_{O^{--},1}^*(\vec{r})\, H(\vec{r})\, \phi_{O^{--},1}(\vec{r})$$

$$\hat{a}' \equiv \int d\vec{r}\ \phi_{O^{--},2}^*(\vec{r} - 2\vec{\rho})\, H(\vec{r})\, \phi_{O^{--},2}(\vec{r} - 2\vec{\rho}).$$

Solving equation (B.5), we obtain:

$$E = \begin{cases} a + 2\epsilon\gamma + \epsilon^2\bar{a}' + \dfrac{4\epsilon^2\bar{\gamma}^2}{a - \hat{a}}\cos^2 2ka \\ \hat{a} + 2\epsilon\gamma + \epsilon^2\bar{a}' - \dfrac{4\epsilon^2\bar{\gamma}^2}{a - \hat{a}}\cos^2 2ka \end{cases} \qquad \text{(B.6)}$$

where $\bar{a} \equiv a' + \hat{a}'$; $\bar{\gamma} \equiv \gamma + \gamma'$. Comparing (B.6) to (B.3), we see that with the choice:

$$\epsilon = -\frac{2\bar{\gamma}}{a' + \hat{a}'}$$

we obtain:

$$\beta = \frac{\pm 2\bar{\gamma}^2}{|a' + \hat{a}'|} \tag{B.7}$$

The sign of β can usually be determined by physical considerations. The result, (B.7), is quite reasonable. It states that the effective cation-cation overlap is proportional to the product of two cation-anion-cation overlaps, which is what we would physically expect. Note that there is always a splitting of the two bands, equal to $|a - \hat{a}|$, the exchange energy, in this simple model. This is characteristic of one-dimensional models, as we saw in Chapter II.

With the result (B.7), we can calculate the important overlap parameter β from the Hartree-Fock wave functions for the V^{++} ion [69] and the O^{--} ion [70]. These Hartree-Fock functions are:

$$F_{O^{--}}(r) = \left[0.078\, e^{-0.71r} + 8.52\, e^{-3.41r} + 1.66\, e^{-1.38r}\right] r^2$$

$$F_{V^{++}}(r) = \left[1.74\, e^{-1.15r} + 19.8\, e^{-2.33r} + 37.9\, e^{-4.42r} + 19.3\, e^{-8.31r}\right] r^3 . \tag{B.8}$$

The potential $V_{O^{--}}$ was obtained by extrapolation from Brown's [71] calculations for Ne and F^-, the potentials being adjusted by scaling both ionic radii to the ionic radius of O^{--}. From Pauling [72]:

$$r_{O^{--}} = 1.76 \text{ Å}$$

$$r_{F^{-}} = 1.36 \text{ Å}$$

$$r_{Ne} = 1.12 \text{ Å} .$$

The extrapolation was linear, by necessity. The best analytic expression for the potential obtained is:

$$V_{O^{--}}(r) = \frac{2}{r}\left[4.42\, e^{-0.82r} + 4.68\, e^{-1.83r} + 0.90\, e^{-17.3r} - 2\right] . \qquad (B.9)$$

From Watson [69], we get for the average 3d electron energy in V^{++}:

$$E_{av} = -2.23 \text{ Ry.} = -30.3 \text{ eV} , \qquad (B.10)$$

Watson [70] gives as the 2p electron energy in O^{--}:

$$a' \approx \hat{a}' \approx -163 \text{ Ry.} = -2.2 \times 10^{3} \text{ eV} . \qquad (B.11)$$

Callaway [73] gives as the expression for the change in the Hartree-Fock energy when the spin of one electron is reversed:

$$E_{ex} = \frac{1}{7}\left[F^{2}(3d, 3d) + F^{4}(3d, 3d)\right] .$$

Using the values calculated by Watson [69] for V^{++}:

$$E_{ex} = \frac{1}{7}(0.669 + 0.417) \text{ Ry.}$$

$$= 0.15 \text{ Ry.} = 1.9 \text{ eV} . \qquad (B.12)$$

From (B.10) and (B.12), we get:

$$a = 2.31 \text{ Ry.} = 31 \text{ eV} ,$$

$$\hat{a} = 2.15 \text{ Ry.} = 29 \text{ eV} . \qquad (B.13)$$

Only γ remains to be evaluated.

We know from the usual tight binding approximations [74]:

$$\gamma \approx \int d\vec{r}\, \phi_{V^{++}}(\vec{r})\, W(\vec{r})\, \phi_{O^{--}}(\vec{r} - \vec{\rho}_3) \qquad \text{(B.14)}$$

where $W(\vec{r})$ is the difference between the one-electron crystalline potential and the potential of an isolated V^{++} ion, and $\vec{\rho}_3 \equiv (001)a$ is the position of a nearest neighbor oxygen ion. We shall make the following assumptions about $W(\vec{r})$:

(i) $W(\vec{r}) = 0 \qquad (r < a/2)$

(ii) $W(\vec{r}) = V(\vec{r}) \qquad (r > a/2)$

where $V(\vec{r})$ is the anion potential centered on the nearest neighbors. Hence:

$$W(\vec{r}) = V_{O^{--}}(\vec{r} - \vec{\rho}_3) \equiv V_{O^{--}}(\vec{r}') \qquad (r > \tfrac{a}{2})$$

$$\phi_{O^{--}}(\vec{r}) = \frac{F_{O^{--}}(r')}{r'} \frac{1}{\sqrt{2}} \left[Y_{1,1}(\theta', \phi') - Y_{1,-1}(\theta', \phi')\right]$$

$$= \sqrt{\frac{3}{4\pi}} \frac{F_{O^{--}}(r')}{r'} \sin\theta' \cos\phi' \qquad \text{(B.15)}$$

$$\phi_{V^{++}}(\vec{r}) = \frac{F_{V^{++}}(r)}{r} \frac{1}{\sqrt{2}} \left[Y_{2,1}(\theta, \phi) - Y_{2,-1}(\theta, \phi)\right]$$

$$= \sqrt{\frac{15}{4\pi}} \frac{F_{V^{++}}(r)}{r} \cos\theta \sin\theta \cos\phi \,.$$

Then (B.14) becomes:

$$\gamma \approx \frac{3\sqrt{5}}{4\pi} \int_{\text{all space}} d\vec{r} \left[\frac{F_{O^{--}}(r')\, V_{O^{--}}(r')\, F_{V^{++}}(r)}{r r'} \cos\theta \sin\theta \sin\theta' \cos^2\phi\right]$$

$$- \frac{3\sqrt{5}}{4\pi} \int_{\text{sphere: } r < 2} d\vec{r} \ [\text{same integrand}] \,. \qquad \text{(B.16)}$$

We shall use prolate spheroidal coordinates, with foci at $\vec{r} = 0$, $\vec{\rho}_3$. Then (B. 16) can be written:

$$\gamma \approx \frac{3\sqrt{5}a}{4\pi} \int_0^{2\pi} d\phi \cos^2\phi \int_{-1}^{1} d\eta \int_1^{\infty} d\zeta \; F_{O^{--}}(r') V_{O^{--}}(r') P_{V^{++}}(r)$$

$$\times \left(\frac{r^2 - r'^2 - a^2}{ra}\right)\left[1 - \left(\frac{r^2 - r'^2 - a^2}{ra}\right)^2\right]^{1/2}\left[1 - \left(\frac{r^2 - r'^2 + a^2}{ra}\right)^2\right]^{1/2}$$

$$- \frac{3\sqrt{5}a}{4\pi} \int_0^{2\pi} d\phi \cos^2\phi \int_{-1}^{0} d\eta \int_1^{1-\eta} d\xi \quad [\text{same integrand}]$$

where:

$$\xi \equiv \frac{r + r'}{a}; \qquad \eta \equiv \frac{r - r'}{a}.$$

Thus:

$$r = \frac{a}{2}(\xi + \eta); \quad r' = \frac{a}{2}(\zeta - \eta); \quad r^2 - r'^2 = a^2\xi\eta.$$

In the case of VO, a = 2.04 Å = 4.0 a.u. The integrals are all elementary, being of the form $\int dx\, x^n e^{-ax}$. After a long, laborious calculation, we obtain from (B. 17):

$$\gamma = 1.06 \text{ Ry.}$$

Thus, from (B. 7) and (B. 11):

$$\beta = \pm 0.0138 \text{ Ry.} = \pm 0.19 \text{ eV}. \qquad \text{(B. 18)}$$

Equation (B. 18) gives the effective value of cation-cation overlap in VO. We must still perform the band calculation for the VO structure. This is extremely lengthy, and we shall just outline it. In obtaining (B. 18), we used only one state, $\phi_1 = \sqrt{15/2\pi}\, y\, z\, F(r)$, of the t_{2g} triplet. We must also consider the other two degenerate states:

$$\phi_2 = \sqrt{\frac{15}{2\pi}}\, xz\, F(r)$$

$$\phi_3 = \sqrt{\frac{15}{2\pi}}\, xy\, F(r)\ .$$

Introduce the notation:

$$\alpha_{mn} \equiv \int d\vec{r}\, \phi_m^*(\vec{r} - \vec{R}_i)\, W(\vec{r} - \vec{R}_i)\, \phi_n(\vec{r} - \vec{R}_i)$$

$$\beta_{mn}(\vec{R}_{ij}) \equiv \int d\vec{r}\, \phi_m^*(\vec{r} - \vec{R}_i)\, W(\vec{r} - \vec{R}_j)\, \phi_n(\vec{r} - \vec{R}_j)\ . \qquad \text{(B. 19)}$$

All off-diagonal elements $\alpha_{mn} = 0$. The diagonal elements are equal, and we have called them $\alpha_{11} = \alpha_{22} = \alpha_{33} \equiv \alpha$. Restricting the overlap integrals to nearest neighbors only, we find:

$$\beta_{12}(R_{xz}) = \beta_{12}(R_{xy}) = \beta_{13}(R_{xz}) = \beta_{13}(R_{yz}) = \beta_{23}(R_{xy}) = \beta_{23}(R_{yz}) = 0$$

$$\beta_{12}(R_{yz}) = \beta_{13}(R_{xy}) = \beta_{23}(R_{xz}) \equiv \beta''$$

$$\beta_{11}(R_{xz}) = \beta_{22}(R_{xy}) = \beta_{33}(R_{yz}) \equiv \beta$$

$$\beta_{11}(R_{yz}) = \beta_{11}(R_{xy}) = \beta_{22}(R_{yz}) = \beta_{22}(R_{xz}) = \beta_{33}(R_{xy}) = \beta_{33}(R_{xz}) \equiv \beta'$$

Since the potential $W(\vec{r})$ is negative everywhere, we can conclude from the definitions, (B. 19), that $\beta > 0$, $\beta' < 0$. We now introduce the spin dependence, which implies a distinction between the potentials for a spin-up and a spin-down electron, W^{α} and W^{β}. This leads to the introduction of the quantities $\hat{\alpha}$, $\hat{\beta}$, $\hat{\beta}'$, $\hat{\beta}''$ for the "excited" band. The secular equation is a 6×6 determinant, which is quite complicated and not worth reproducing here. Since we are really interested in just the antiferromagnetic splitting, we set $\beta'' = 0$, which essentially factors the secular determinant into three equivalent 2×2 sub-determinants. For simplicity, we also make the assumptions

$\hat{\beta} = \beta$, $\hat{\beta}' = \beta'$, which are undoubtedly quite accurate within our range of error. The secular equation is now simply:

$$0 = \begin{vmatrix} a + 2\beta\cos(k_x - k_z)a + 2\beta'[\cos(k_y + k_z)a + \cos(k_x + k_y)a] - E & 2\beta\cos(k_x + k_z)a + 2\beta'[\cos(k_y - k_z)a + \cos(k_x - k_y)a] \\ 2\beta\cos(k_x + k_z)a + 2\beta'[\cos(k_y - k_z)a + \cos(k_x - k_y)a] & \hat{a} + 2\beta\cos(k_x - k_z)a + 2\beta'[\cos(k_y - k_z)a + \cos(k_x - k_y)a] - E \end{vmatrix} \tag{B.20}$$

Noting from (B.12) and (B.18) that $|\beta|, |\beta'| \ll |a - \hat{a}|$, the solution of (B.20) can be expressed:

$$\begin{aligned} E_c = {} & a + 2\beta\cos(k_x - k_z)a + 2\beta'[\cos(k_x + k_y)a + \cos(k_y + k_z)a] \\ & + (a - \hat{a})^{-1}\{4\beta^2\cos^2(k_x + k_z)a + 4\beta'^2[\cos(k_x - k_y)a \\ & + \cos(k_y - k_z)a]^2 + 4\beta\beta'\cos(k_x + k_z)a[\cos(k_x - k_y)a \\ & + \cos(k_y - k_z)a]\} \\ E_v = {} & \hat{a} + 2\beta\cos(k_x - k_z)a + 2\beta'[\cos(k_x + k_y)a + \cos(k_y + k_z)a] \\ & - (a - \hat{a})^{-1}\{\text{same expression as in curly brackets above}\} \end{aligned} \tag{B.21}$$

with both the valence and conduction bands three-fold degenerate. Since VO has three 3d electrons per cation, the valence band in this approximation will be completely filled and the conduction band completely empty provided that E_c and E_v do not overlap.

From (B.21), the top of the valence band occurs at the two

points in the first Brillouin zone:

$$\vec{k} = \frac{\pi}{4a}\ (1, -1, 1)$$
$$\vec{k} = \frac{\pi}{4a}\ (-1, 1, -1)\ . \qquad \text{(B.22)}$$

At these points:

$$(E_v)_{max} = \hat{a} + 2\beta + 4|\beta'|\ . \qquad \text{(B.23)}$$

It is much more difficult to find the bottom of the conduction band, since there is no point in k-space where the terms in E_c are individually minimized.

Up until this point, we have been completely general. It is now necessary to put in values for β, β', a, $\hat{a}$ in order to proceed. However, note that the bottom of the conduction band must be higher than:

$$(E_c)_{min} > a - 2\beta - 4|\beta'| - \frac{4\beta^2 + 16(\beta')^2 + 16\beta|\beta'|}{a - \hat{a}}\ .$$

Thus, there is always an energy gap if:

$$(a - \hat{a}) > 4\beta + 8|\beta'| + \frac{4(\beta + 2|\beta'|)^2}{a - \hat{a}}\ . \qquad \text{(B.24)}$$

In order to evaluate β', we use the relationship found by Fletcher [75] for the ratio of the same overlap integrals in the case of the 3d electrons of metallic nickel:

$$\frac{\beta'}{\beta} = -0.297$$

Equation (B.18) then yields:

$$\beta' = -0.041 \text{ Ry.} = -0.06 \text{ eV}\ . \qquad \text{(B.25)}$$

We can now use (B.12), (B.18), and (B.25) to test equation (B.24). We find:

$$a - \hat{a} = 1.9 \text{ eV}$$

$$4\beta + 8|\beta'| + \frac{4(\beta + 2|\beta'|)^2}{a - \hat{a}} = 1.4 \text{ eV} .$$

Thus equation (B.24) is satisfied, and the true energy gap is at least 0.5 eV.

We can also easily obtain an upper limit for the band width. From (B.21), it is clear that:

$$E_b < 4\beta + 8|\beta'| + \frac{4(\beta + 2|\beta'|)^2}{a - \hat{a}}$$

$$< 1.4 \text{ eV} .$$

In order to find the real values of E_c and E_b, we must locate the conduction band minimum. Since $\beta > |\beta'|$, the minimum occurs near the planes, $k_x = k_z \pm \pi/a$. Minimizing the other terms subject to this constraint, it can be seen that the bottom of the conduction band is in the vicinity of the twelve points equivalent to:

$$\vec{k} = \frac{\pi}{4a}(1, 1, -3) .$$

The conduction band minimum is approximately:

$$(E_c)_{min} = a - 4\beta - 4|\beta'| + \frac{4\beta'^2}{a - \hat{a}} \qquad (B.26)$$

Comparing (B.26) to (B.23), we conclude:

$$E_g = (a - \hat{a}) - 4\beta - 4|\beta'| + \frac{4(\beta')^2}{a - \hat{a}}$$

$$= 0.9 \text{ eV} , \qquad (B.27)$$

It is clear from (B.21):

$$E_b = 4\beta + 4\beta' - \frac{4(\beta')^2}{a - \hat{a}}$$

$$= 1.0 \text{ eV} , \qquad \text{(B.28)}$$

It is also useful to calculate the effective masses. The effective mass of holes in the valence band is easily determined from (B.21). It is found that the band is extremely anisotropic near the maximum; the diagonalized effective mass tensor can be expressed, in units of the free electron mass:

$$m_1^* = 4; \quad m_2^* = 10; \quad m_3^* = 90. \qquad \text{(B.29)}$$

Defining a "density-of-states" effective mass as:

$$m^* \equiv M(m_1^* m_2^* m_3^*)^{1/3}$$

(B.29) shows:

$$m^* = 31. \qquad \text{(B.30)}$$

The final results, (B.27) and (B.28), are each about a factor of 5 greater than we expected from the experimental observations in Chapters IV and V. This is undoubtedly due to proportional overestimates of the important band parameters $(a - \hat{a})$, β, and β'. Such overestimates are a general characteristic of band calculations. The explanation may be in covalency effects, most of which are neglected in this type of calculation, or it may be due to a serious deviation of the ionic wave functions in the crystal from those of the isolated ions. Note that the effective mass value, given by (B.30) is quite reasonable for VO.

Appendix C

HYDROGEN MOLECULE AND MOLECULAR ION WITH DELTA-FUNCTION INTERACTIONS

In section II D, we solved the problem of a one-dimensional crystal with two cations per unit cell, the cations attracting the 3d electrons by means of a delta-function interaction. We demonstrated that, when there is one 3d electron per cation, such a crystal will be semiconducting due to the doubling of the periodicity arising from the pairing of cations. As we showed in section II D, excitation of an electron across this energy gap tends to decrease the gap. However, it is not obvious that such excitation also tends to increase the average distance between the closely-spaced cations.

In order to demonstrate the decrease of crystalline distortion as electrons move from bonding to antibonding bands, we used an analogy relating to the hydrogen molecule and the hydrogen molecular ion. With both electrons in an H_2 molecule in bonding orbitals, the equilibrium distance between the two H^+ ions is 0.74 Å [76]. If one of the two electrons is placed in an anti-bonding orbital, the molecule is no longer bound, and the equilibrium distance becomes infinite. In the band situation, it is more reasonable to look at one electron being taken out of a bonding orbital and put into an antibonding orbital in another unit cell. Thus, we should compare the H_2 equilibrium distance with that of an H_2^+ molecular ion, whose H^+ ions are 1.06 Å apart [77]. Therefore, the H^+ ions move apart a factor of 1.43 when an electron is removed from a bonding orbital.

However, the first case worked out in section II D is for electrons attracted to the cations by delta-function interactions, which are essentially infinitely screened Coulomb interactions, and are very different from pure Coulomb potentials as can be seen from the work of Kohn [31] discussed in Chapter I. Therefore, it is important to see if the hydrogen molecule analogy holds up if the electrons are attracted to the H^+ ions by means of a delta-function potential. Such a calculation is the purpose of this appendix.

Consider an "H_2^+" molecular ion, with the following Hamiltonian:

$$H = -\frac{\hbar^2}{2m}\frac{d^2}{dx^2} - V\,\delta(x) - V\,\delta(x - X) + \frac{e^2}{X} \qquad (C.1)$$

where $X > 0$ is the distance between the H^+ ions. Take the zero of energy at e^2/X. Then Schrödinger's equation can be written:

$$H\,\phi(x) = E_+\,\phi(x)\ . \qquad (C.2)$$

The true energy is:

$$E = E_+ + \frac{e^2}{X}\ . \qquad (C.3)$$

Let:

$$k \equiv \sqrt{\frac{-2m\,E_+}{\hbar^2}}$$

For $x = (-\infty, 0)$, equations (C.1) and (C.2) give:

$$\phi''(x) - k^2\,\phi(x) = 0\ . \qquad (C.4)$$

Solving (C.4), and applying the boundary condition at $x = -\infty$:

$$\phi(x) = A\,e^{kx}\ . \qquad (C.5)$$

Similarly, for $x = (0, X)$, the solution of equation (C.2) is:

$$\phi(x) = B\, e^{kx} + C\, e^{-kx} . \qquad (C.6)$$

Finally, in the region $x = (X, \infty)$, the solution of (C.2), using the boundary condition at $x = \infty$, is:

$$\phi(x) = D\, e^{-kx} . \qquad (C.7)$$

From (C.5) and (C.6), continuity at $x = 0$ implies:

$$A = B + C . \qquad (C.8)$$

Similarly, from (C.6) and (C.7), continuity at $x = X$ yields:

$$B\, e^{2kX} = D + C . \qquad (C.9)$$

Integrating (C.4) from $x = 0^-$ to $x = 0^+$:

$$\phi'(0^+) - \phi'(0^-) = -\eta\, \phi(0) \qquad (C.10)$$

where:

$$\eta \equiv \frac{2mV}{\hbar^2}$$

Similarly, integration of (C.4) from $x = X^-$ to $x = X^+$ implies:

$$\phi'(X^+) - \phi'(X^-) = -\eta\phi(X) . \qquad (C.11)$$

Using (C.5), (C.6), and (C.7), equations (C.10) and (C.11) yield:

$$B - C - A = -\frac{\eta}{k} A \qquad (C.12)$$

$$D - C + B\, e^{2kx} = \frac{\eta}{k} D . \qquad (C.13)$$

Solving (C.8), (C.9), (C.12), and (C.13):

$$B = \frac{\eta}{2k}\, e^{-2kx}\, D$$

$$B = \frac{(2k - \eta)^2}{2k\eta}\, D . \qquad (C.14)$$

Equations (C. 14) have a non-trivial solution only if:

$$\eta^2 e^{-2kX} = (2k - \eta)^2 . \qquad \text{(C. 15)}$$

Let $\gamma \equiv 2k - \eta$. Then (C. 15) can be written:

$$e^{-\frac{1}{2}(\eta+\gamma)X} = \pm\gamma \qquad \text{(C. 16)}$$

Let $a \equiv e^{-\frac{1}{2}\eta X}$. Then (C. 16) becomes:

$$\pm\frac{\gamma}{a} = a^{\frac{\gamma}{\eta}} = (a^a)^{\frac{\gamma}{\eta a}} \qquad \text{(C. 17)}$$

Let $M \equiv \gamma/\eta a$; $N \equiv a^a$. Equation (C. 17) is now expressed:

$$\pm M = N^M . \qquad \text{(C. 18)}$$

There are thus two solutions to Schrödinger's equation. Taking the positive sign of (C. 18), we find:

$$M = N^M = N^{N^{N^{\cdots}}} = \eta(N) . \qquad \text{(C. 19)}$$

The solution (C. 19) corresponds to:

$$k = \frac{\eta}{2}\left[1 + 3^{-\frac{1}{2}\eta x}\,\eta(N)\right]$$

$$E_+ = -K\left[1 + a\,\eta(a^a)\right]^2 . \qquad \text{(C. 20)}$$

where $K \equiv m V^2/2\hbar^2$. The negative sign in (C. 18) yields:

$$(-M) = (a^a)^M . \qquad \text{(C. 21)}$$

The solution of (C. 21) is clearly:

$$M = -\frac{1}{a}$$

which corresponds to:

$$k = 0$$

$$E_+ = 0 .$$

Hence, this solution does not produce a bound state. There is one and only one bound state, given by (C.20). From (C.3), the total energy of this state is:

$$E = -K\left[1 + \alpha\,\eta(a^{\alpha})\right]^2 + \frac{e^2}{X} . \qquad (C.22)$$

The equilibrium distance, X_o, is relatively close to $X = 0$. Note that in the vicinity of $X = 0$, (C.20) implies:

$$E_+ \approx -4K(1 - \eta X) . \qquad (C.23)$$

Now, consider the "H_2" molecule, with the Hamiltonian:

$$H_o = -\frac{\hbar^2}{2m}\frac{\partial^2}{\partial x_1^2} - \frac{\hbar^2}{2m}\frac{\partial^2}{\partial x_2^2} - V\,\delta(x_1) - V\,\delta(x_1 - X)$$

$$- V\,\delta(x_2) - V\,\delta(x_2 - X) + V\,\delta(x_1 - x_2) + \frac{e^2}{X} . \qquad (C.24)$$

Schrödinger's equation is:

$$H_o\,\psi(x_1, x_2) = E\,\psi(x_1, x_2) \qquad (C.25)$$

Since the "H_2^+" molecular ion had only one bound state, we know that the solution of (C.24) and (C.25) neglecting the electron-electron interaction, is:

$$\psi(x_1, x_2) = \phi(x_1)\,\phi(x_2)\left[\alpha_1\beta_2 - \alpha_2\beta_1\right] \qquad (C.26)$$

From (C.5), (C.6), and (C.7), using equations (C.8), (C.9), (C.12),

and (C.13), we find:

$$\phi(x) = \begin{cases} \frac{2k - \eta}{\eta} \; e^{kx} & (-\infty, 0) \\ \frac{(2k - \eta)^2}{2k\eta} \; e^{kx} + \frac{2k - \eta}{2k} \; e^{-kx} & (0, X) \\ e^{-kx} & (X, \infty) \; . \end{cases} \tag{C.27}$$

Taking into account the electron-electron interaction, the solution of (C.24) and (C.25) is:

$$E = 2E_+ + \frac{e^2}{X} + E' \tag{C.28}$$

where:

$$E' \equiv \frac{V \int_{-\infty}^{\infty} dx \, |\phi(x)|^4}{\left[\int_{-\infty}^{\infty} dx \, |\phi(x)|^2 \right]^2} \tag{C.29}$$

Near $X = 0$, (C.27) and (C.29) give:

$$E' \approx 2K(1 - \tfrac{1}{2} \eta X) \; . \tag{C.30}$$

For large X, (C.27) and (C.29) show:

$$E' \to 2K \; , \tag{C.31}$$

Analogous to the case of the real hydrogen molecule, the electron-electron interaction is relatively independent of the distance between the H^+ ions, and hence doesn't affect the calculation of equilibrium distance in a major way. Using (C.30) and (C.31), (C.28) yields:

$$E = \begin{cases} -6K\left(1 - \frac{7}{6}\ X\right) + \frac{e^2}{X} & (X \approx 0) \\ \\ \frac{e^2}{X} & (X \to \infty)\ . \end{cases} \qquad \text{(C. 32)}$$

Comparing (C. 23) with (C. 32), we see that for the "H_2" molecule, the equilibrium distance is:

$$X_{oo} = \sqrt{\frac{4}{7}}\ X_o = 0.76\ X_o\ . \qquad \text{(C. 33)}$$

Equation (C. 33) shows that removal of an electron from a bonding orbital in "H_2" increases the separation of the ions by a factor of 1. 32, very close to the value in the real case. Hence, the hydrogen molecule analogy used in section II D remains valid for delta-function interactions.

BLANK PAGE

REFERENCES

1. J. H. deBoer and E. J. W. Verwey, Proc. Phys. Soc. (Lond) A49, 59 (1937).
2. F. J. Morin, Bell Syst. Tech. J. 37, 1047 (1958).
3. G. H. Jonker and S. van Houten, Halbleiterprobleme VI, F. Sauter, ed., Friedr. Vieweg und Sohn, Braunschweig, 1961, p. 118.
4. E. J. W. Verwey, P. J. Haaijman, F. C. Romeijn, and G. W. van Oosterhout, Philips Res. Rep. 5, 173 (1950).
5. R. R. Heikes and W. D. Johnston, J. Chem. Phys. 26, 582 (1957).
6. L. D. Landau, Physik. Z. Sowjetunion 3, 664 (1933).
7. J. Yamashita and T. Kurosawa, J. Phys. Soc. Japan 15, 802, 1211 (1960).
8. P. W. Anderson, Solid State Physics, Vol. 14, F. Seitz and D. Turnbull, eds., Academic Press, N.Y. (1963).
9. N. F. Mott, Proc. Phys. Soc. (Lond.) A62, 416 (1949).
10. T. Holstein, Ann. of Phys. 8, 325, 343 (1959).
11. H. Frohlich, Adv. in Phys. 3, 325 (1954).
12. J. C. Slater, Phys. Rev. 82, 538 (1951).
13. J. Hubbard, Proc. Roy. Soc. A276, 238 (1963).
14. N. Perakis, J. phys. radium 8, 473 (1927).
15. C. T. Anderson, J. Am. Chem. Soc. 58, 564 (1936).
16. M. Foex, Compt. rend. 223, 1126 (1946), 227, 193 (1948).
17. M. Foex and J. Loriers, Compt. rend. 226, 901 (1948).
18. J. Jaffray and A. Dumas, J. des recherche du C.N.R.S., Bellevue (Paris) 5, 360 (1954).

REFERENCES (cont.)

19. A. D. Pearson, J. Phys. Chem. Solids 5, 316 (1958).

20. F. J. Morin, Phys. Rev. Letters 3, 34 (1959).

21. J. Feinleib, Tech. Rep. No. HP-11, Gordon McKay Laboratory, Harvard University, 1963 (Unpublished).

22. J. Yahia and H. P. R. Frederikse, Phys. Rev. 123, 1257 (1961).

23. S. C. Abrahams, Phys. Rev. 130, 2230 (1963).

24. D. Adler and J. Feinleib, Phys. Rev. Letters 12, 700 (1964).

25. J. Callaway, Proc. Int. Conf. Phys. Semiconductors, Exeter, 1962, p. 582.

26. N. F. Mott, Nuovo Cim. Suppl. 7, 312 (1958).

27. N. F. Mott, Phil. Mag. 6, 287 (1961).

28. J. B. Goodenough, Phys. Rev. 120, 67 (1960).

29. J. B. Goodenough, J. Phys. Chem. Solids 6, 287 (1958).

30. J. B. Goodenough, Phys. Rev. 117, 1442 (1960), J. Appl. Phys. Suppl. 31, 359S (1960), Magnetism and the Chemical Bond, Interscience Publishers, N.Y. (1963).

31. W. Kohn, Phys. Rev. 133, 171A (1964).

32. J. Hubbard, to be published.

33. T. Figielski, Phys. stat. sol. 3, 1876 (1963).

34. Tables Relating to Mathieu Functions, U.S. Natl. Bur. Standards, Columbia U. Press, N.Y., 1951.

35. W. Ehrenberg, Proc. Roy. Soc. (Lond.) A63, 75 (1950).

36. E. P. Warekois, J. Appl. Phys. Suppl. 31, 346S (1960).

37. S. Minomura and H. Nagasaki, J. Phys. Soc. Japan 19, 131 (1964).

38. P. H. Carr and S. Foner, J. Appl. Phys. Suppl. 31, 344S (1960).

REFERENCES (cont.)

39. A. Paoletti and S. J. Pickart, J. Chem. Phys. 32, 308 (1960).

40. J. Wucher, Compt. rend. 241, 288 (1955).

41. S. Teranishi and K. Tarama, J. Chem. Phys. 27, 1217 (1957).

42. A. J. MacMillan, Tech. Rep. 172, Lab. for Insulation Research, M.I.T., 1962 (unpublished).

43. I. G. Austin, Phil. Mag. 7, 961 (1962).

44. G. Goodman, Phys. Rev. Letters 9, 305 (1962).

45. International Critical Tables, Vol. III, McGraw-Hill Book Co., N.Y. (1929).

46. P. G. De Gennes and J. Friedel, J. Phys. Chem. Solids 4, 71 (1958).

47. R. Heckingbottom and J. W. Linnett, Nature 194, 678 (1962).

48. W. G. Rudorff, G. Walter, and J. Stadler, Z. anorg. und allgem. Chem. 297, 1 (1958).

49. T. Kawakubo and T. Nakagawa, J. Phys. Soc. Japan 19, 517 (1964).

50. J. S. Kasper, to be published.

51. C. H. Neuman, A. W. Lawson, and R. F. Brown, to be published.

52. M. Foëx and J. Wucher, Compt. rend. 229, 882 (1949).

53. H. P. R. Frederikse, J. Appl. Phys. Suppl. 32, 2211 (1961).

54. M. Blume, to be published.

55. J. Feinleib, ref. 21, p. IV-38.

56. C. Kittel, Introduction to Solid State Physics, John Wiley and Sons, N.Y. (1956), p. 293.

57. J. Feinleib, to be published.

58. C. Kittel, loc. cit., p. 265.

REFERENCES (cont.)

59. J. B. Gibson, J. Phys. Chem. Solids 1, 27 (1956).

60. N. F. Mott and H. Jones, Theory of Metals and Alloys, Dover Publications, N.Y. (1936), p. 19.

61. S. Minomura and H. G. Drickamer, J. Appl. Phys. 34, 3043 (1963).

62. E. Conwell and V. F. Weisskopf, Phys. Rev. 77, 388 (1950).

63. R. A. Smith, Semiconductors, Cambridge U. Press, Lond. (1961), p. 152, 153.

64. G. A. Acket and J. Volger, Physica 28, 277 (1962); R. R. Heikes and W. D. Johnston, ref. 5; J. Yamashita and T. Kurosawa, ref. 7; S. van Houten, J. Phys. Chem. Solids 17, 7 (1960).

65. A. P. Young, W. B. Wilson, and C. M. Schwartz, Phys. Rev. 121, 77 (1961).

66. H. Brooks, Advances in Electronics and Electron Physics, Vol. VII, L. Marton, ed., Academic Press, N.Y. (1955), p. 121.

67. A. C. Switendick, Quarterly Progress Report No. 49, Solid State and Molecular Theory Group, M.I.T., p. 41 (1963).

68. J. Yamashita, Proc. Buhl Int. Conf. on Transition Metal Compounds (1963), to be published.

69. R. Watson, Technical Report No. 12, Solid State and Molecular Theory Group, M.I.T., 1961 (unpublished).

70. R. Watson, Phys. Rev. 111, 1108 (1958).

71. F. W. Brown, Phys. Rev. 44, 219 (1933).

72. L. Pauling, Nature of the Chemical Bond, Cornell U. Press, Ithaca, N.Y. (1945), p. 346.

REFERENCES (cont.)

73. J. Callaway, Phys. Rev. 99, 502 (1955).

74. J. R. Reitz, Solid State Physics, Vol. 1, F. Seitz and D. Turnbull, eds., Academic Press, N.Y. (1955), p. 46.

75. G. C. Fletcher, Proc. Phys. Soc. (Lond.), A65, 192 (1952).

76. W. Kauzmann, Quantum Chemistry, Academic Press, N.Y. (1957), p. 396.

77. Ibid., p. 381

ACKNOWLEDGMENTS

I wish to express my deep gratitude to Professor Harvey Brooks, who guided this research at all stages, made innumerable helpful suggestions, and provided much insight into solid state theory in general.

Special thanks are also due to Dr. Julius Feinleib for many long discussions relating to both the theory and the experimental situation in transition metal oxides.

I should also like to thank Professors William Paul, Henry Ehrenreich and Arthur Bienenstock, and Dr. Gerald Peterson for useful conversations and encouragement at various stages of this work.

Finally, I am indebted to the National Science Foundation and the Advanced Research Projects Agency for continuous support during the course of this research.

Advanced Research Projects Agency – Contract SD-88 – Distribution List*

Program in the Materials Sciences

Technical

Asst. Director of Materials Sciences
Advanced Research Projects Agency
The Pentagon [5]
Washington, D. C. 20301

Defense Documentation Center
Cameron Station [20]
Alexandria, Virginia 22314

Director, Materials Science Center
Cornell University
Ithaca, New York

Dr. H. Brooks, Dean
Div. Eng. and Applied Physics
Harvard University
Cambridge, Massachusetts 02138

Dr. C. Flow
Massachusetts Institute of Technology
Cambridge, Massachusetts 02139

Dr. M. E. Fine
Materials Research Center
Northwestern University
Evanston, Illinois

Dr. J. N. Hobstetter
Director, LRSM Program
University of Pennsylvania
Philadelphia, Pennsylvania 19104

Dr. R. A. Huggins
Stanford University
Stanford, California 94305

Dr. H. W. Leverenz
Associate Director
David Sarnoff Research Center
Radio Corporation of America
Princeton, New Jersey

Dr. R. W. Morse
Brown University
Providence, Rhode Island

Dr. R. Myers
Department of Physics
University of Maryland
College Park, Maryland 20742

Dr. E. D. Palmetier
Department of Physics
University of North Carolina
Chapel Hill, North Carolina

Dr. P. N. Powers
Purdue University
West Lafayette, Indiana 47907

Prof. F. Seitz, Dean
Graduate College
308 Administration East
Urbana, Illinois 61803

Dr. W. H. Zachariasen
University of Chicago
Chicago, Illinois 60637

*Two copies to each address, unless otherwise indicated by numbers enclosed in brackets.